Hybrid Plasma Reactor/Filter for Transportable Collective Protection Systems
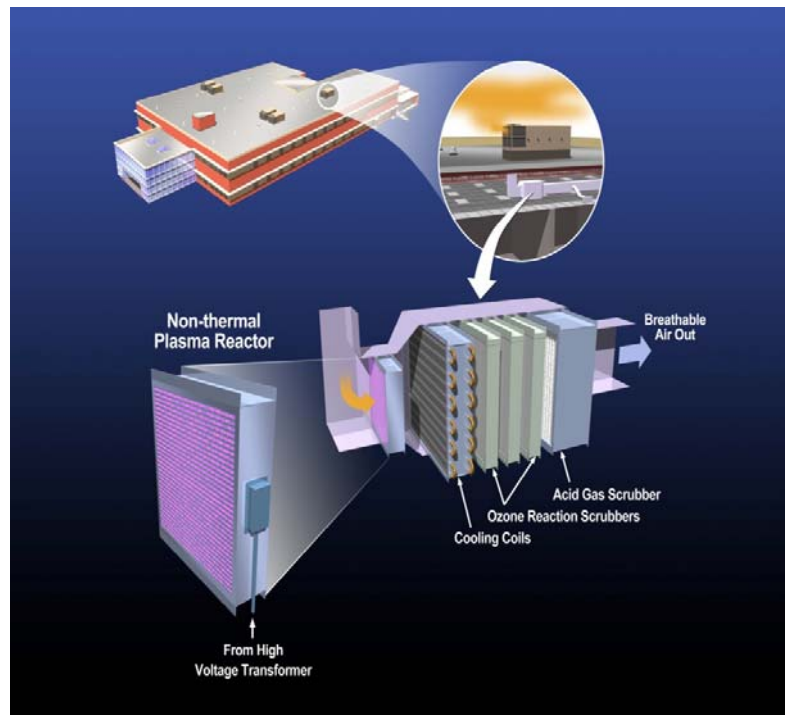## Control: BA07PRO040

GB Josephson   BJ Riley
RG Tonkyn   KG Rappe
JG Frye

March 2011

Non-thermal Plasma Reactor

Breathable Air Out

Acid Gas Scrubber
Ozone Reaction Scrubbers
Cooling Coils

From High Voltage Transformer

Pacific Northwest
NATIONAL LABORATORY

Annual Report for Hybrid Plasma Reactor/Filter for Transportable Collective Protection Systems—Phase 1C
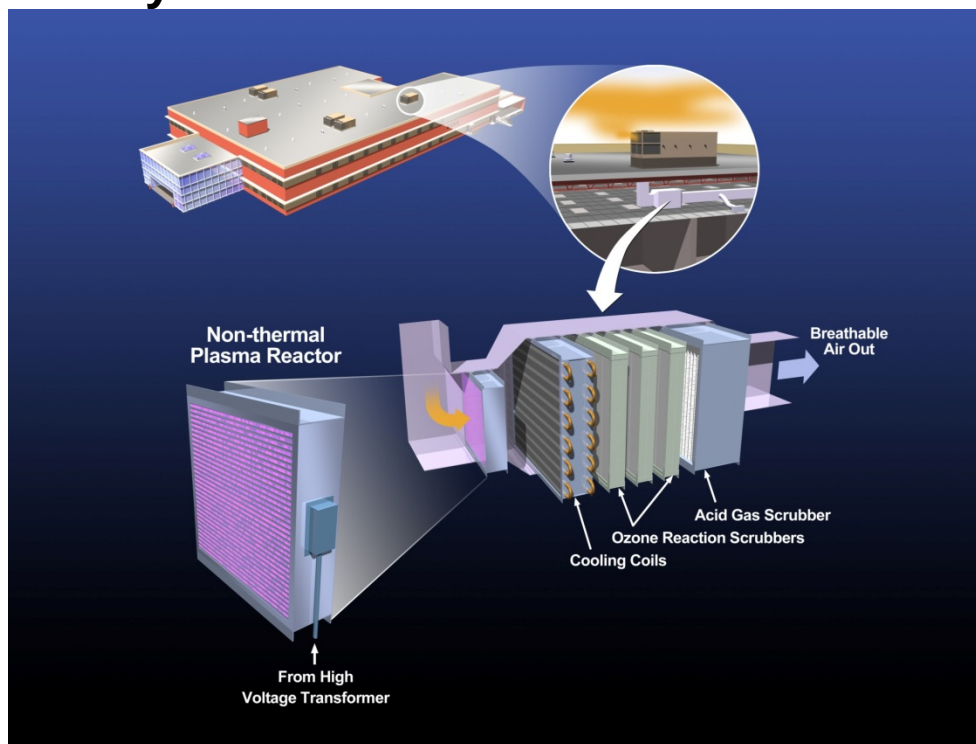
GB Josephson
RK Tonkyn
JG Frye
BJ Riley
KG Rappe

March 2011

Control: BA07PRO040

Executive Summary

Conventional collective protection systems typically employ HEPA filters for biological/radiological protection and activated carbon filters for chemical agent protection. Pacific Northwest National Laboratory (PNNL) has performed an assessment of a Hybrid Plasma/Filter system as an alternative to conventional methods for collective protection. The key premise of the hybrid system is to couple a nonthermal plasma (NTP) reactor with reactive adsorption to provide a broader envelope of protection than can be provided through a single-solution approach. The first step uses highly reactive species (e.g. oxygen radicals, hydroxyl radicals, etc.) created in a nonthermal plasma (NTP) reactor to destroy the majority (~75% - 90%) of an incoming threat. Following the NTP reactor an O_3 reactor/filter uses the O_3 created in the NTP reactor to further destroy the remaining organic materials. The complete system has four components:

- NTP reactor—destroys majority of warfare agents and organic TICs,
- O_3 reactor/filter—completes destruction of organics and removes O_3 from breathing air,
- Acid gas scrubber—removes acid threats/agents and acid gas reaction byproducts from reactor effluent, and
- Heat exchanger—removes heat imparted by the NTP reactor during an attack.

A conceptual depiction of the full system integrated in a building ventilation system is shown on the front cover.

The operating concept is to continuously operate the NTP reactor in a stand-by mode at very low power. When any elevated concentration of material is detected in the air inlet the power is immediately raised to full-protection level and operated there until the inlet air again returns to normal. No heat up time is necessary.

This report summarizes the laboratory development of the Hybrid Plasma Reactor/Filter to protect against a 'worst-case' simulant, methyl bromide (CH_3Br), and presents a preliminary engineering assessment of the technology to Joint Expeditionary Collective Protection performance specifications for chemical vapor air purification technologies.[1]

Methyl bromide was used as the 'worst-case' simulant because it has a high vapor pressure and is quite non-reactive. It is difficult to control by conventional means of adsorption and reaction. The Hybrid Plasma Reactor/Filter meets protection standards by employing a modified ZSM5 substrate in the NTP reactor and O_3 reactor filter. The NTP gets excellent reactivity by adding Ag to the ZSM5 in the NTP reactor and Ag and Mn (or Fe) to the ZSM5 in the O_3 reactor filter.

A summary of the conceptual design is shown below and compared to the JECP performance standards.

(Note: the preliminary engineering design is an estimate based upon limited laboratory testing. This estimate is provided as a basis to determine whether the Hybrid Plasma Reactor/Filter provides sufficient promise to warrant further development through the TRL levels and advance both the technical maturity and confidence levels of the design.)

---

[1] TTA #08-JECP-07-003 rv. 6.

Hybrid Plasma Reactor/Filter Conceptual Design Specifications to protect against two serial attacks of CH$_3$Br.[1]

	NTP reactor:						Heat Ex.		O3 scrubber reactor			acid gas scrubber	
	power, J/L	destruction in NTP	Power for 220CFM		Reactor vol. ft3	dim.	~ wt. lbs	ft2	lbs.	packing wt. lbs.	bulk density lb/ft3	packing vol. ft3	Zr(OH)4 wt. lbs	Zr(OH)4 vol. ft3
Normal Operation	30		3.1	kW										
Attack Operation	200	95%	20.8	kW	1.5	1.9'x2'x6"	200	284	67	412	62	6.6	6.2	0.05

wt. does not include housing

Hybrid Plasma Reactor/Filter Performance Specifications Comparison to JECP Performance Thresholds[2]

Attribute	Performance Threshold	Hybrid Plasma
Chemical Performance CH$_3$Br	55,000 mg-min/m^3	Conceptual design to 110,000 mg-min/m^3 (2 exposures)@ 2000 mg/m^3 conc.
Acid-gas (Cl$_2$)	100,000 mg-min/m^3	Conceptrual design to 200,000 mg-min/m^3 (2 exposures)@ 2000 mg/m^3 conc.
Unit Weight	5 lbs/cfm	4.2 lbs/cfm [3]
Unit Volume	0.3 ft^3/cfm	0.055 ft^3/cfm[4]
Unit Power	0.12 kW/cfm	Continuous Power—0.014kW/cfm Peak Power—0.1 kW/cfm
Consumables	5 yrs.	TBD

[1]Design basis is to protection against two serial attacks w/o opportunity to replace consumable reactants.
[2]Performance specifications are estimates based upon laboratory studies scaled to 220CFM.
[3]Weight estimates are based upon the process functional elements (packing, electrodes, heat exchanger surfaces, and transformer). Weights of vessel shells, controls, and supporting structure have not been estimated.
[4] Volume estimates are based upon the active process volumes only. Equipment is expected to be close-packed as shown in illustration, but no open space has been estimated between elements. Volume of supporting structure is not included.

Table of Contents

1 Technical Approach

The technical approach for Hybrid Plasma Reactor/Filter assessment was selected to arrive at a near-optimum selection of substrate and catalyst for the two primary components in the system—the NTP reactor and the O_3 reactor filter. The approach covered a wide-range of potential catalyst/substrate combinations and identified a substrate/catalyst combination that would provide a reasonable assessment of the system's potential performance. The target for the assessment was the "contaminant" CH_3Br.

Simply stated the technical approach consisted of two steps:

1) Down selection of a preferred substrate/catalyst system, followed by
2) Performance testing of the NTP reactor, O_3 reactor, and integrated system.

The total number of potential combinations of substrates and catalysts is too large to encompass in a single material development effort. In order to select a near-optimum combination with a limited amount of testing, a three-stage down-selection approach was employed for the O_3 reactor, followed by performance testing on the final preferred combination(s). The first stage focused on selecting preferred substrates from among many commercially available adsorbent materials and PNNL prepared SAMMs®[2] materials that would be resistant to decomposition by O_3. Carbon and polymeric adsorbents were not considered because they would react with O_3 and decompose.

Potential catalysts were added to a selection of substrate candidates to facilitate the decomposition of ozone. The first stage of down selection consisted of testing each candidate system for (1) adsorption of CH_3Br in high humidity, and (2) O_3 decomposition. The second stage of down selection tested those metals that provided the best O_3 decomposition on the two-best commercially available substrates plus modified SAMMs materials that were expected to perform better in high-humidity environments. The third round of down selection focused on a two-metal catalyst system that merged as promising from the first two rounds of testing. Further improvements could be expected from further manipulation of catalyst loadings and/or incorporation of a third metal. Nevertheless, this final catalyst/substrate system should be a good baseline for a reasonable assessment of the potential of the Hybrid Plasma Reactor/Filter.

Earlier phases of Hybrid Plasma Reactor/Filter testing had identified a Pr/Ce oxide blend ($Pr_{0.1}Ce_{0.9}O_2$) on an alumina substrate to be a preferred general oxidation catalyst for the NTP reactor. A literature search also indicated that an amorphous manganese oxide would be especially effective for the destruction of CH_3Br. Samples of each of the materials were prepared for limited testing in the NTP reactor. Results from the O_3 catalyst/substrate testing indicated ZSM5 with silver may also be effective in the NTP reactor so a third material was added and tested. Samples with better performance were further tested coupled with the O_3 reactor for overall performance.

---

[2] SAMMS (Self-Assembled Monlayers on Mesoporous Supports) is a PNNL developed technology that can be tailored to achieve high adsorption of a variety of contaminants.

2 Experimental Methods

The test system consisted of the gas manifold, the NTP reactor, the ozone reactor and the Fourier Transform Infrared (FTIR) spectrometer. They are depicted in simplified form in the following **Figure** 1. For safety reasons most of the system is housed in a closed, separately ventilated room. An electrical interlock system prevented anyone from entering the room while the high voltage was on.
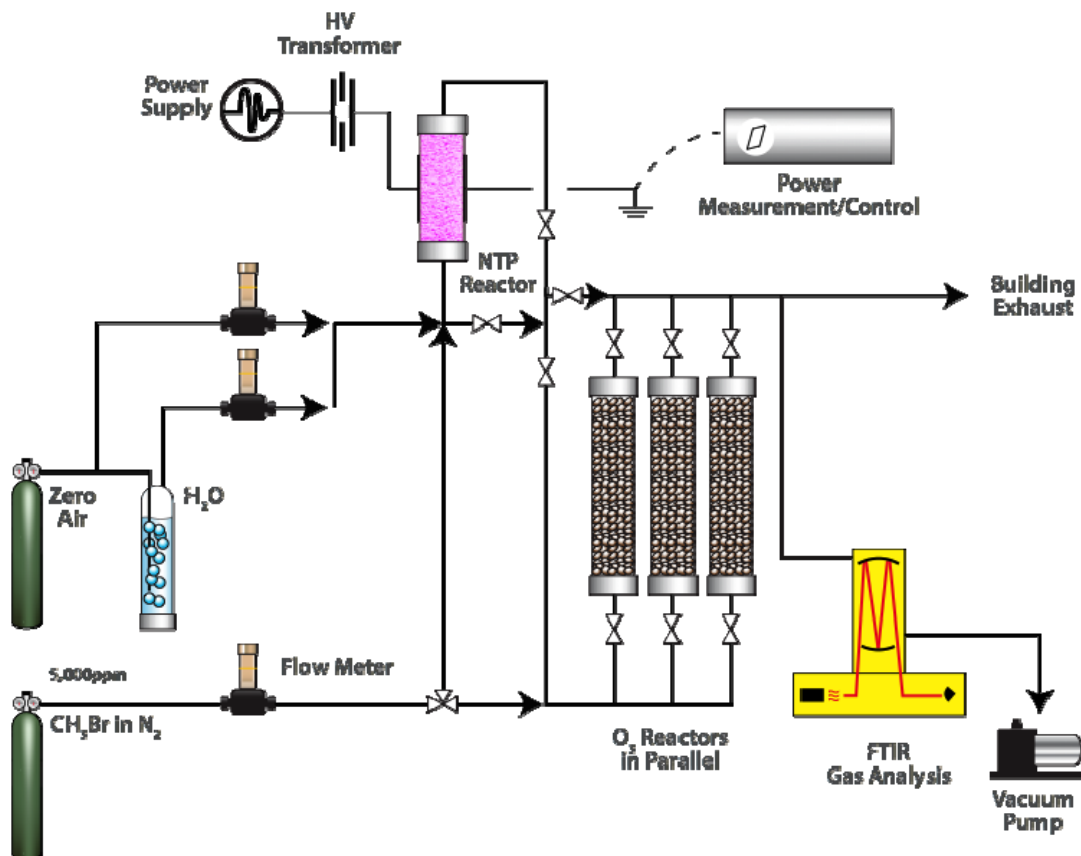
Figure 1. Hybrid Plasma Reactor/Filter Test Bench Schematic

A cylinder of dry, CO_2-free air supplied the main gas flow. Mass flow controllers directed a fraction of the total flow (typically 80%) through a large water bubbler to set the relative humidity. The contaminant of interest was added to the flow either before or after the non-thermal plasma (NTP) reactor. Flow was controlled with the ability to bypass either the NTP reactor or the ozone reactor manifold as desired.

For most of the experiments described in this report a dilute mixture of methyl bromide (CH_3Br) or acrylonitrile (CH_2CHCN) in nitrogen was employed for contaminant blending to the desired concentration. For poisoning tests, triethyl phosphate (TEP) was added by placing a small bubbler in a gently heated beaker of water. TEP vapor pressure, flow-rate through the bubbler, and the water bath temperature determined the subsequent TEP concentration. The tubing between the bubbler and the main gas flow was heated well above the water bath temperature to prevent condensation of TEP.

Non-thermal plasma was generated in one of two quartz-tube packed bed reactors, ½ inch or 1 inch OD. The high voltage was delivered via a stainless steel central electrode and the ground electrode was formed from copper tape (1 to 2 inches in height) wrapped around the outside of the tube. The position of the ground electrode defined the plasma region, which was filled either with 3 mm glass beads or small beads of the catalyst of interest.   A computer controlled AC voltage (200 to 400 Hz) was amplified and delivered to a high voltage transformer designed for this frequency range. The transformer output voltage was connected directly to both the stainless steel inner electrode and a high voltage probe. The outer, copper tape electrode was connected directly to ground through a large (1.96 µF) capacitor. The computer monitored both the voltage input and the voltage across the capacitor. The energy per cycle was determined by calculating the area inside a Lissajou figure formed by plotting the high voltage signal vs. the capacitor voltage. The plasma power (in Watts) was maintained at a pre-set value by controlling the source voltage with PID control.

The ozone reactor manifold consisted of ten (10) parallel, 1-inch diameter stainless steel tubes with shutoff solenoid valves at each entrance and exit port. For some tests larger diameter quartz tubes were installed to accommodate higher catalyst volume testing. Flow could be delivered to any of ten packed reactors, or the manifold could be bypassed entirely.

Gas flow to the FTIR was controlled by a mass flow controller (typically set at 1 SLPM) upstream of the measurement cell; pressure was controlled in the measurement cell by a pressure control valve located between the measurement cell and a small vacuum pump. The pressure control valve adjusted the exhaust flow such that the FTIR cell pressure remained at 100 torr. For this flow rate and a cell volume of ~ 2 liters, the nominal residence time in the cell was approximately 15 seconds.

The FTIR utilized a 10 meter path length, stainless steel White cell containing gold coated mirrors and zinc selenide input and output windows. Although the cell can be heated, for these experiments the cell was kept at room temperature. The FTIR resolution was set to 0.5 cm^{-1}.

2.1 *Experimental protocols*

The reactivity of the test gases was measured in the NTP reactor alone, in the ozone reactor alone and with both systems in combination. For tests of reactivity in the NTP reactor, both quasi-steady state and dynamic exposure (CT) tests[3] were employed. Dynamic exposure tests (CT) inject a concentration of contaminant for a given period of time and monitor the output contaminant concentration during and after the end of the contaminant input. Such tests are necessary for systems rely on a limited adsorption capacity to provide some or all of the protection. Reactivity of the ozone reactor or the full-system was established through with CT tests.

The "quasi-steady state" NTP tests consisted of packing the reactor with a known mass of catalyst followed by initiating the desired conditions of flow, relative humidity, test gas concentration and plasma power. Using OMNIC's series software allowed monitoring of the FTIR responses of 5 separate analytes in real time. The collected spectra could also

---

[3] CT tests are derived from concentration/time exposure testing as done on carbon filters.

be analyzed after the experiment for other reaction products. Due to the very large pore volume and surface area of the zeolite catalysts, the system was often slow to respond to changes in the challenge conditions. In some cases steady state was reached, but more often the system *approached* a condition of either true steady state or possibly slowly changing output due to self-poisoning of the catalyst. At this point plasma power was changed and the measurement repeated for the new condition. These quasi-steady state results, while not completely satisfying, at least allowed comparison of catalysts in a fairly even manner.

All CT tests were carried out in similar manner for the NTP reactor alone, O_3 reactor alone, or combined system. The test consisted of switching between two flow conditions. In the baseline condition a set amount of air was directed through the bubbler to establish the desired %RH. "Balance air" was combined with the humidified air to achieve the desired total flow (usually 2SLPM). During the contaminant injection condition, concentrated contaminant was metered into the "balance air" flow at the proper flow rate to obtain the desired concentration and the flow of the "balance air" was reduced accordingly to maintain the 2SLPM total flow. The flow through the bubbler remained the same in order to keep the relative humidity constant. The system was prepared in the former setup, including running the NTP reactor as desired. The flow was switched to include the test gas for a set period of time before switching back to the initial condition. Bypass measurements were taken as desired before, during and after the test gas exposure, and the post-exposure behavior was monitored as necessary.   These two procedures will be illustrated below in the results sections of this report.

2.2 *Catalyst Preparations*

2.2.1 Catalyst Requirements
The catalyst requirements derive from the process application described below:

1) The system would employ a high frequency, high energy plasma discharge chamber, near the air intake. The plasma could run intermittently or at low power most of the time, but in the event of a threat attack, the unit would be capable of almost instantaneously going to full power.

2) While the plasma is capable of destroying most organic matter contained in a threat scenario, complete destruction at short residence times in the plasma chamber would require very high power requirements. The solution for this technology is to put a catalyst and a support material into the plasma chamber that would adsorb and retain threat materials long enough to ensure destruction or at least partial destruction of the incoming threat agent.

3) To insure that toxic materials that might escape the plasma chamber are fully removed from the breathing air downstream catalyst and adsorbent beds are also required. Since a considerable amount of residual ozone escapes from the plasma chamber, even during a threat attack, an "ozone" catalyst is employed immediately downstream of the plasma chamber. The ozone catalyst utilizes unreacted ozone to complete the oxidative destruction of the residual threat agent or degradation products. If sufficient catalyst(s) is used the threat agent is neutralized and residual ozone will also be degraded to O2 by the catalyst.

10

4) As some materials are degraded, they result in the production of acid gases, and NOx and nitric acid are also formed in the plasma chamber. This necessitates the use of an acid gas scrubber/adsorber near the exit end of the system. Therefore it was deemed necessary that all of the catalyst supports used in the combined system would have to be stable in a strongly oxidizing, strongly acidic, high moisture environment. Materials that would be considered for use in the plasma chamber needed to be poor electrical conductors to avoid shorting out the plasma discharge.

2.2.2 Catalyst Supports

Catalyst supports that were investigated for use in the Hybrid Plasma Reactor System consisted mostly of synthetic zeolite materials and engineered silicas. It was felt that these materials would offer the best long term resistance against degradation by ozone, acid gases, and most potential threat agents. All of the support materials evaluated were commercially available commodities, with moderate to high surface areas and porosities. Effective pore diameters varied between different zeolitic or porous silica structures. Support materials were selected that displayed low affinity for water so that water would interfere less with the adsorption of the gaseous threats. The materials selected for testing had different but generally low levels of "hydrophilicity". Some materials were chemically modified to adjust this attribute. All support materials were initially screened to determine to what extent that they adsorbed CH_3Br both dry and in the presence of water vapor, and to insure that the supports did not result in unacceptably high pressure drops. None of the support materials by themselves (without catalyst components added to them or without the aid of a plasma discharge) were capable of destroying **any** CH_3Br. Also, only small pore zeolites (~5 Angstrom pore diameter MFI type zeolites) displayed significant CH_3Br adsorption capacity. Uncatalyzed larger pore zeolites (such as Faujasites and beta), mesoporous silicas (such as MCM41), and macroporous silicas displayed **no** adsorptive capacity for CH_3Br.

2.2.3 Catalytic Components

Much of the catalyst development focused on the development of an "ozone" catalyst which would be located downstream of the NTP reactor. Contaminant not destroyed in the NTP reactor (or partial oxidation products) would be captured in the downstream ozone catalyst and be destroyed by active species (e.g. O• radical) formed during the decomposition of the residual ozone.

Following a review of the catalyst literature, and subsequent discussions with Dr. Joe Rossin, a number of catalyst supports were chosen upon which the catalysts would be prepared. The list of potential catalytic components to be investigated was narrowed to Mn, Fe, Pt, Re, Cu, Ag, and Au (either alone or in combination with each other).

A few catalysts were also prepared and tested in the NTP reactor to improve the performance of the overall system and reduce the demands on the O_3 reactor.

- A Pr/Ce blended-oxide catalyst had shown promise as a general low-temperature oxidation catalyst. The catalyst was applied to alumina beads for testing with the NTP reactor.
- An amorphous manganese oxide was reported in the literature to be effective for photocatalytic degradation of CH_3Br. The literature preparation was a fine powder

that was not expected to be appropriate to use under the higher gas flow rates of Hybrid Plasma Reactor System. Thus the preparation was modified and deposited on 1 mm alumina beads.

- In addition, several of the "ozone" catalysts that had been prepared and tested as downstream catalysts were also tested within the plasma chamber.

All of the catalyst preparations and the results of the down selection testing are described in the following section.

Synthesis methods for each of the catalysts prepared are discussed in Appendix A.

3 Results

3.1 *Down selection Testing*

The best combination of substrate and catalyst/reactant were selected through three rounds of testing. Following down selection, the performance of the NTP reactor and O_3 reactor/filter were quantified in performance testing. And finally, the impacts of a known catalyst poison, triethylphosphate (TEP), were quantified.

3.1.1 Round 1 Objectives/Summary

Table 1 lists the various catalysts that were made and tested in the 1st round of the ozone catalyst screening. The objective of the first round screening was to test as many of the support materials as were initially available with or without catalytic metals added, and employing different catalytic preparation methods. As can be seen from the Table 1, there were so many different catalyst preparations that the 1st round catalysts had to be tested in 2 groupings. One of the key objectives was to identify which supports displayed significant CH_3Br adsorption.

All of the catalysts that were prepared on either ZSM-5 or Silicalite displayed good to very good adsorption of CH_3Br. Catalysts that were prepared on the mesoporous MC-1381 silica supports displayed very poor CH_3Br adsorption. Catalysts prepared on the Perlkat 97-0 macroporous silica support displayed no CH_3Br adsorption at all. A second key objective was to identify catalyst compositions that performed catalyzed ozone decomposition, and to what degree. A final objective was to identify catalyst compositions or preparations that displayed conversion of CH_3Br either in the presence of ozone or without it. As can be seen from Table 1, all of the metal containing catalysts tested in the 1st round showed some ozone decomposition activity. The most active ozone decomposition catalysts all contained either Mn or Fe. The most active ozone decomposition catalysts are not necessarily the best catalysts for the decomposition of CH_3Br, in fact they were among the worst. The two best catalysts for the decomposition of CH_3Br were a Ag-exchanged ZSM-5 and a Mn-exchanged ZSM-5 that had been post impregnated with H_2-reduced Pt. The Pt-containing catalyst displayed good reactivity with CH_3Br, and much of the converted CH_3Br carbon was converted to CO_2. The Ag-exchanged ZSM-5 catalyst appeared to be unique. It was a poor ozone decomposition catalyst, showed the most reaction with CH_3Br, but made almost no CO_2 in the process. This catalyst did however convert much of the CH_3Br to methanol (CH_3OH), even in the absence of ozone. It was uncertain whether the Ag was facilitating a hydrolysis reaction

12

of the CH_3Br or whether the Ag was reacting stoichiometrically with CH_3Br (forming an inactive AgBr phase). Irrespective of which of these may be the case, the presence of the Ag component allowed more of the CH_3Br to be converted to something (CH_3OH) which is more strongly adsorbed and held in the catalyst.

Table 1. Round 1 O_3 Reactor/Filter Substrate/Catalyst Down Selection Testing Summary

Round 1a							
Substrate	Catalyst	Catalyst I.D.	CH3Br Adsorption	CH3Br Reaction	CO/CO2 Generation	O_3 Decomposition	other comment
Silicalite	1% Au	60433-5-1	GOOD	POOR	POOR	FAIR	
Silicalite	0.5% Au + 0.14% Mn	60433-11-1	VERY GOOD	FAIR	FAIR	FAIR	
Silicalite	1% Pt (reduced)	60433-8-1	GOOD	FAIR	FAIR	FAIR	
Perlkat 97-0	3% Pt + 2.86% Re (reduced)	60433-14-1R	NONE	NONE	NONE	FAIR	
ZSM-5	Mn-Exch'd. + 1.8% Pt (reduced)	60433-25-1R	VERY GOOD	GOOD	GOOD	GOOD	
Perlkat 97-0	2.95% Re (reduced)	60433-18-1R	NONE	NONE	NONE	FAIR	
ZSM-5	Ag-Exch'd.	60433-21-1	VERY GOOD	VERY GOOD	POOR	POOR	Makes CH_3OH from CH_3Br in absence of O_3
Perlkat 97-0	NONE-Support Only	60433-1-2	NONE	NONE	NONE	NONE	
ZSM-5	H-Exch'd. Form of Support Only	60433-1-3	GOOD	NONE	NONE	NONE	
Round 1b							
Substrate	Catalyst		CH3Br Adsorption	CH3Br Reaction	CO/CO2 Generation	O_3 Decomposition	other comment
MC1381	Cu(OAc)$_2$		POOR	POOR	POOR	POOR	
MC1381	NONE-Support Only		NONE	NONE	NONE	POOR	
MC1381	Cu/Mn		POOR	POOR	POOR	VERY GOOD	
MC1381	AgNO$_3$		POOR	POOR	POOR	POOR	
None	Mn(OAc)2		POOR	POOR	POOR	VERY GOOD	
Al$_2$O$_3$	Precip. FeO(OH)		POOR	POOR	POOR	FAIR	Adsorbs CO_2 in absence of O_3
NONE	Precip. FeO(OH)		POOR	POOR	POOR	GOOD	Adsorbs CO_2 in absence of O_3
ZSM-5	Mn-Exch'd. + 1.8% Pt	60433-25-1	GOOD	FAIR	FAIR	GOOD	
Perlkat 97-0	3% Pt + 2.86% Re	60433-14-1	NONE	POOR	POOR	POOR	

3.1.2 Round 2 Objectives/Summary

Table 2 lists those catalysts that were prepared and tested in round 2 testing. The first of the SAMMS-type hydrophobic catalysts were tested during this round and gave similar results to the previously tested mesoporous silica results. The presence of the hydrophobic coatings and precursor failed to improve CH_3Br adsorption on the mesoporous supports, and no evidence of CH_3Br reaction was observed for any of these catalysts (including the Ag-containing catalyst). Several catalysts had been made as perturbations of some of the round 1 catalysts to determine whether ion exchange prepared catalysts were more effective or selective for some of the desired reactions. It was decided to first investigate Mn, which had been used in some of the more successful round 1 catalysts. A Mn(II)-Exch'd ZSM-5 catalyst (without any additional promoters) was tested to establish its catalytic properties. Its CH_3Br adsorption was rated as good, its ability to convert CH_3Br and to generate CO_2 as a product were both rated as fair, and its ozone decomposition ability was also rated as fair. This suggested that Mn located in ion exchange sites (where Mn is expected to be atomically dispersed) is not nearly as active of an ozone decomposition catalyst as is a bulk Mn oxide. But, nonetheless does display some ability to convert CH_3Br to largely CO_2. Another catalyst was prepared from the same batch of the Mn(II)-Exch'd ZSM-5 catalyst where an equal amount of additional Mn was impregnated into the catalyst. This change did not seem to affect the CH_3Br adsorption, but the ozone decomposition activity increased at the expense of the CH_3Br reactivity and the CO_2 generation. Another similar catalyst was also prepared on the Mn(II)-Exch'd ZSM-5 catalyst by co-impregnating an additional amount of both Mn and Ag. This resulted in a catalyst that performed nearly identical to the previous Mn-Exch'd ZSM-5 +1.8%Pt (reduced) catalyst from the round 1 candidates. A Cu-exch'd ZSM-5 catalyst was prepared also for comparison to other metal-exch'd ZSM-5 materials. This material similarly displayed good adsorption of CH_3Br, but no CH_3Br reactivity, no CO_2 production, nor any ability to decompose ozone.

A SAC-13 catalyst was obtained from Engelhard for testing also. This material is an H-Nafion Ion Exchange resin supported on a macroporous silica support. The intent was to see if the acidity of this catalyst, in the presence of CH_3Br and water vapor, would promote the CH_3Br hydrolysis (resulting in CH_3OH) as observed on some of the Ag-containing catalysts. Under the test conditions no reaction with CH_3Br was observed.

Since some of the precipitated FeO(OH) materials that had been obtained from Dr. Joe Rossin at Guild Associates, had showed significant ozone decomposition activity, it was decided to investigate Fe-containing catalysts as well. Previously the as-received precipitated FeO(OH) materials displayed poor CH_3Br adsorption. It was decided to add 3wt% of Ag to this material in an attempt to increase CH_3Br reaction capacity. Unfortunately, this approach showed no benefit. An Fe(III)-Exch'd ZSM-5 material post-impregnated with 3wt% of Ag, however, displayed very good CH_3Br adsorption and good CH_3Br reactivity. That catalyst was only fair at producing CO_2 and at decomposing ozone.

A Carrulite commercial ozone decomposition catalyst was obtained and also tested as an ozone reactor catalyst. The Carrulite material decomposed ozone completely, but

15

displayed no adsorption for CH_3Br, showed no reaction with CH_3Br, and produced no CO_2. A 3.6%Mn +1%Ag composition prepared on the silicalite support proved to be nearly as active as the commercial Carrulite catalyst at decomposing ozone and with considerably less active metals content. It did adsorb CH_3Br very well, but no CH_3Br reaction was observed nor CO_2 produced.

Table 2. Round 2 O_3 Reactor/Filter Substrate/Catalyst Down Selection Testing Summary

Round 2a							
Substrate	**Catalyst**	**Catalyst I.D.**	**CH3Br Adsorption**	**CH3Br Reaction**	**CO/CO2 Generation**	**O_3 Decomposition**	**other comment**
NONE	Precip. FeO(OH)		POOR	POOR	POOR	VERY GOOD	Adsorbs CO_2 in Absence of O_3
ZSM-5	Mn-Exch'd. + 1.8% Mn + 3% Ag	60433-46-1	VERY GOOD	GOOD	GOOD	GOOD	
ZSM-5	Mn-Exch'd.	60433-33-1 SAC-13 (Engelhard Corp.)	GOOD	FAIR	FAIR	FAIR	
SiO$_2$	H-Nafion Resin		NONE	NONE	NONE	NONE	
ZSM-5	Mn-Exch'd. + 1.8% Mn	60433-43-1	GOOD	POOR	POOR	GOOD	
ZSM-5	Cu-Exch'd.	60433-40-1	GOOD	NONE	NONE	NONE	
Silicalite	3.6% Mn + 1.0% Ag	60433-37-1	VERY GOOD	NONE	NONE	EXCELLENT	
MC1382	Mn(pfb)2 on C8F13 SAMMS		NONE	NONE	NONE	FAIR	
MC1381	Ag(pfb)		NONE	NONE	NONE	NONE	
MC1382	Cu(pfb) on C8F13 SAMMS		NONE	NONE	NONE	NONE	
Round 2b							
Substrate	**Catalyst**		**CH3Br Adsorption**	**CH3Br Reaction**	**CO/CO2 Generation**	**O_3 Decomposition**	**other comment**
MC1381	Cu(pfb)		NONE	NONE	NONE	POOR	
NONE	Precip. FeO(OH) + 3% Ag	60433-54-1	POOR	POOR	POOR	VERY GOOD	Adsorbs CO_2 in Absence of O_3
ZSM-5	Fe^{+3}-Exch'd. + 3% Ag	60433-49-1	VERY GOOD	GOOD	FAIR	FAIR	Makes CH_3OH and CO_2
Al$_2$O$_3$	Precip. FeO(OH)		POOR	POOR	POOR	GOOD	Increasing O_3 Decomposition Activity
NONE	Carrulite		NONE	NONE	NONE	EXCELLENT	

17

3.1.3 Round 3 Objectives/Summary

From results that had been obtained from round 1 and round 2 ozone catalyst testing, an optimum material for CH_3Br treatment began to emerge. Only small pore ZSM-5 type zeolite structures appeared effective at adsorbing methyl bromide. Larger pore mesoporous and macroporous materials tested simply did not retain any significant amount of methyl bromide. Even when catalytic materials were contained within the pores of these materials, CH_3Br was seemingly unaffected. While many of the catalysts tested did display significant ozone decomposition activity (including larger pore mesoporous and macroporous materials) catalysts that were also promoted with Ag or Pt demonstrated an enhanced ability to convert CH_3Br and to also produce more CO_2. In the catalyst, if ozone decomposition is too facile, then there may not be sufficient ozone in the catalyst to participate in CH_3Br decomposition.

Catalysts prepared containing bulk MnO_x and FeO_x appeared to be very potent ozone destruction catalysts, while catalysts containing Mn^{+2}, Fe^{+3}, or Ag^{+1} ions in chemical exchange sites displayed considerably less ozone decomposition capacity. The combination of a Mn^{+2}- or Fe^{+3}-exchanged ZSM-5 zeolite, post-impregnated with Ag, appeared to offer the best option for enhancing methyl bromide destruction on the downstream ozone catalyst. Planning for the phase 3 catalyst preparation included variations of the amount of post-impregnated Ag to be added to the catalysts, as well as catalyst variations using silicalite (material that showed the highest CH_3Br adsorption capacity), and zeolite Y (a larger pore zeolite, but with a much larger fraction of ion exchange sites).

As can be seen from Table 3 a couple of new larger pore support materials were tested for their ability to adsorb CH_3Br. These materials were considered for two reasons. First, as catalytic metals were added to the small pore ZSM-5 and Silicalite materials they adsorbed CH_3Br better. This seemed to be the case whether or not the catalytic metals reacted to form CO_2 and may be related as much to a physical blocking of the pores as catalytic reaction. Secondly, the zeolite Y material has a much lower silica to alumina ratio, and thus has many more cation exchange sites that can be populated with active metals (this is somewhat true of the zeolite Beta material as well). However, in spite of our optimistic view, neither of the two catalysts prepared on the Y zeolite material showed any adsorption or reaction of CH_3Br, however both were excellent ozone decomposition catalysts. Several catalysts made using either a Mn-exch'd ZSM-5 or a Fe-exch'd ZSM-5 post impregnated with several different levels of Ag, showed very convincingly that a little added Ag is good, and more is even better. These materials, without catalysts added, did not adsorb any significant amount of CH_3Br.

Two of the most promising round 1 catalysts were tested again, due to a change in test protocol. The first catalyst was the Ag-exch'd ZSM-5 catalyst that had exhibited good CH_3Br conversion. On the repeat testing, this catalyst seems to have improved with respect to its ability to produce CO_2 in the presence of CH_3Br and ozone. The 2nd catalyst was Mn-exch'd ZSM-5 post impregnated with 1.8% reduced-Pt. On retesting, this catalyst appears to have lost much of its ability to convert CH_3Br and generate CO_2.

The reason for the poor performance was attributed to instability in an oxidizing environment, but was further investigated. Further performance testing was conducted using the ZSM-5 based catalysts, because they performed better.

Table 3. Round 3 O_3 Reactor/Filter Substrate/Catalyst Down Selection Testing Summary

Round 3a

Substrate	Catalyst	Catalyst I.D.	CH3Br Adsorption	CH3Br Reaction	CO/CO2 Generation	O_3 Decomposition	other comment
Silicalite	NONE-Support Only		GOOD	NONE	NONE	NONE	
Na-Y-Zeolite	NONE-Support Only		NONE	NONE	NONE	NONE	
H-Zeolite-Beta	NONE-Support Only		NONE	NONE	NONE	NONE	
ZSM-5	Mn-Exch'd. + 3% Ag	60433-67-1	VERY GOOD	GOOD	GOOD	FAIR	
ZSM-5	Fe^{+3}-Exch'd.	60433-73-1	FAIR	NONE	NONE	FAIR	
ZSM-5	Mn-Exch'd. + 1.8% Pt (reduced)	60433-25-1R	FAIR	POOR	POOR	FAIR	
ZSM-5	Mn-Exch'd. + 1.8% Mn + 3% Ag	60433-46-1	GOOD	GOOD	VERY GOOD	VERY GOOD	
Silicalite	1.8% Fe (as hydroxide) + 3% Ag	60433-69-1	GOOD	FAIR	VERY GOOD	VERY GOOD	
Silicalite	1.8% Mn, post impreg. w/3% Ag	60433-63-1	GOOD	NONE	NONE	EXCELLENT	

Round 3b

Substrate	Catalyst	Catalyst I.D.	CH3Br Adsorption	CH3Br Reaction	CO/CO2 Generation	O_3 Decomposition	other comment
ZSM-5	Ag-Exch'd.	60433-21-1	VERY GOOD	VERY GOOD	GOOD	POOR	Makes CH_3OH from CH_3Br in Absence of O_3
ZSM-5	Mn-Exch'd. + 6% Ag	60433-81-1	VERY GOOD	VERY GOOD	VERY GOOD	VERY GOOD	
ZSM-5	Mn-Exch'd. + 12% Ag	60433-81-2	VERY GOOD	VERY GOOD	VERY GOOD	EXCELLENT	
Na-Y-Zeolite	Fe^{+3}-Exch'd. + 6% Ag	60433-75-1	NONE	NONE	NONE	EXCELLENT	
ZSM-5	Fe^{+3}-Exch'd. + 6% Ag	60433-78-1	VERY GOOD	VERY GOOD	VERY GOOD	V.G. to POOR	CH_3Br Destroys O_3 Decomposition Activity
Silicalite	0.05% Mn + 3% Ag	60433-91-1	GOOD	POOR	NONE	GOOD	
ZSM-5	Fe^{+2}-Exch'd. + 3% Ag	60433-85-1	VERY GOOD	FAIR	GOOD	FAIR	
ZSM-5	Fe^{+3}-Exch'd. + 3% Ag	60433-49-1	VERY GOOD	FAIR	FAIR	FAIR	
Na-Y-Zeolite	Mn-Exch'd. + 12% Ag	60433-88-1	NONE	NONE	NONE	EXCELLENT	

3.1.4 Plasma Chamber Catalyst Objectives/Summary

Materials/catalysts were placed into the plasma chamber and screened for their suitability to perform as plasma chamber catalysts or packings. Ideally, such a material would not possess any significant electrical conductivity which would result in shorting out the plasma system, but would enhance CH_3Br destruction in the Plasma. The results of the plasma chamber testing are summarized in Table 4.

The Pr/ Ce blended-oxide catalyst (10wt% coated on 1mm alumina beads) facilitated complete destruction of the CH_3Br at high plasma power. Almost all of the organic carbon contained in the CH_3Br appeared to be converted to CO_2. The AMO catalyst was rated as good on CH_3Br destruction in the plasma reactor and most of the organic carbon from the CH_3Br conversion appeared as CO_2. The fresh AMO catalyst shows very good ozone decomposition activity, but after exposure to CH_3Br, this capability seems to be lost.

With the plasma chamber filled with 3mm glass beads, there is no adsorption of the CH_3Br (as expected), but under maximum plasma power ~30% of the CH_3Br is destroyed and converted largely to CO_2. No ozone decomposition is facilitated by the glass beads.

When the H-ZSM-5 substrate material is used in the plasma reactor CH_3Br destruction is much better than with glass beads alone. Most of the converted CH_3Br material shows up as CO_2, yet the catalyst doesn't seem to degrade ozone appreciably.

The Ag-Exch'd ZSM-5 catalyst was the best choice for the plasma reactor catalyst. The catalyst exhibited very good CH_3Br adsorption capacity, and with a slightly oversized plasma catalyst bed demonstrated complete CH_3Br destruction at moderate plasma power levels while converting the carbon to CO_2. The Ag-exch'd ZSM-5 catalyst also generates moderate quantities of ozone in the NTP reactor, which is a desirable feature for the NTP reactor catalyst. Glass beads generate the most O_3 in the NTP reactor, which is an advantage for optimum performance in the O_3 reactor/filter. But the superior performance for destroying CH_3Br in the NTP reactor outweighs the higher O_3 generation of glass beads.

Table 4. Plasma Chamber Substrate/Catalyst Down Selection Testing Summary

Substrate	Catalyst	Catalyst I.D.	CH3Br Adsorption	CH3Br Reaction	CO/CO2 Generation	O_3 Generation	other comment
1mm Al_2O_3 Beads	10% Pr-doped CeOx Coating	58562-85-1	POOR	EXCELLENT	VERY GOOD	GOOD	Complete CH_3Br Destruction at Very High Power
1mm Al_2O_3 Beads	10% Amorphous MnOx Coating	60433-99-1	POOR	GOOD	VERY GOOD	GOOD	Br Seems to Poison O3 Decomp. Activity
Glass Beads Only	none		POOR	FAIR	GOOD	VERY GOOD	Only ~30% Max. CH_3Br Destruction @ Max. Power
H-ZSM-5 Granules	none	60433-1-3	GOOD	GOOD	VERY GOOD	GOOD	Better CH_3Br Destruction than with Glass Beads
ZSM-5	Ag-Exch'd.	60433-109-1	VERY GOOD	EXCELLENT	EXCELLENT	GOOD	Complete CH_3Br Destruction with Larger Catalyst Bed & Moderate Plasma Power

3.1.5 Catalyst Preparation for Performance Testing

Two large batches of the two best O_3 reactor/filter catalyst compositions were prepared and tested to insure that the new batches of catalyst perform as had the previous smaller catalyst batches in the baseline testing. Additionally, the AMO catalyst and Pr/ Ce blended-oxide catalyst, prepared for the NTP reactor were tested to establish reactivity without the plasma.

The AMO catalyst prep that was developed displayed no capacity for adsorption or conversion of CH_3Br in the O_3 reactor, nor did it generate any CO_2, but it was a fair ozone decomposition catalyst. Therefore this catalyst would not be considered for use as a downstream ozone catalyst, and is undesirable in the NTP reactor, from which O_3 is to be generated to drive the following O_3 reactor/filter.

Pr/ Ce blended-oxide catalyst fared no better than did the AMO catalyst as a catalyst in the O_3reactor/filter, but it did not decompose the O_3, which is an advantage for an NTP reactor catalyst.

As can be seen from Table 5, the two large batches of the Mn-exch'd ZSM-5 +12%Ag catalyst and the Fe-Exch'd ZSM-5 + 6%Ag catalyst both performed similarly to those catalysts tested in round 3.

Table 5. Large Batch Testing in O_3 Reactor/Filter of Final Catalyst Preparations

Substrate	Catalyst	Catalyst I.D.	CH3Br Adsorption	CH3Br Reaction	CO/CO2 Generation	O_3 Decomposition	other comment
1mm Al_2O_3 Beads	10% Amorphous MnOx Coating	60433-99-1	NONE	POOR	POOR	V.G. -> POOR	Br Seems to Poison O3 Decomp. Capability
ZSM-5	Mn-Exch'd. + 12% Ag (Large Batch)	60433-96-1	VERY GOOD	VERY GOOD	VERY GOOD	EXCELLENT	
ZSM-5	Fe^{+3}-Exch'd. + 6% Ag (Large Batch)	60433-105-1	VERY GOOD	VERY GOOD	VERY GOOD	V.G. -> POOR	Br Seems to Poison O3 Decomp. Capability
1mm Al_2O_3 Beads	10% Pr-doped CeOx Coating	58562-85-1	NONE	POOR	NONE ?	POOR	

3.1.6 Catalyst Selections and Performance

The Ag-Exchanged ZSM-5 catalyst is the preferred choice as the plasma chamber catalyst. The performance testing did not identify a clear preference between the Mn-Exchanged + 12% Ag impregnated ZSM-5 catalyst or the Fe-Exchange+6% Ag impregnated ZSM-5 as the downstream O_3 reactor/filter catalyst. Both materials lose activity toward CH_3Br with continued exposure. The Fe-exchanged material appears to initially react faster than the Mn-exchanged material, but is poisoned more rapidly. As an O_3 decomposition catalyst the Fe-exchanged material deteriorates more rapidly than the Mn-exchanged catalyst.

Post reaction testing of both materials shows that the Ag is consumed in the reaction with CH_3Br. This suggests that Ag is not participating catalytically in the reaction with CH_3Br, but rather as consumed reactant. The reaction is reason for the favorable performance with CH_3Br, but the consumed reactant must be considered in design.

The Ag held in the ion exchange sites of the ZSM-5 catalyst shows very little ability to decompose ozone or to facilitate the production of CO_2. However, when Ag is impregnated onto a Mn-exchanged ZSM-5 catalyst, the ability of that catalyst to convert CH_3Br and produce CO_2 are both greatly enhanced, but its ability to decompose ozone remains unchanged.

This is similar to observations with Mn with respect to its ability to decompose ozone. Mn in an exchange site is a poor O_3 decomposition catalyst, while Mn dispersed throughout the substrate as an oxide is a very potent O_3 decomposition catalyst. In the case of Ag it appears to have very good activity as an oxidation catalyst as a bulk oxide, but is still a poor ozone decomposition catalyst (which is what we were trying to take advantage of).

Although optimization can still provide additional benefits, it is obvious that Ag is important in the NTP reactor and Ag combined with Mn (or Fe) is necessary as a bi-metal reactant/catalyst for best performance in the O_3 reactor/filter.

3.2 *Performance Testing*

3.2.1 Destruction of CH_3Br in an NTP Reactor
Ag exchanged ZSM5

This material clearly performed the best in the NTP moderated destruction of CH_3Br, although the reaction is not catalytic in nature.

Many of the aspects involved with the destruction of CH_3Br by Ag exchanged ZSM-5 in the plasma reactor are illustrated by the following experiment.
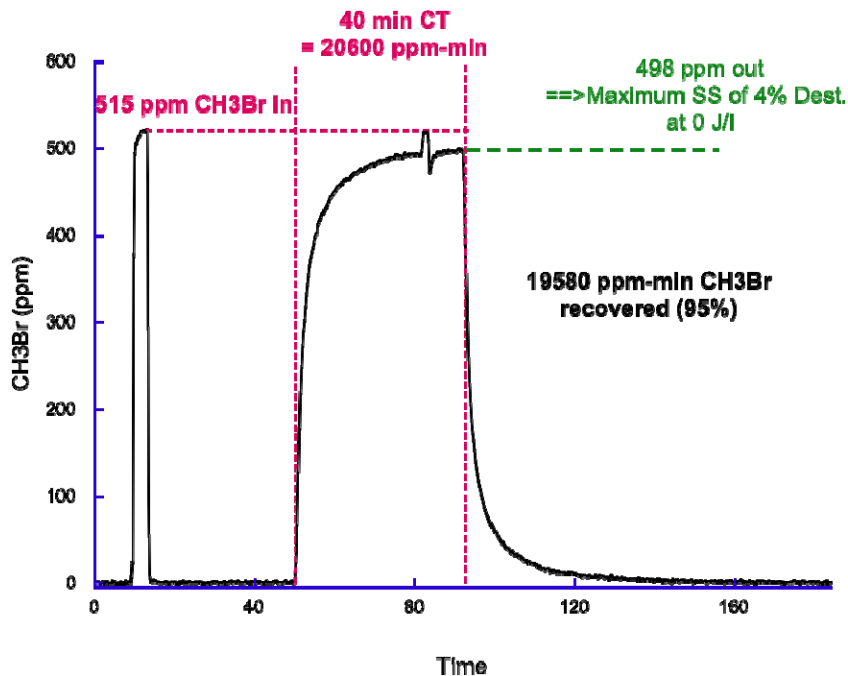
Figure 2. Adsorption of CH₃Br onto Ag-ZSM5 with no plasma present.

The interesting behavior of ZSM5 is illustrated in Figure 2. In this experiment the small (1/2" dia.) NTP reactor was filled with 2.3 ml or 1.8 g of fresh material covered by a 1" high ground electrode. Three consecutive CH₃Br exposures tests were run at 2 slm total flow (GHSV ~ 53000/Hr) without changing the catalyst or the gas flow conditions. In the first exposure, shown in Figure 2, plasma was left off and the catalyst exposed to CH₃Br for 40 minutes. When CH₃Br is introduced the concentration begins to rise almost immediately. This indicates that the substrate does not have a rapid adsorption rate, the kinetics are slow. However, it takes a long time for the outlet concentration to reach steady-state, thus there is significant capacity. By comparison, CH₃Br reached inlet levels within a minute or so for many non-adsorbing catalysts. Towards the end the of the exposure the bypass input concentration was checked to confirm that the flow was stable.

We observed a small, "steady state" reaction between CH₃Br and Ag-ZSM5 accounting for ~ 4% of the input. The only product observed was a small methanol signal. This indicates that even w/o plasma there was some reaction albeit small. After the CH₃Br was turned off the outlet concentration dropped rapidly but had a rather long tail. This again indicates a significant capacity, but slow kinetics.

The impacts of plasma power on the steady-state destruction of CH₃Br are illustrated by two successive tests with increasing plasma power. After the first test the plasma was turned on to 1W (30 J/l) and then a third exposure conducted at 6.7W (200 J/l). The next figure compares the results of all three CT exposures on the same time-scale. Included in the figure are the measured ppm-minutes of CO, CO₂ and CH₃OH detected in each case, as well as the overall CH₃Br destruction calculation.
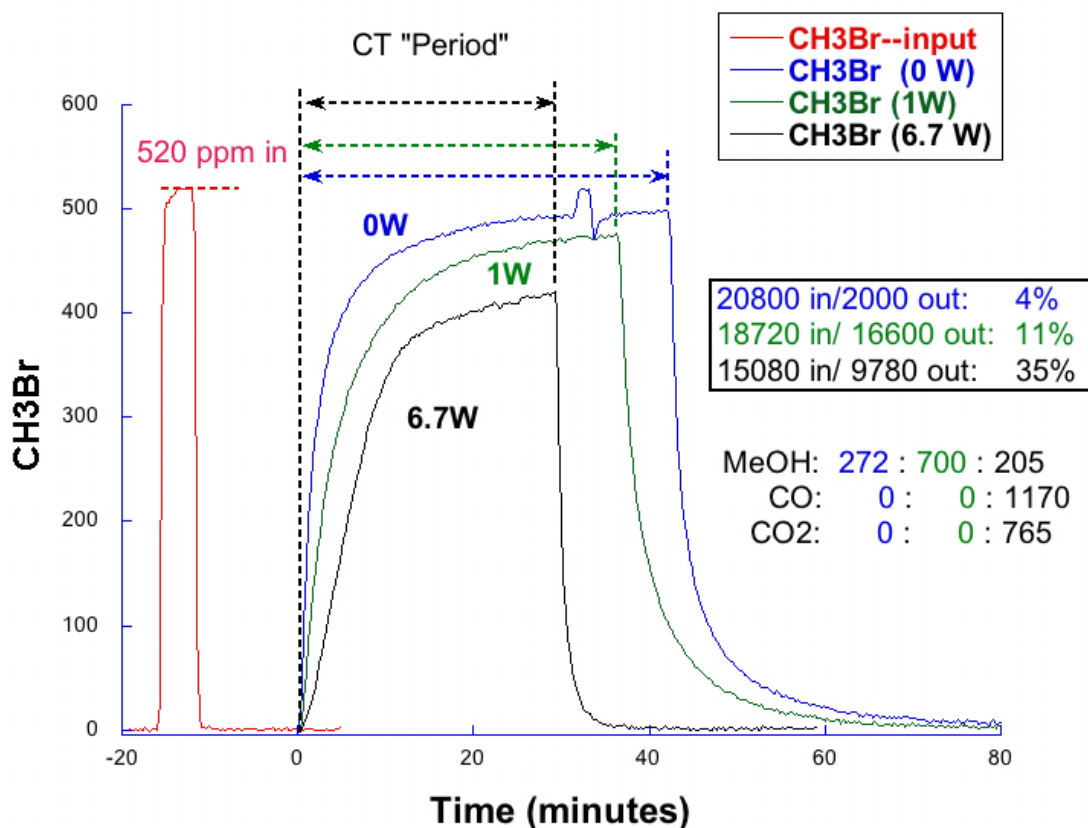
26

Figure 3. Three consecutive destructions of CH₃Br with increasing NTP power.

In the first experiment, (0 J/l), CH_3Br rose up to ~ 96% of input levels with a very small amount of CH_3OH formed. The net and quasi-steady state destruction was ~4%, meaning that 96% of the stored (un-reacted) CH3Br came back off. There was no CO or CO_2 formed. In the second case, (30 J/l), the final "steady state" result was ~91% of input levels with more CH_3OH formed but still no measurable CO or CO_2 produced. The total destruction was ~ 11% suggesting that perhaps a small amount of stored CH_3Br was eventually destroyed. Finally at 200 J/l a noticeable amount of CO and CO_2 (more CO than CO_2) were formed and the total destruction measured ~ 35%. The final near "steady-state" value of 20% destruction and the almost complete lack of CH_3Br out after turning off the input suggests that most of the stored CH_3Br was destroyed before making it out of the catalyst bed. Very little CH_3OH was seen, perhaps because at this power level any CH_3OH formed was itself destroyed. Although only ~ 40% of the missing CH_3Br reappeared as CO or CO_2, it was apparent that more CO/CO_2 would have been measured if the experiment had continued longer. As a side note, the percentage of CO dropped dramatically once the CH_3Br was turned off, indicating that strongly adsorbed CH_3Br fully oxidizes to CO_2.

As mentioned above, the reaction is known to be non-catalytic under these conditions. Subsequent analyses of the reactor packing showed AgBr and Ag_2BrNO_3 deposited on the packing. Therefore, the catalyst was only "fresh" for the first run. The second run was affected by consumption of the Ag in the 0 J/l test and the third run was affected by

27

the first two exposures. Evidently, the reaction is initiated and enhanced by the non-thermal plasma, but it is not catalytic.

For comparison purposes the amount of CH_3Br missing after 29 minutes (the length of the final exposure) was calculated. The amount increased from 19% to 27% to 39% of the input as the plasma power was increased. The plasma dramatically increased the amount of reactant on the catalyst, with more reacted at higher power.

A similar experiment on a larger bed (4.5 ml) of fresh AgZSM-5 is shown below. In this case the plasma was maintained at 300 J/l for both runs.
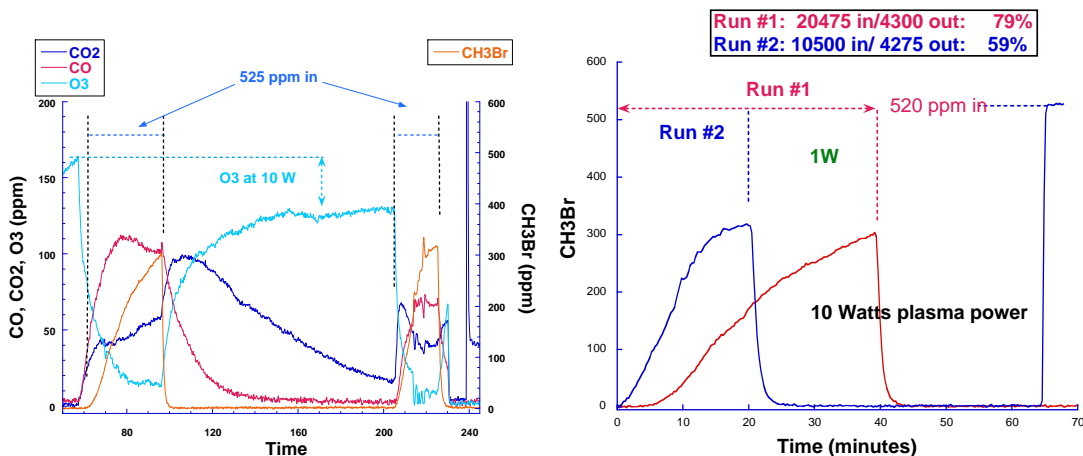

Figure 4. Consecutive Exposures of CH_3Br to same catalyst showing "poisoning".

The figure on the left includes the time data for O_3, CO_2 and CO as well, while the figure on the right shows the two CH_3Br breakthrough curves on the same time-scale. As you can see the CH_3Br adsorption and destruction performance dropped significantly between runs. No CH_3OH was observed in either case, but in both a majority of CO is produced during the exposure and a majority of CO_2 is produced after the exposure. Integrating the CO_2+CH_3Br concentrations vs. time for the first exposure test 78% of the carbon can be accounted. It is unclear how long the CO_2 "tail" would have continued but clearly carbon was still held up in the reactor when the first test was concluded and the second exposure begun.

The improved CH_3Br destruction may have been due to two factors: 1) an increase in catalyst bed size (2.1 to 4.5 ml), and 2) increased in plasma power (200 to 300 J/l). Although we were unable to do a comprehensive study of the various contributions to the observed reaction of CH_3Br the following sections expound the two main factors.

Effect of bed volume:

We show in Figure 5 two examples of varying the catalyst volume at a constant plasma power. In both cases the larger the catalyst bed the higher the efficiency. At high power and with a large enough bed we can eliminate virtually all the CH3Br. It is important to note that changing the volume of the catalyst changes both the residence time and the plasma discharge volume. This changes the local intensity of the discharge, thereby changing the ion/radical product distribution in a complex manner. Nevertheless, the results conform to our expectation that the extent of reaction increases at constant power with more "catalyst" present.
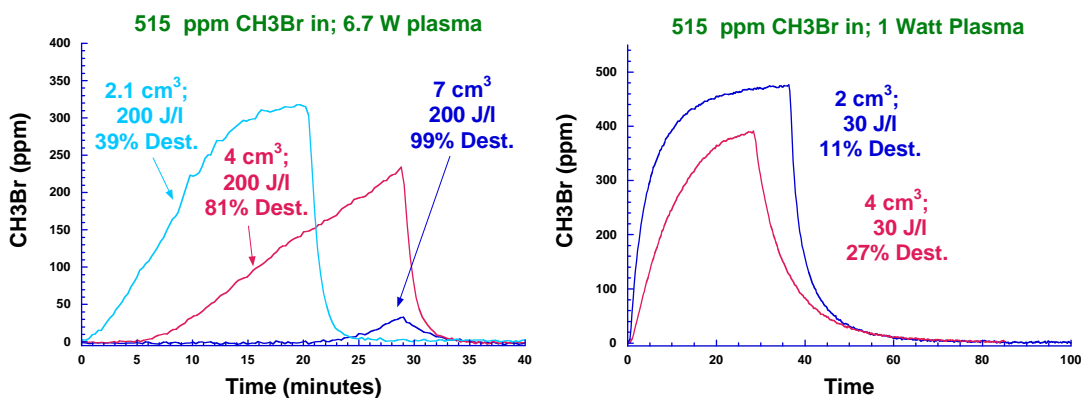
28

Figure 5. Effect of NTP bed volume on plasma destruction with same input power.

Effect of plasma power:

Several tests were conducted comparing the same catalyst volume at different plasma power levels. Shown below are the results for three separate tests using 4 cm^3 of catalyst and turning on the power at progressively higher levels (fresh catalyst was used for each test).
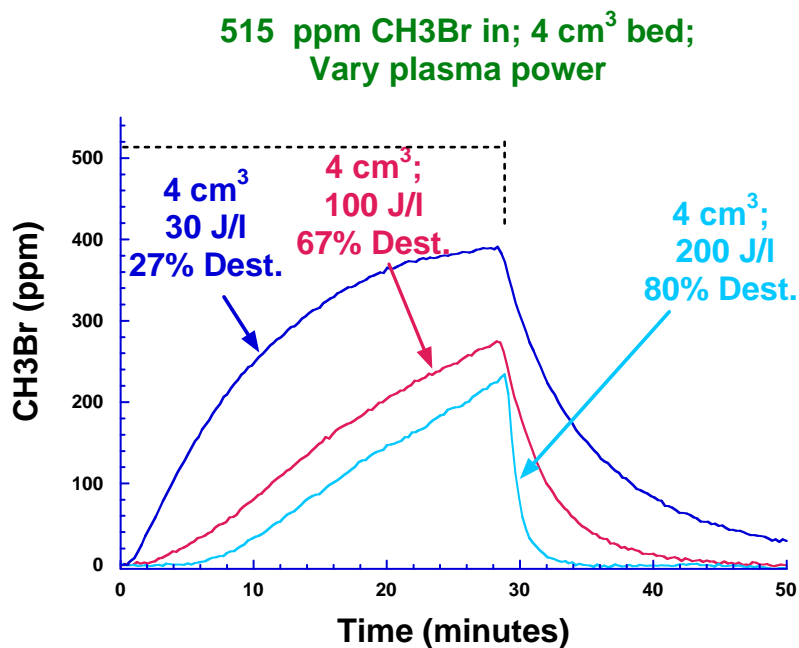

Figure 6. NTP destruction vs. power.

As typically witnessed in NTP reactions, more plasma power leads to a greater rate of CH$_3$Br destruction. The relationship between input power and destruction often follows first order kinetics. This is so common the NTP plasma literature has adopted a common means of comparing NTP reactivity by the specific energy, β. The specific energy of a chemical is the amount of energy required to achieve a 1/*e* reduction of the inlet concentration. Specific energies depend on the chemical being treated and on the NTP

system. Low specific energies show that less energy is required to achieve a target level of destruction. NTP systems that demonstrate lower specific energies on the same compound are more efficient. Compounds that have lower specific energies in the same system are easier to destroy. For CH_3Br with an Ag-ZSM-5 packing the specific energy is ~100 J/L. Comparably, the specific energy for CH_3Br with glass beads was ~425 J/L.

Effect of relative humidity—80%RH is the more stringent test for Hybrid Plasma)

The water content of the gas, or relative humidity, can be expected to affect the system performance in several ways. In the first place, ZSM-5 catalysts have a strong affinity for water, and one might expect there to be fewer available adsorption sites when the system is "saturated" at a higher relative humidity. If water is more strongly bound than the challenge molecule it could easily displace it and prevent, or at least reduce the reaction efficiency. A second issue arises simply because the overall plasma discharge physics change as the water content changes. Generally speaking at high humidity there are many more micro-discharges per cycle, but the average intensity of each one is smaller. This almost certainly means the number of high energy electrons produced is reduced, which generally reduces the formation of reactive species in the plasma (e.g. O•). For example, O_3 production is strongly affected, usually in the negative direction, as the relative humidity increases. Finally, the formation of HNO_3 is a concern, but at high humidity it seems to be efficiently "scrubbed" from the gas via adsorption onto any moist surface, but it is more readily produced. This can make quantification difficult, but beyond that the presence of nitrate in the catalyst may well contribute to the overall reaction scheme.

A systematic study of the effect of relative humidity on the CH_3Br destruction efficiency was not within the scope of this project. Nevertheless, the system was tested a high and low relative humidity to verify the expected behavior that high humidity would have poor performance and to estimate how much difference there might be. Figure 7, below, shows the time-behavior of the NTP reactor with 4 cm^3 of catalyst at 200 J/l at low and high relative humidity. The second one shows the CH_3Br breakthrough curves on a similar time-scale.
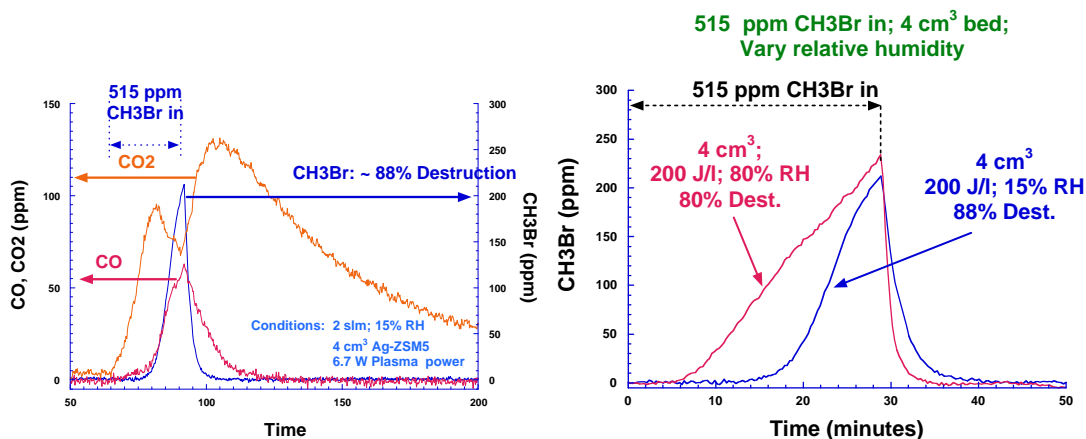

Figure 7. Impact of %RH on NTP reactor destruction of CH_3Br

30

At lower RH the initial breakthrough took significantly longer to occur, indicating that CH_3Br and H_2O do, indeed, compete for the same adsorption sites. It is interesting to note that at lower relative humidity CO_2 was the main reaction product during the exposure rather than a majority of CO. This, again, could be caused by stronger adsorption keeping the carbon in the plasma longer, or alternatively by a change in the electron energy distribution leading to more efficient oxidation. The important thing to note is that while there is some decay in system efficiency at higher relative humidity the overall effect is moderate at most. Testing at 80% RH was the more stringent test condition, as we suspected from the start.

Performance degradation:

It has already been shown how the performance degrades as the NTP "catalyst" is exposed to CH_3Br with 300 J/l of plasma power. The example below illustrates what happens at a more modest 100 J/l. In this experiment three consecutive exposures were conducted on the same catalyst at 100 J/l before increasing the power and running one test with 200 J/l NTP power.
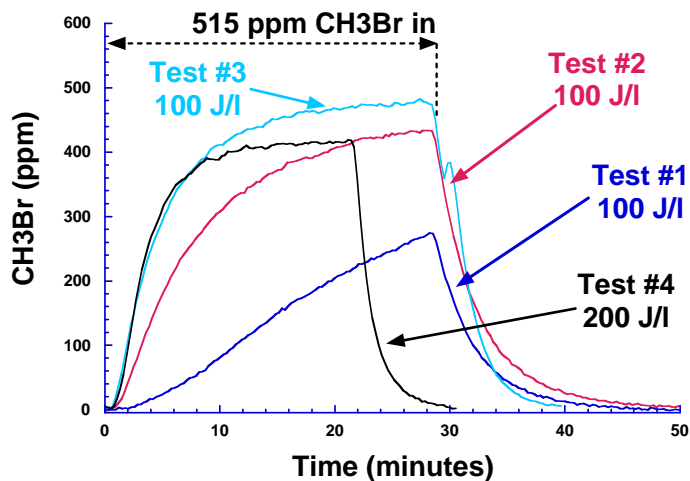

Figure 8. Performance degradation with multiple exposures to CH_3Br—"poisoning".

As you can see the performance degrades with each test. After the third test the "catalyst" appears fully degraded. The CH_3Br output quickly rises after it is introduced and levels off, appearing to reach a steady-state destruction. This likely is due to the loss of all reactive sites.

The degradation of the reaction rate along with characterizations of used packing (see section 5) confirm that the destruction of CH_3Br is by a plasma-induced reaction with Ag-ZSM5, leading to AgBr products. Clearly a fresh catalyst surface at high power will hold up a considerable amount of CH_3Br long enough for reaction to occur. The overall destruction is quite impressive but limited by stoichiometry. The reaction is not catalytic, Ag is consumed by reaction with CH_3Br and destruction efficiency drops. However, some destruction occurs at treatment power (~25% at 200J/l in our case) even after the reactive Ag is fully consumed.

Ag-ZSM5 packing is the preferred packing material for the NTP reactor due to its favorable performance on the target compound, CH_3Br. Other NTP packing materials

(catalysts) were also tested: glass beads, 1% Pt on silicalite, 10% amorphous MnOx on Alumina (Sasol) beads, 10% Pr doped-CeOx on alumina beads. Test results for those packing materials are in Appendix B.

3.2.2 Destruction of CH_3Br in O_3 Reactor/Filter

For tests of the ozone reactor capabilities CH_3Br inlet was moved from upstream of the plasma to downstream of the plasma. The plasma reactor was filled with glass beads in order to produce a stable concentration of ozone. Generally speaking a glass bead filled non-thermal reactor reaches a higher O_3 output concentration than the other (adsorbing) packings tested.

The CH_3Br was added directly to the plasma reactor exhaust, where it mixed with the main gas before passing through any of several ozone reactors in a multi-reactor manifold. Externally controlled solenoid valves were used to direct the gas either through the desired catalyst bed or around it, and then to the FTIR for analysis. Ozone and CH_3Br did not noticeably interact outside of the catalyst beds. Only the two most promising materials, namely Fe-exchanged ZSM-5 with 6% Ag impregnated and Mn-exchanged ZSM-5 with 12% Ag impregnated, were performance tested. Results of the preliminary down selection testing are captured as summarized conclusions in Section 3.1 Tables 1-4.

Fe-ZSM-5 with 6% Ag Results:

Figure 9 below illustrates how the ozone reactor operates. The time has been adjusted such that the exposure begins at t = 0. For this experiment the plasma reactor supplied approximately 600 ppm O_3. The flow was 2 slm, the relative humidity was 15% and the reactor had 10 cm^3 of fresh catalyst (GHSV ~ 12000/Hr). The catalyst was exposed to ozone for a short time (17 min) prior to CH_3Br addition. Ozone was completely consumed during the pre-conditioning period, but started to break through the catalyst bed a short while after CH_3Br addition. Prior to that CO_2 appeared, and grew to a nearly steady value that was far short of carbon balance.
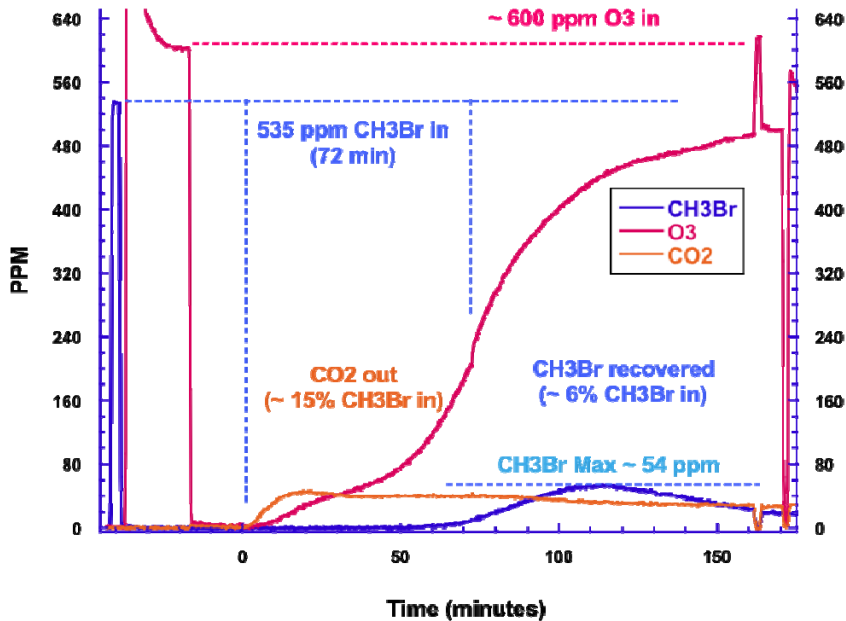
Figure 9. Reaction of CH₃Br in O₃ Reactor/Filter w/Fe-exchanged ZSM5+6% Ag @ 15% RH

In this case no appreciable amount of either CO or methanol was detected. Note that CO_2 continued to appear in the exhaust stream long after the CH_3Br was shut off. Clearly, the carbon balance would have improved with time. The most interesting observation is that CH_3Br concentration reached a maximum of approximately 10% of the input value 30-40 minutes after the exposure was over. This is a useful feature—simply by adsorbing and slowly desorbing the compound one can reduce the maximum concentration significantly.

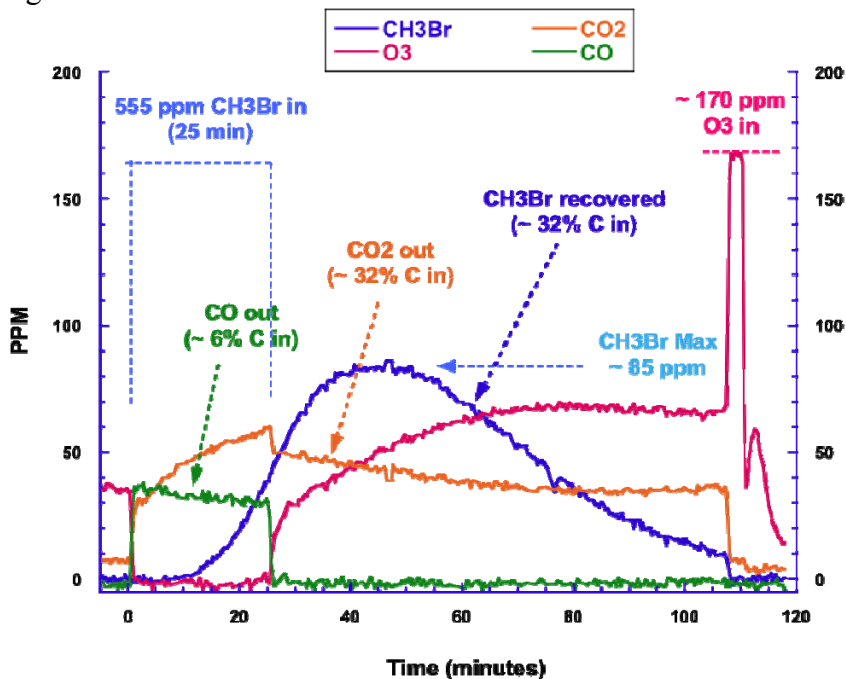Figure 10 shows the results for the same test at 80% RH.

Figure 10. Reaction of CH₃Br in O₃ Reactor/Filter w/Fe-exchanged ZSM5+6% Ag @ 80% RH

33

Performance (CH_3Br destruction) was qualitatively similar but quantitatively not as appealing. The peak CH_3Br concentration was higher indicating less destruction occurred and the peak occurred earlier than @ 15% RH, indicating that adsorption capacity was diminished. Under these conditions we did observe CO formation, but only during the exposure. Possibly CO was formed in the previous (15% RH) case as well but was further oxidized by the excess O_3. Again, the CH_3Br "peak" concentration occurred after the exposure ended, and the CO_2 formation was still quite high at the end of the experiment. Two factors can contribute to the poorer O_3 reactor performance at 80% RH: 1) the higher water content reduces adsorption of CH_3Br in the reactor, and/or 2) the lower O_3 concentration reduces the reaction rate of CH_3Br.

The above test was run with a high O_3 concentration generated with high power in the NTP reactor. Several tests were conducted at lower power to determine the effect of lower O_3. For these tests we reduced the quantity of catalyst to 5 cm^3, doubling the GHSV to 24000/Hr. The CH_3Br results are shown in upper left quadrant of Figure 11 below. The CO_2, CH_3OH and O_3 results are shown in the next three quadrants.
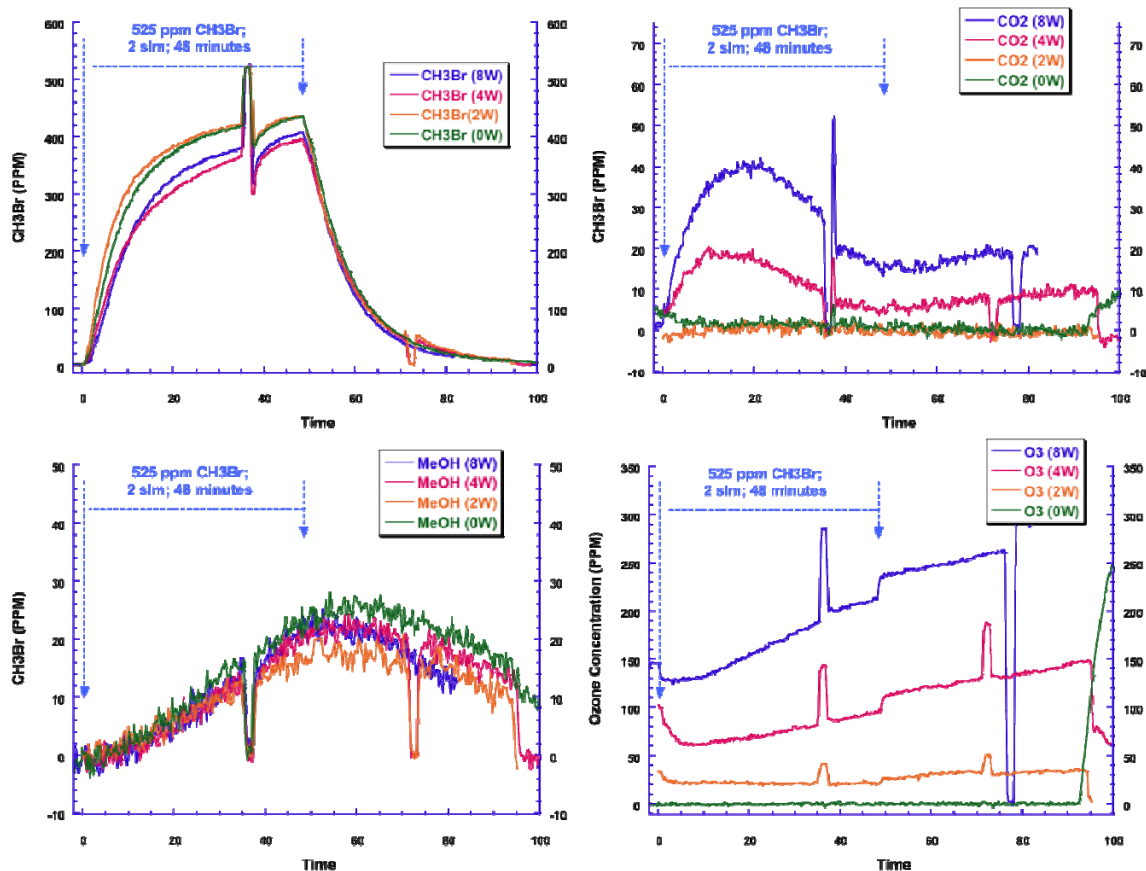

Figure 11. Impacts of ozone concentration in O_3 reactor filter w/ Fe-ZSM5+6%Ag @ 80%RH

In the figures, the "spikes" are caused by switching the flow to the bypass position to check the inlet concentrations. Clearly greater plasma power increases the CO_2 formation and aids the overall CH_3Br destruction process. Presumably this is due to changes in the ozone concentration. In every case there was a small, stepwise increase in

ozone concentration when the exposure was ended which is consistent with the direct reaction of ozone with CH_3Br. Also, in every case the methanol formation appears to be independent of plasma power, and is at its maximum 10 minutes or more after the end of the exposure. The methanol formation likely results from hydrolysis of CH_3Br, which would also produce a Br. Initially, it was expected the Br would exit as HBr. However, HBr was never detected in the off-gas. Post reaction analysis of the packing material showed formation of AgBr. Acid gas was not formed from the CH_3Br test contaminant.

Mn-ZSM-5 with 12% Ag Results:

Similar tests were conducted with the Mn-ZSM-5+12% Ag catalyst. A typical experimental result is shown in Figure 12 below.
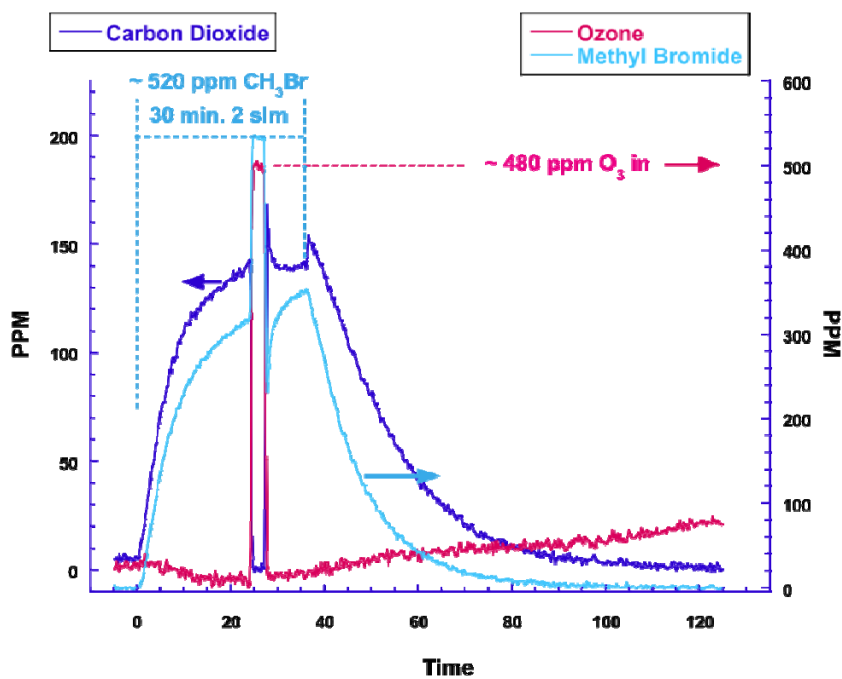

Figure 12. Reaction of CH_3Br in O_3 Reactor/Filter w/Mn-exchanged ZSM5+12% Ag @ 80% RH

For this test we packed the reactor with 5 cm^3 of catalyst, set the relative humidity to 80% and used a flow of 2 standard liters per minute (GHSV ~ 24000/Hr). The CH_3Br was added after the plasma reactor. In comparison to the Fe-ZSM-5, a much larger CO_2 signal was observed. In this case the CO_2 concentration mirrored the CH_3Br concentration, which peaked at the end of the exposure. No CO was observed, and only a trace of methanol escaped the catalyst. The catalyst very efficiently destroyed ozone, but appeared to lose that ability over time. The Mn exchanged catalyst appears to be a superior oxidation catalyst compared to the Fe-ZSM-5, but the overall CH_3Br destruction is comparable.

Figure 13 shows the effect of increasing the catalyst volume from 5 to 15 cm^3 (GHSV decreased from 24000 to 8000 Hr^{-1}). The same gas velocity was used so the larger bed volume increases the reaction time of the gases and increases the number of reaction sites.
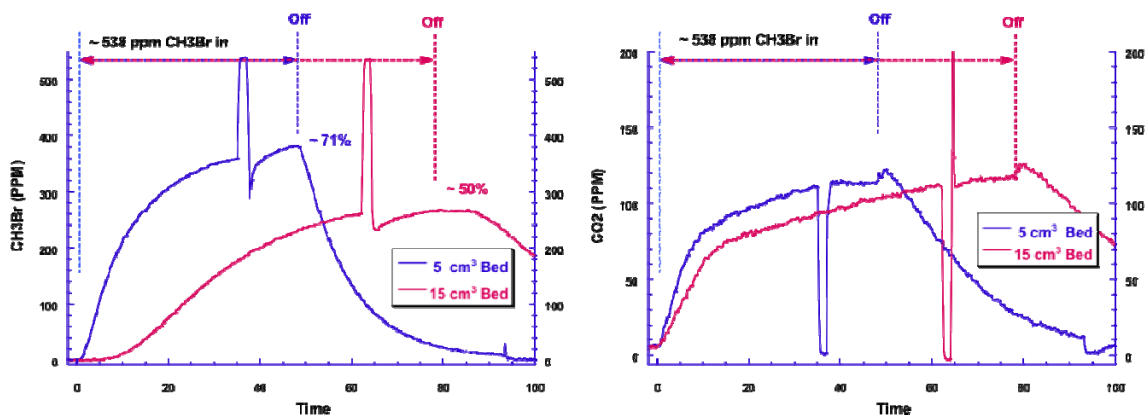
Figure 13. Reaction of CH₃Br in Mn-ZSM5+12%Ag @ 80

During both tests the CH_3Br input was continued until the output CH_3Br appeared to "level off" indicating that the adsorption part of CH_3Br removal was satisfied. The $5cm^3$ reactor continued for about 50 minutes. The 15 cm^3 reactor continued longer, but not 3X longer. It seemed to level off after 90 minutes of exposure. Towards the end of each exposure the instantaneous carbon balance was pretty good—approaching 95% for the smaller bed and 77% for the larger one. No CO was observed in either case.

The "quasi-steady state" concentration was significantly lower with the larger bed indicating a greater level of CH_3Br destruction. The total net CH_3Br destruction for the 5 cm^3 bed was ~ 30%. For the 15 cm^3 case we could not measure the net CH_3Br destruction but it was certainly higher with more catalyst. At the end of the test time the adsorbed, but un-reacted, CH_3Br was not fully desorbed so the overall carbon balance couldn't be closed.

The O_3 reactors were all preconditioned by running air through them at the designated relative humidity prior to any experiments. Both ZSM-5 catalysts hold a large amount of water under high humidity conditions. Since the adsorption of CH_3Br is so crucial to its removal from the gas stream, preconditioning the bed is necessary so that the overall destruction efficiency isn't confused by adsorption that wouldn't occur during an attack situation. We should also note that at low humidity the ozone production for at given plasma power is generally much higher, so a straightforward comparison is complicated.

Impact of humidity:

Figure 14 shows results of testing with $5cm^3$ of the Mn-ZSM5+12% Ag tested at 15% relative humidity. This is directly comparable to the 5 cm^3 test @ 80% RH shown in Figure 13.
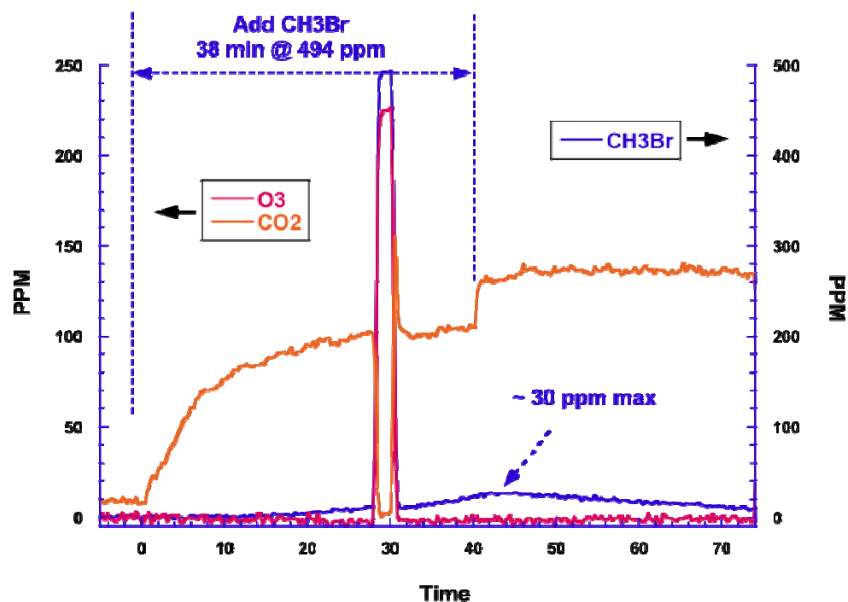
Figure 14. Reaction of CH₃Br in Mn-ZSM5+12%Ag @ 15%RH

As was the case for the Fe exchanged material, the CH₃Br activity was much greater in at lower humidity. We attribute this to a much larger number of adsorption sites available due to decreased competition from H_2O. The overall destruction efficiency was excellent, and the maximum observed CH₃Br output was only ~30 ppm, just after the end of the exposure. Considerable CO_2 was formed, but evidently was generated from material stored (for quite some time) in the catalyst. For this test at least there was no degradation in the ozone reactivity. The plasma power was relatively low, at 2.1 W or only ~ 60 J/l but the ozone production was reasonably good. No methanol was observed, and only a trace of CO (not shown) was found.

Mn-Fe Catalyst Comparison:

The Fe and Mn exchanged catalysts were very similar in CH₃Br "activity", but the Mn exchanged material produced much more CO_2 and also did a better job of destroying ozone. It seems likely that both acted as reactants with CH₃Br rather than as catalysts, although the subsequent oxidation to CO_2 may well be catalytic in nature. Figure 15 compares the results for two directly comparable experiments.
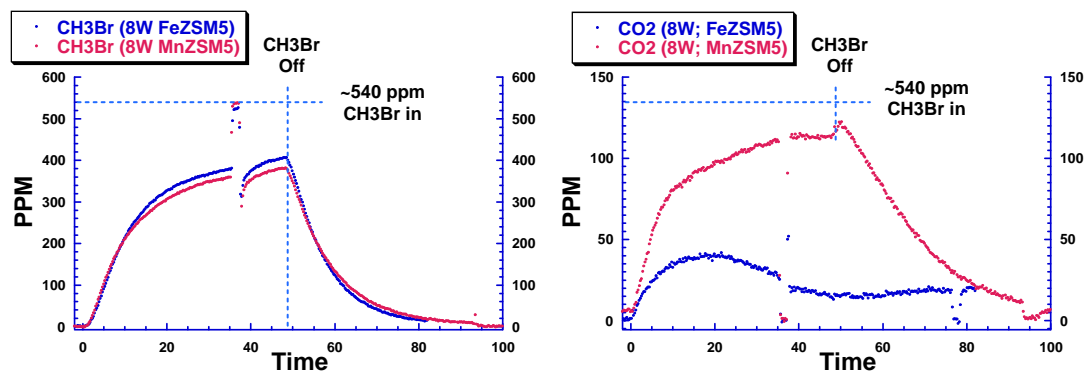
Figure 15. Reaction of CH₃Br in Fe and Mn exchanged ZSM5 reactors. CH₃Br(left), CO₂(right)

As you can see, the CH_3Br out concentrations are very close while the CO_2 formation rate is significantly higher in the MnZSM-5 case. Both catalysts are of interest for further study, since they are successful at destroying CH_3Br.

3.2.3 CT Tests

Four separate tests of the NTP-Ozone Reactor combined system were conducted to determine efficiency using our best catalysts. To test the system we added a 2000 mg/m³(515 ppm) of CH_3Br for a given period of time (fixed concentration * time, or CT) to achieve an over-all capacity test of 55,000 mg-min/m³, while monitoring the output of the entire system[4]. We chose two ozone catalysts, namely the Mn exchanged ZSM5 with 12% Ag impregnated (Mn-ZSM5-Ag) and the Fe exchanged ZSM5 with 6% Ag impregnated (Fe-ZSM5-Ag) as the ozone catalysts. We tried three separate packing materials for the NTP reactor, including glass beads, Pr-CeO₂, and Ag-ZSM5. In the first instance we don't expect much if any reaction in the NTP but hope for a relatively high ozone concentration coming out. In the case of Pr-CeO₂ and Ag-ZSM5 we sacrifice much O_3 production in the hopes of destroying more CH_3Br in the NTP reactor itself.

The first test utilized a 15 cm³ NTP reactor filled with Pr-CeOx beads followed by an ozone reactor containing 25 cm³ Mn-ZSM5-Ag + 50 cm³ Fe-ZSM5-Ag. We added 528 ppm CH_3Br to the flow for 27.3 minutes while simultaneously raising the plasma power from 1 to 10 W (30 to 300 J/l). At the end of the exposure the plasma power was turned back down to 1 W. In retrospect that may have significantly changed the result, since at that level almost no ozone was made. The relevant results are shown in Figure 16 below.

---

[4] The concentration and over-all capacity correspond to established performance tests for CH_3Br in TTA # 08-JECP-07-003 (rev. 6).
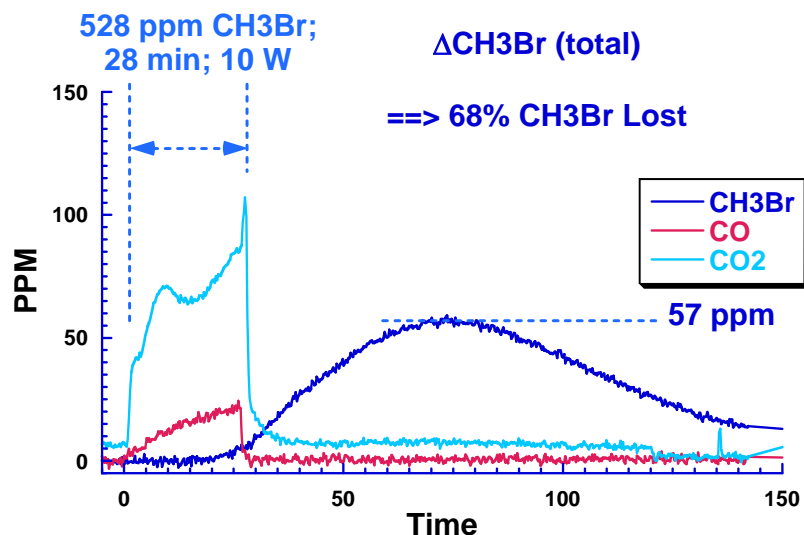
Figure 16. CT test with Pr-CeOx catalyst in NTP reactor + Mn and Fe ZSM5 in O_3 reactor

The results were encouraging during the exposure, but as monitoring continued after the exposure a peak of CH_3Br emerged indicating that ~ 30% of the CH_3Br simply adsorbed and then desorbed later. The net destruction was 68%; the adsorption/desorption process did succeed in reducing the maximum concentration out by a factor of 10 or so. A measurable amount of CO_2 (and CO) was formed while the plasma was on, but both dropped precipitously once the plasma was turned down. Late in the experiment (not shown) we turned the plasma back up to 180 J/l and observed an instantaneous production of CO_2, so some oxidizable carbon was left on at least one of the catalyst beds.

The next test used glass beads in the NTP reactor followed by 40 cm^3 of Fe-ZSM5-Ag and 20 cm^3 of Mn-ZSM5-Ag. The flow and relative humidity remained at 2 slpm and 80%, respectively.
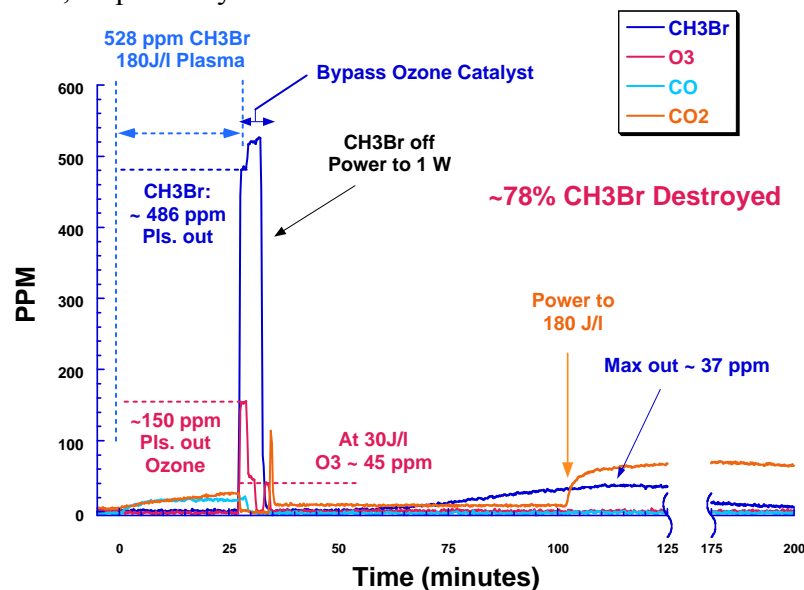

Figure 17. CT test with glass beads in NTP reactor + Mn and Fe ZSM5 in O_3 reactor.

In this experiment we ran a similar 27 minute exposure at 528 ppm of CH_3Br but before turning down the plasma power and turning off the CH_3Br we checked the NTP out concentrations. At 180 J/l the glass bead filled NTP only destroyed ~ 8% of the CH_3Br, but did produce ~ 150 ppm of ozone for use downstream. The ozone concentration dropped to no more than 45 ppm at 30 J/l, which is where we set the power prior to sending the gas back through the ozone catalyst.

Figure 17 clearly shows the result was better but CH_3Br had the same long slow release well after the CT test was over. The overall efficiency was 78% and the maximum CH_3Br out was ~ 37 ppm, or 7% of the inlet value. Once again a late increase in plasma power did result in more CO_2 detected but did not effect the evolution of CH_3Br off the catalyst. Since this destruction surely took place almost entirely on the ozone catalyst it would have been wiser to keep the plasma power up "post-exposure".

Both experiments demonstrated insufficient CH_3Br destruction in the NTP reactor.

For the next experiment we decided to set up an "overkill" reactor in order to demonstrate that the O_3 reactor filter could completely prevent CH_3Br from escaping the system. The ozone reactor contained 50 cm^3 of the Fe-ZSM5-w/6%Ag catalyst on top (upstream) of 25 cm^3 of Mn-ZSM5-w/12%Ag. Additionally, a new type of NTP packing was tested. Due to the outstanding performance of the ZSM5 in the O_3 reactor it was tested in the NTP reactor. The Fe and Mn catalysts were not included because we wanted O_3 to be generated in the NTP reactor and not destroyed. The Ag catalyst was included due to its performance for CH_3Br destruction in the O_3 reactor. The NTP reactor was filled with ~ 4.5 cm^3 of Ag-ZSM5 catalyst. The CT test flow was dropped from 2 to 1 slpm and the following result obtained.
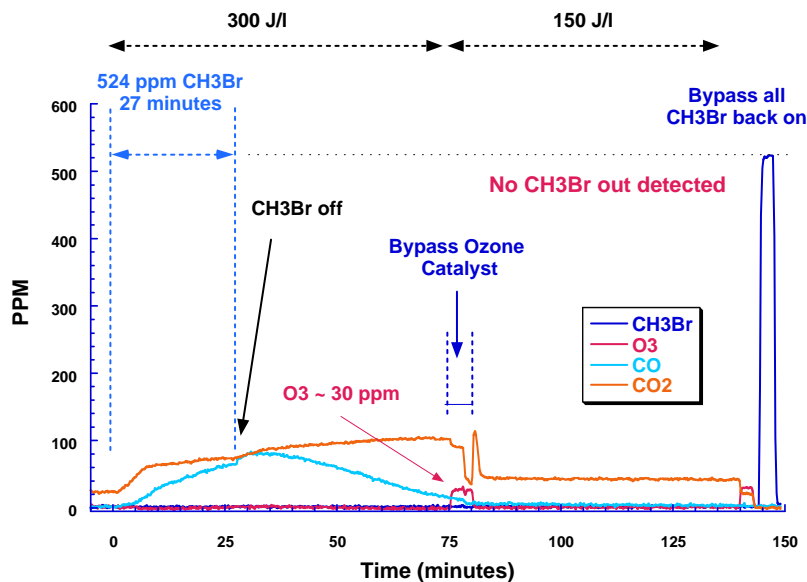

Figure 18. "Overkill" CT Test with Ag-ZSM5 in NTP reactor and Mn+Fe catalysts in O_3 reactor

For this test we didn't reduce the plasma power until well after the CT exposure was finished, and as a result observed CO and CO_2 continuously generated. Monitoring of the

outlet continued for 2 hours after the end of the exposure without detecting ANY CH_3Br.

It is clear that with enough catalyst relative to the overall flow rate it is possible to completely eliminate CH_3Br from the gas stream. We suspect from our NTP tests that most of the work was done on the AgZSM5, although we did not monitor the plasma output.

From an engineering perspective we still need to optimize the system. In particular it would be useful to reduce the size of the catalyst beds until CH_3Br barely breaks through. This would obviously be important in any scale up of the system, where size, weight, cost and so forth become important.

In our final CT test we kept the NTP reactor the same, employing 4.4 cm^3 of fresh catalyst, but reduced the energy density from 300 to 200 J/l. We dropped the total ozone catalyst volume from 75 to 33 cm^3 while doubling the flow rate from 1 to 2 slm. In a sense, we increased the difficulty of the challenge by a factor of 4.6 while decreasing the power density by 33%. The ozone catalyst had the same 2:1 ratio of Fe-ZSM5-Ag:Mn-ZSM5-Ag. The Fe catalyst was placed upstream because the Mn catalyst completely destroys O_3 and O_3 is necessary to drive the CH_3Br destruction.

The result is shown in the next 2 figures. The system was "pre-oxidized" during the two hour period shown prior to the exposure. Somewhere in the system a fair amount of CO_2 was formed during this time. Once most of the CO_2 was cleaned off we began the test. Under these conditions we destroyed 94% of the input CH_3Br, and the maximum out concentration occurred approximately 40 minutes after the end of the test at ~ 15 ppm. At 200 J/l the NTP reactor was supplying roughly 100 ppm ozone to the ozone reactors.
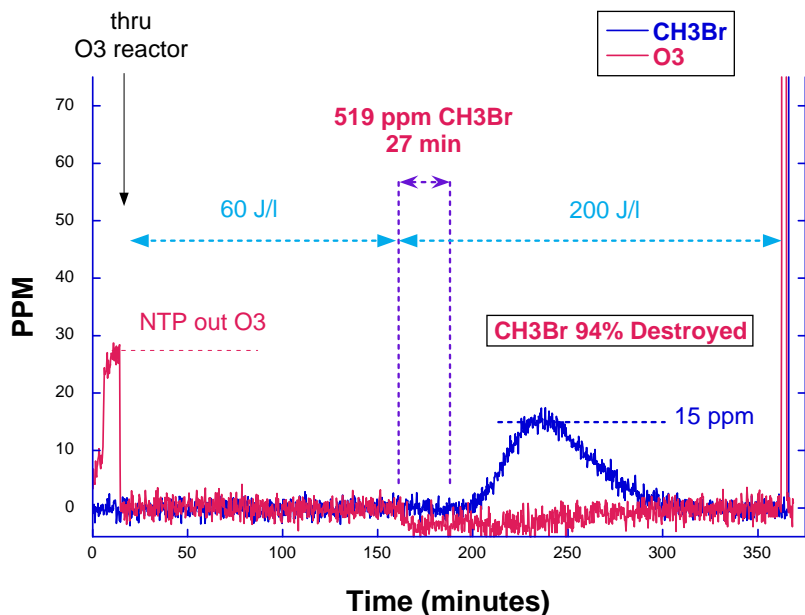

Figure 19. CT test with Ag-ZSM5 in NTP reactor and 33cm^3 O_3 reactor.

Figure 20 below simply shows the CO and CO_2 out on the identical timescale. In this test the amounts produced were comparable during the exposure, but CO_2 dominated in the post-exposure stage.
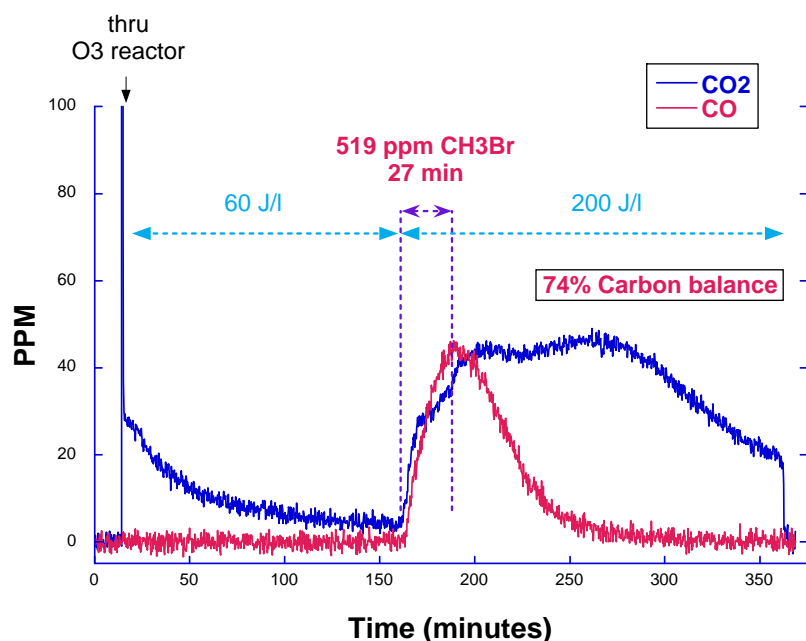
41

Figure 20. CO and CO$_2$ generation during and after CH$_3$Br CT test.

These results demonstrate that the Hybrid Plasma Reactor/Filter system will be able to meet the performance standards and provide volumes of material that can be scaled for an engineering assessment.

System optimization to establish an optimum NTP power input, NTP reactor volume, and O$_3$ reactor volume can be accomplished with appropriate model development and validation testing. Nevertheless, these empirical data provide a sound basis for an engineering assessment of the Hybrid Plasma Reactor/Filter against performance objectives for size, weight, and power.

3.2.4 Post-Reaction Packing Characterization

 The Ag-ZSM5 packing performed best among all of the substrate:metal combinations tested during down selection. Catalyzing the packing with Fe or Mn to decompose O$_3$ was necessary in the reactor after the NTP reactor, but was not necessary in the NTP reactor, where ample reactive species are created by the plasma. In both systems, it was observed that the performance of the reactor deteriorated with continued exposure to CH$_3$Br. Therefore, it was concluded that the catalysts were quickly poisoned OR the chemistry was not catalytic, but was reactive and some vital reactant on the packing was being consumed. It was initially suspected that the Ag may be reacting to form AgBr in the same manner that Ag reacts with Cl in photofilms.

Samples of packing from the NTP reactor and from the O$_3$ reactor/filter were examined the SEM-EDS, XRD, and XPS.

Figure 21 is a dot map SEM-EDS image showing an abundance of Br on the surface of a reacted particle and shows that the Br is co-located with Ag (or with Al).

42
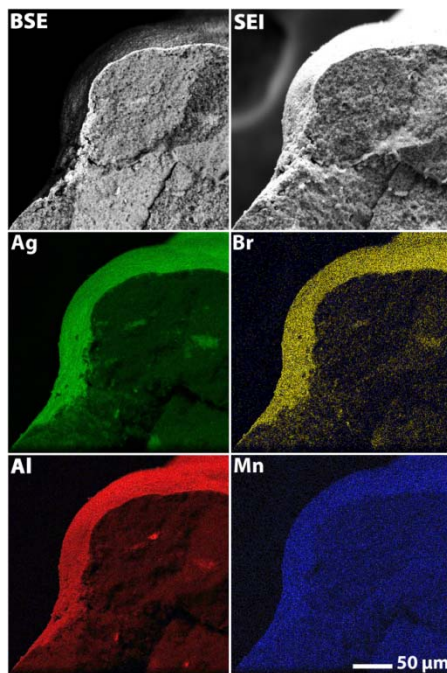
Figure 21. SED-EDS dot map showing elemental co-location of Br with Ag (or Al).

The EDS identifies specific atoms, but does not identify compounds. Figure 22 shows and XRD plot of the particle that identifies crystal phases, but doesn't specifically identify the location of those phases.
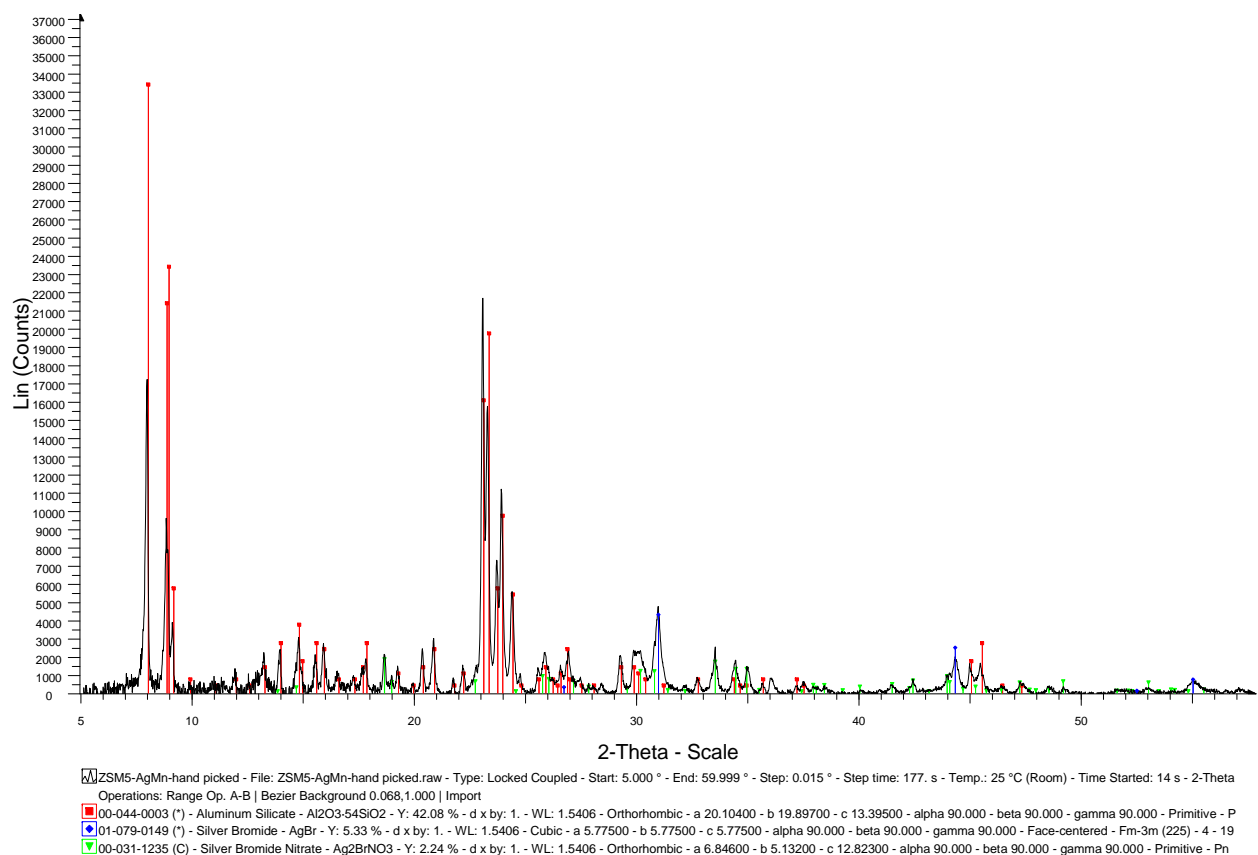
Figure 22. XRD spectrum of reacted Mn-ZSM5 w/12%Ag from O₃ reactor.

The red lines correspond to alumino-silicate, which is the basic ZSM5 substrate. The blue lines correspond to AgBr, confirming the assumed Ag halide chemistry. The green lines correspond to an unexpected reaction product, Ag_2BrNO_3. The final product provides an explanation why NO or NO_2 were not detected as reaction products when the system was exposed to CH_3Br.

The post-reaction characterization confirms that the reaction of CH_3Br with the Hybrid Plasma Reactor/Filter packing materials is a stoichiometric reaction which consumes the Ag. It is not catalytic.

Appendix C contains the complete SEM-EDS and XRD characterization data.

3.2.5 Destruction of acrylonitrile (CH₂CHCN) in Hybrid Plasma system

3.2.5.1 Destruction in an NTP Reactor

Acrylonitrile, CH2=CH-CN was chosen as a surrogate for cyanide containing compounds (e.g. HCN, ClCN, or C_2N_2) and as an organic compound that isn't expected to poison the Ag based "catalysts" in the NTP and O_3 reactors. Because acrylonitrile (or ACr) is a relatively low boiling liquid it could only be obtained as a relatively low concentration (1011 ppm) gas mixture in nitrogen. This limited the maximum concentration at a given relative humidity because we used a bubbler with zero air to add water. For a flow of 80% humidity at most 20% of the gas comes from the ACr source, which limited ACr concentration to approximately 200ppm in the mixture.

The chemical formula for acrylonitrile is C_3H_3N, suggesting the following possible "balanced" partial oxidation reaction:

$$C_3H_3N + 3/2\ O_2 \quad ===> \quad CO + HCN + HCOOH$$

Of course CO, HCOOH and presumably HCN can all oxidize further to CO_2, but as we show below, all three products and CO_2 are detected under various conditions.

The initial test indicated that ACr is strongly adsorbed on Ag-exchanged ZSM5, and that upon reaction most of the adsorbed material can be recovered as CO_2. To facilitate testing and reduce long lead times needed to establish steady-state conditions due to strong adsorption it was decided to operate with a relatively small amount of packing/catalyst. Fresh catalyst (2.1mL) was placed into a small diameter (1/2"OD) quartz reactor with a 1" outer ground electrode and a 1/16" inner high-voltage electrode. For a flow rate of 2 slpm the gas hourly space velocity (GHSV) for this reactor was ~57,000/Hr.

Destruction of ACr in a NTP plasma was studied using both steady-state destruction and dynamic injection, CT test, as shown in Figure 23.
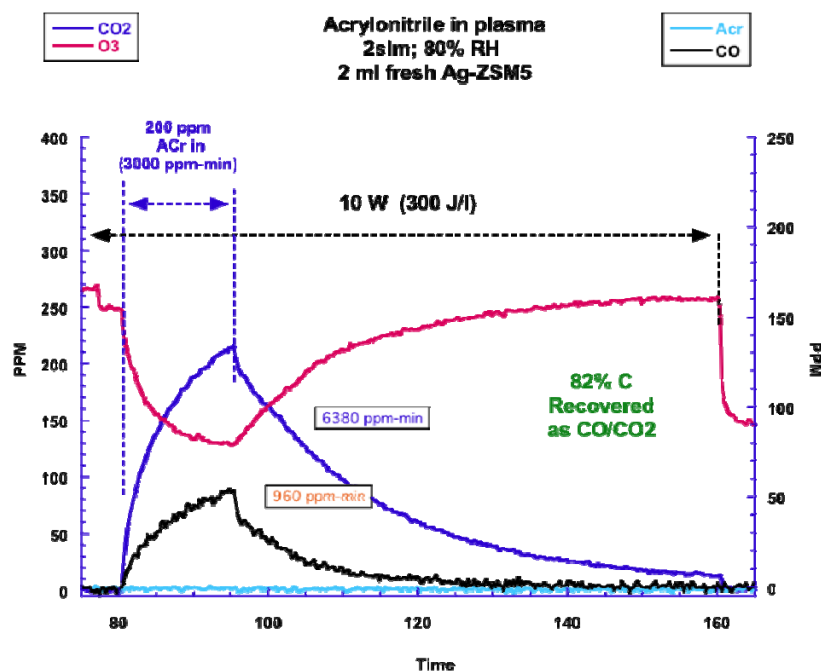

Figure 23. Acrylonitrile CT destruction in NTP reactor with Ag-ZSM5 packing.

45

In the CT experiment shown in Figure 23 no ACr was recovered at all, indicating that 300 J/l on a fresh catalyst completely destroys ACr. The CO/CO_2 concentrations rose quickly and eventually accounted for ~ 82% of the missing ACr. No hydrogen cyanide (HCN) or formic acid (HCOOH) was found; presumably they were completely oxidized in the plasma. The shape of the CO and CO_2 curves are reminiscent of a typical adsorption curve, with neither one reaching steady state during the exposure. This suggests that adsorption of ACr gradually increases the rate of reaction.

In the "steady state" test at lower powers we identified both HCN and HCOOH products. These are indicated in Figure 24, using externally obtained reference spectra.
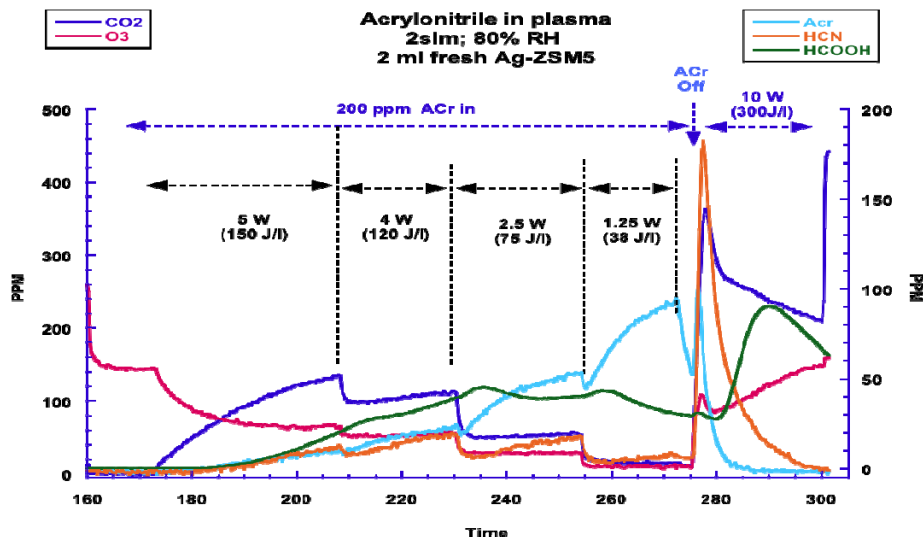
Figure 24. Power vs. Destruction of Acrylonitrile in NTP reactor w/Ag-ZSM5 packing.

As is evident in Figure 24, the test did not attain true "steady state" conditions for any specific condition. Nevertheless, the power vs. destruction data fits a nice exponential decay with a 1/e power (specific energy, β) of ~ 50 J/l as shown in Figure 25. Interestingly, at the end of the experiment when ACr was turned off and the plasma power turned up to burn off excess carbon we observed a huge surge in the HCN concentration. Evidently, material adsorbed on the catalyst still contains the C-N bond. Further tests are required before we can determine the fate of the nitrogen in ACr.
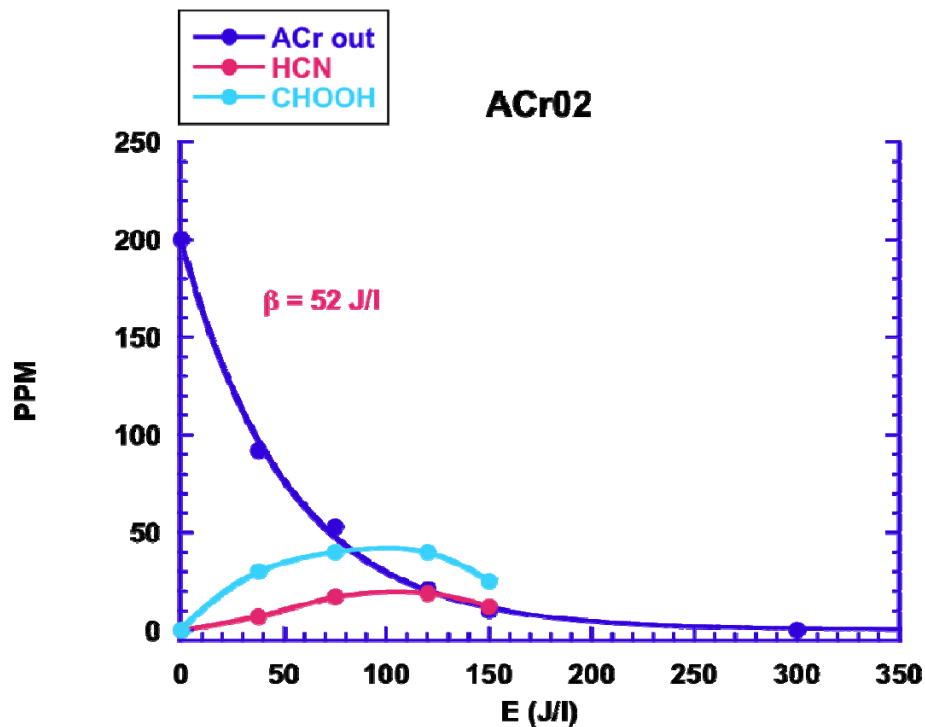
Figure 25. Destruction of acrylonitrile vs. power in NTP reactor w/ Ag-ZSM5 packing

At low powers both HCN and HCOOH increase with power and then disappear at higher powers.

To determine the impact of the Ag catalyst another reactor was filled with 2.3 ml of the original H-ZSM5 (from Joe Rossin) in the NTP reactor and measured the ACr destruction versus power. Without Ag the results were significantly different. Figure 26 shows the fate of all the detected carbon.
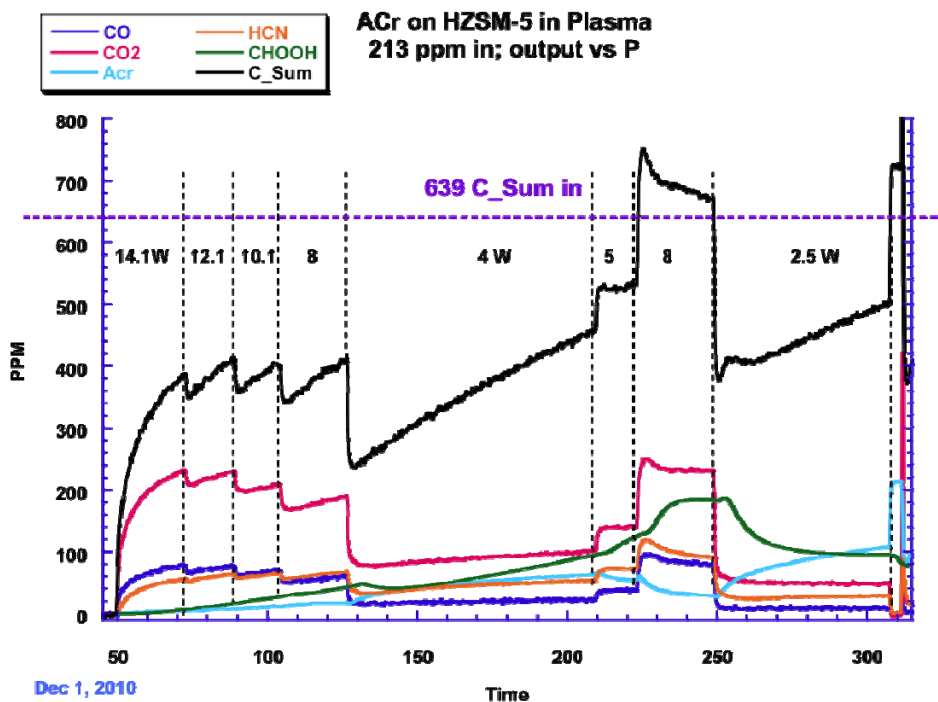
Figure 26. Acrylonitrile destruction in NTP reactor with ZSM5 substrate no catalyst (Ag).

47

We clearly observe more CO, HCN and CHOOH than with Ag-ZSM5. Evidently, the presence of silver facilitates full mineralization to CO_2. Without silver the oxidation reactions in the plasma bed went way down. The H-ZSM5 still has good adsorptive capacity, but considerably less reactive capacity.

When plotted versus power all these trends become more obvious. The measured β value increased from 52 to 103 J/l, or in other words the energy required to destroy ACr went up a factor of 2. Furthermore, the formation of HCN and CO increased as well. Evidently, the exchanged Ag is intimately involved in the total oxidation process in plasma.
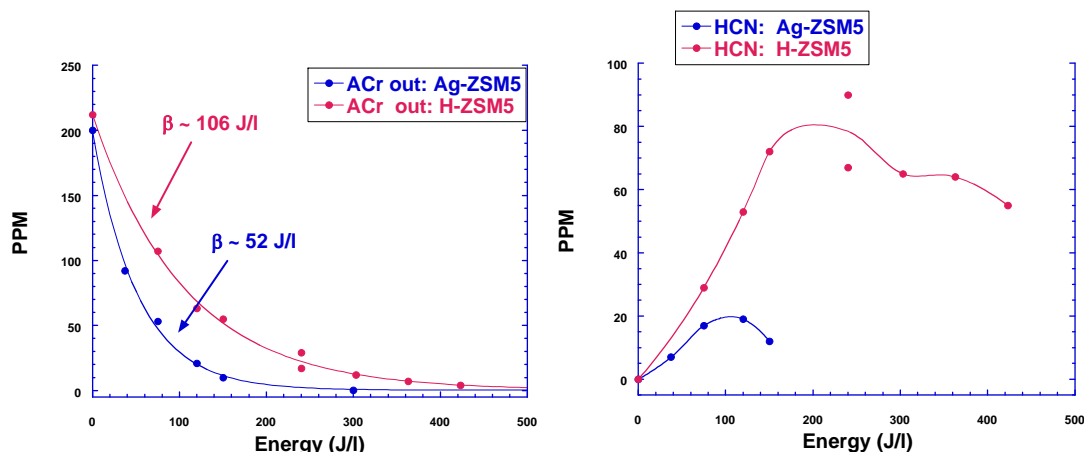
Figure 27. Acrylonitrile destruction in NTP reactor (left) HCN generation in NTP reactor (right)

The measurement of ACr destruction on H-ZSM5 was hampered by a slow drift in the concentration of CO and CO_2 over time. Some discolored catalyst beads were observed at the upstream end of the bed, indicating that there was some catalyst coking going on. This explains the slowly increasing CO and CO_2 values observed. We also observed that that formic acid sticks quite strongly to either the tubing walls or the H-ZSM5 catalyst. A long, slow release of formic acid was observed overnight without any plasma power. The released carbon brought the carbon balance into good agreement.

A second test on the same bed of H-ZSM5 catalyst resulted in consistent data, indicating that not much degradation of the catalyst (outside of some coking) occurred. The combined results of all the packing materials are shown in the power vs. destruction curves in Figure 28.
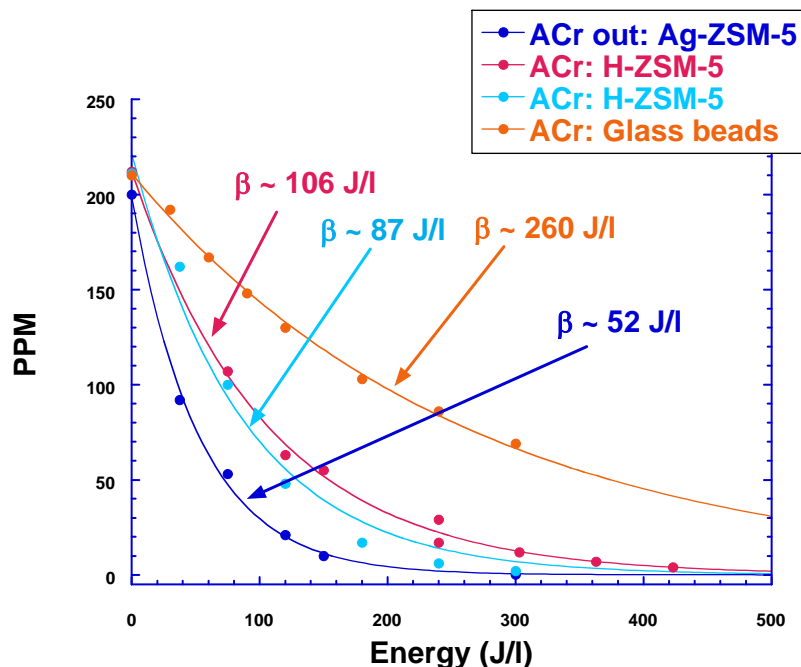
Figure 28. Destruction of Acrylonitrile in NTP Reactor—Effects of packing.

Clearly, there is a big difference in the effectiveness of the ACr destruction depending on the plasma reactor packing. The data includes a test with 3 mm glass beads for comparison. The H-ZSM5 packing is an improvement on glass beads, probably because of the long ACr residence time in the plasma region. However, the Ag-ZSM5 catalyst is the best performer by a significant margin.

3.2.5.2 Destruction in an Ozone Reactor

Figure 29 illustrates ACr destruction in the O_3 reactor section of the Hybrid Plasma Reactor/Filter.
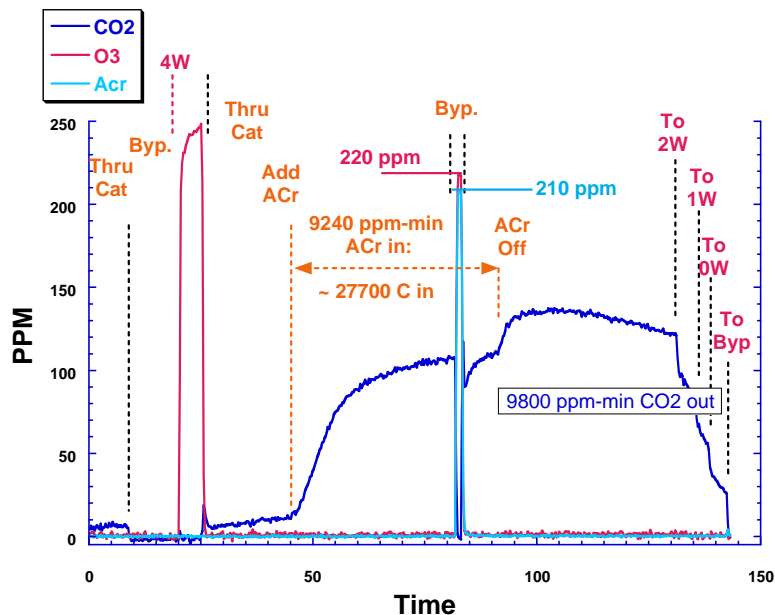
Figure 29. Reaction of acrylonitrile in O_3 Reactor/filter with Mn-ZSM5+12%Ag

49

The catalyst tested was 5 ml of fresh Mn- exchanged ZSM5 with 12% Ag impregnated after exchange. For these tests a glass bead filled NTP reactor was used to generate O_3 and ACr was added downstream of the plasma reactor. At 2 slm, a 5 cc catalyst bed corresponds to a GHSV of 24000/Hr.

Figure 29 clearly indicates that CO_2 was created in the reactor, but the concentration is not enough to explain the complete loss of acrylonitrile. Evidently, the catalyst adsorbs ACr quite well, and at least some of it (between ⅓ and ½) can react quickly with ozone to make CO_2. No CO, HCN, HCOOH or ACr left the ozone reactor.

To more completely close the carbon balance low levels of ozone were run through the reactor for 15 hours. The ozone was made using ambient air so there was a significant CO_2 background, which made quantification impossible. Nevertheless, Figure 30 shows the output CO_2 decreased steadily over the course of the experiment indicating CO_2 continued to be generated from organic material remaining on the packing after the day's testing. Even low concentrations of O_3 generated by low plasma power continued to drive the oxidation. The amount of CO_2 generated over the 15 hours still leaves about 1/3 the carbon unaccounted. It could be the unaccounted C could be still associated as –CN on the packing. This would need to be investigated further.
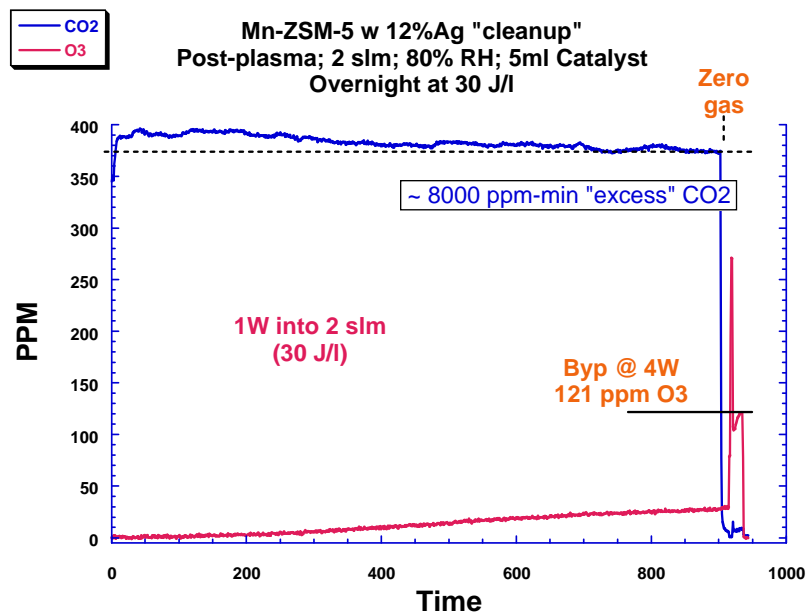
Figure 30. O_3 Reactor/filter output for extended exposure (16 hr).

Figure 30 also shows that O_3 gradually broke through the Mn-ZSM5 catalyst. Either the ozone reaction on Mn is not purely catalytic or the catalyst is slowly poisoned in some fashion. This, also, must be investigated further.

Recognizing the unanswered questions the main point is that the ozone reactor with Mn-ZSM5+12%Ag completely eliminated acrylonitrile from the inlet air stream. The reaction of ozone with the bed led to CO_2 formation and no other reaction products could be detected.

3.2.6 Poisoning of catalyzed ZSM5 with Tri-ethyl Phosphate

Catalyst poisoning by phosphorus was studied by exposing a fresh Hybrid plasma system (the system contained both an NTP reactor and O_3 reactor/filter in series) to triethylphosphate (TEP), and then looking at the remaining activity for ACr and CH_3Br destruction. Triethylphosphate is a clear, high boiling liquid (b.p. = 215°C) used as a surrogate for phosphorus containing agents. We added TEP to the gas flow using a bubbler, and calculated the subsequent concentration using the vapor pressure curve obtained from:

$$P(mm\ Hg) = 10^{\left(7.4321 - \frac{1482.76}{(T+248.44)}\right)}\ [5]$$

where T is the temperature in °C.

The liquid temperature was measured by a thermocouple immersed in the TEP, and we assumed 100% equilibration in the bubbles. In order to reach the desired concentration the bubbler was heated in a warm water bath (~48°C) and the lines between the bubbler and the main flow were heat traced and insulated to maintain a higher (~70°C) temperature. Once diluted into the main flow the TEP was assumed to remain in the gas phase for any concentration less than 240 ppm. Unfortunately, TEP is either quite sticky or quite reactive, and was very slow to equilibrate with the tubing and/or FTIR cell walls. It was difficult to quantify the initial concentrations very well.

The TEP exposure was conducted twice. The first test only exposed the NTP reactor with glass beads. The second test exposed a combined Hybrid Plasma Reactor/Filter with Ag-ZSM5 packing in the NTP reactor and Mn-ZSM5+12% Ag catalyst in the O_3 reactor/filter.

In both exposures no TEP exited the NTP reactor regardless of the plasma power. Very little CO_2 was generated so TEP was not fully oxidized in the plasma but it was completely immobilized. For the second test (hybrid plasma system) the exposure was continued at a calculated concentration of 145 ppm for 3 hours. The total flow rate was 2 slpm and the relative humidity was 80%, the plasma reactor contained 4.3 grams of catalyst, and the power was turned up to 200 J/l. The calculated exposure CT was a molar phosphorous equivalent to a 150,000 mg-min/m^3 exposure of Sarin. Only a trace of CO_2 was observed, so it is not included in Figure 31, below. The spikes in the ozone concentration indicate times when flow to the FTIR was switched from after the O_3 reactor to after the NTP reactor. At the end of the test flow was by-passed around the NTP reactor and TEP came up immediately, so we are confident that TEP was entering the NTP reactor during the test.

---

[5] From Yaws' Handbook of Antoine Coefficients for Vapor Pressure (2nd Electronic Ed.)
http://www.knovel.com/web/portal/browse/display?_EXT_KNOVEL_DISPLAY_bookid=1183
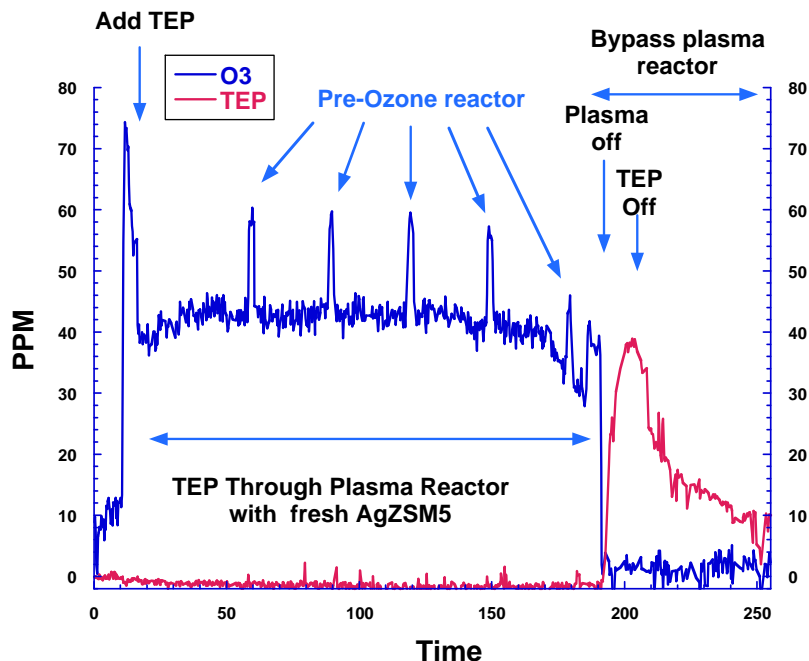
Figure 31. TEP removed in NTP reactor, but no CO_2 is formed.

Effects of TEP exposure on reactor performance—"poisoning":

Two tests were conducted on the NTP catalyst to determine the impact of the TEP exposure. The first was a test of the catalyst's ability to destroy acrylonitrile (ACR), shown in Figure 32.
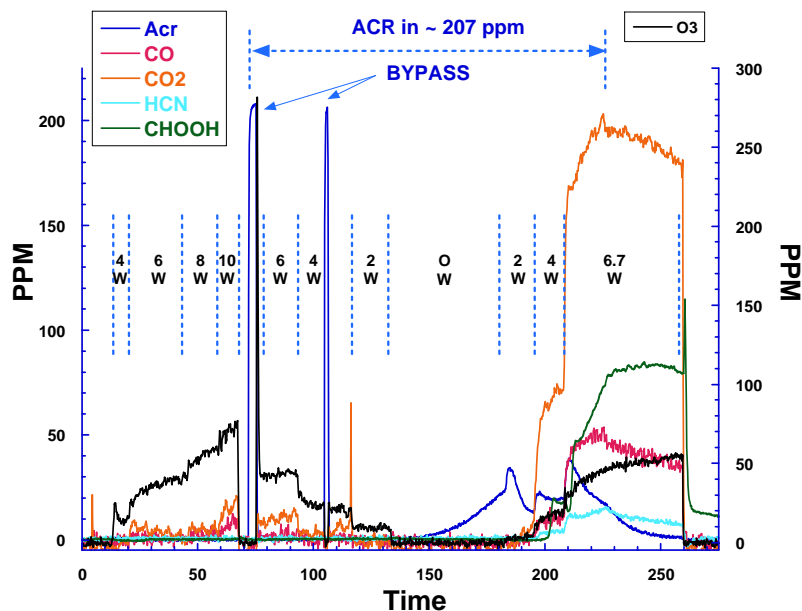
Figure 32. Reaction of acrylonitrile in NTP reactor after "poisoning" by TEP

The results indicated a major change in the catalyst's activity. The ACR was still completely removed by the NTP reactor, but without the expected CO_2 production. After running for quite some time the power was turned off with continuing to flow ACr until it "broke through" the catalyst bed. At this point, turning on the plasma produced a large CO_2 signal as well as smaller

concentrations of CO, formic acid and HCN. Each of these is a known product of ACr decomposition; they do NOT indicate any removal of TEP from the catalyst.

Evidently, the reaction with ACr resulted in lots of carbon left behind on the catalyst. We cleaned this off by running air through the catalyst overnight with the plasma power set at 120 J/l. Then the tests were conducted with CH_3Br and the destruction efficiency was measured on both the "poisoned" catalyst and a fresh batch.
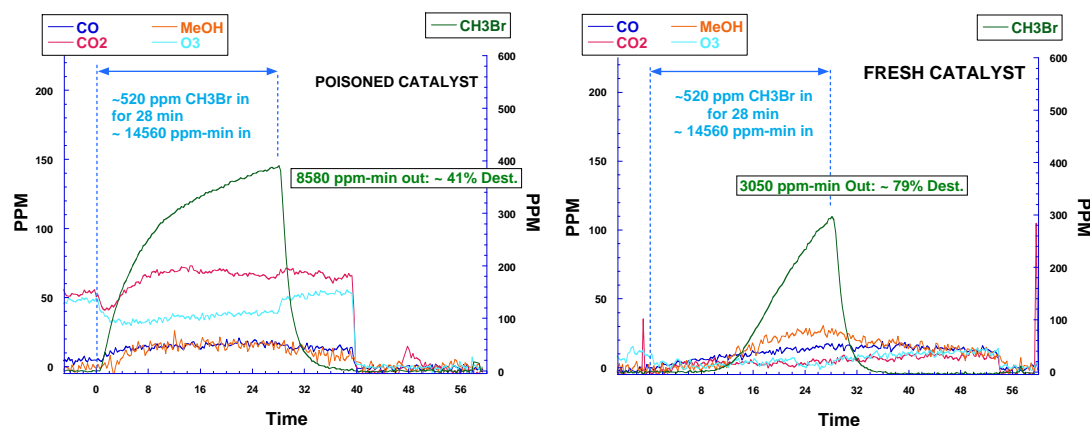
Figure 33. Reaction with CH₃Br in NTP reactor after poisoning w/TEP (left) and fresh (right).

As can be seen in Figure 33, there were major changes in the destruction of CH_3Br after exposure to TEP, indicating a large change in the catalyst's activity. Interestingly, the NTP reactor still maintained a respectable 43% destruction even after exposure to TEP. However, this is significantly less than 79% destruction measured on fresh catalyst. Other differences include changes in the CO_2, O_3, CO and even methanol output concentrations.

In principle the Mn-ZSM5+12% Ag ozone catalyst was also exposed to whatever TEP exited the NTP reactor, but nothing did so a post-poisoning test was not conducted on the ozone reactor.

3.2.7 HNO3 Generation in NTP

During NTP testing HNO_3 frequently, but intermittently appeared in the FTIR spectra. At times, such as when starting up the gas flow slugs of HNO_3 would appear in the spectra and then disappear with time or as humidity was added to the system to condition it for operation at 80% RH. It seemed as if drying the packings and associated system tubing would release accumulated HNO_3. With these clues that HNO_3 was being generated during some times of the NTP operation this task was undertaken to quantify the amount and the conditions that caused HNO_3 generation. Although it is important to understand how much HNO_3 may be generated during high power operation, when the system is under attack, it is most important to understand how much HNO_3 would be generated during the normal 24/7 operation while the system is in stand-by mode waiting for an attack.

While it is possible to quantify HNO_3 by FTIR it is difficult due to the "sticky" nature of the gas. Nitric acid sticks very easily to the walls of the cell, the mirrors and the windows and has a much longer residence time in the gas cell than the background gas. Additionally, even after "steady state" is achieved, small changes in relative humidity produce large "bursts" of measured HNO_3 unrelated to the plasma conditions at the moment. We therefore wanted to measure acid gas

formation using a different technique. Since HNO_3 is trivial to scrub we decided to bubble the NTP output gas through a water column with a minimal amount of piping to hold up the HNO_3 and then measure the nitrate using ion exchange chromatography. We extended this technique to include Br- formed in the plasma-induced reaction of CH_3Br on Ag exchanged ZSM5 pellets.

The experiment was set up as follows. We sent 2 SLM of humidified (80% RH) air through a small plasma reactor loaded with 2 grams of Ag exchanged ZSM5 and turned on the plasma at a given power. From the gas exiting the plasma reactor we diverted 500 sccm through a small bubbler containing a known mass (~ 14 gms) of water. We used a short piece of 1/8" Teflon tubing to reduce HNO_3 "sticking" on the tubing walls. The following table shows four test conditions. Three of the test conditions were conducted with only air flowing through the reactor. In the fourth test we added CH_3Br to the flow and searched for bromide anion as well. The outlet gas from the bubblers was also analyzed by the FTIR and no HNO3 was detected after passing through the bubbler, although O_3 quickly reached pre-bubbler levels.

The water samples from each test were analyzed by ion chromatography (IC) for nitrate ion and Br⁻ ion. A "blank" of the initial water was also analyzed; nitrate was very low, as expected.

Table 6. HNO_3 Quantification Conditions

Test #	Plasma power	Time (minutes)	Mass of water (g)	NO3⁻ detected (mg/l)	Br⁻ detected (mg/l)
1	1 W = 30 J/l	150	14.2	5.54	None
2	0.5 W = 15 J/l	225	14.05	4.45	None
3	6 W = 300 J/l	112	14.14	190	None
4	6W = 300 J/l	29	14.2	13.8	11.6
5	0—Blank			0.18	None

From the ion chromatography results we can calculate the concentration of HNO_3 in the gas leaving the plasma reactor. The small NO3⁻ detected in the blank was ignored.

Table 7. HNO_3 Quantification Gas Concentrations

Test #	Total gas flow (moles)	Total NO3⁻ detected (mg)	Total Br⁻ detected (mg)	[HNO3] in gas (ppm)	[Br⁻] in gas (ppm)
1	3.35	0.079	0	0.38	0
2	5.02	0.063	0	0.20	0
3	2.50	2.687	0	17.33	0
4	0.65	0.196	0.16	4.88	0.82

Under these conditions we detected very small amounts of nitrate at low plasma power, but at high power the amount was significant. The TWA value for HNO_3 in air is 3ppm. When the NTP reactor is operating at high power scrubbing of HNO_3 is necessary, but HNO_3 concentrations are within the allowable limits for breathing air when the NTP reactor is at "idling" conditions. Nevertheless, under 24/7 operating conditions the amount of HNO_3 generated may be sufficient that it will, overtime, consume the acid-gas scrubber capacity. It has always been assumed that the Hybrid Plasma system will be operated at with an "idle" power constantly, but that isn't really necessary. Because the NTP can be turned on essentially instantly, the standby condition of the system may at zero power with occasional power ups to verify availability of full protection and purge accumulated ambient VOCs from the system. Either operating mode could be used; an optimum can be determined with operational testing at a later stage of development.

Interestingly, the presence of CH_3Br actually reduced the NO_3 concentration noticeably. This is completely consistent with the identification of Ag_2BrNO_3 on the reactor packings after exposure to CH_3Br. HNO_3 co-reacted with CH_3Br and deposited NO_3^- onto the packing with most of the Br^-. A small amount (i.e. 0.82 ppm) of the 520 ppm of Br entering with the CH_3Br slipped through the system, but the vast majority (99.8+%) was captured in the system.

4   Engineering Assessment

Performance objectives have been established for chemical vapor purification units as a common basis of comparison for different technical approaches. Based on the experimental laboratory work described in earlier sections a conceptual design for a Hybrid Plasma Reactor/filter has been prepared. The basis of the design is a system that the system will remove (destroy) chemical threats from two attacks and maintain a safe breathable output concentration to the war fighter. This design is based upon CH_3Br as being the design limiting threat. The critical performance protection criteria are:

Capacity	Challenge Conc.	Max. Effluent Conc.
55,000 mg-min/m^3	2000 mg/m^3	4 mg/m^3
14,300 ppm-min	520 ppm	1 ppm

The Hybrid-plasma reactor/filter is illustrated in Figure 34
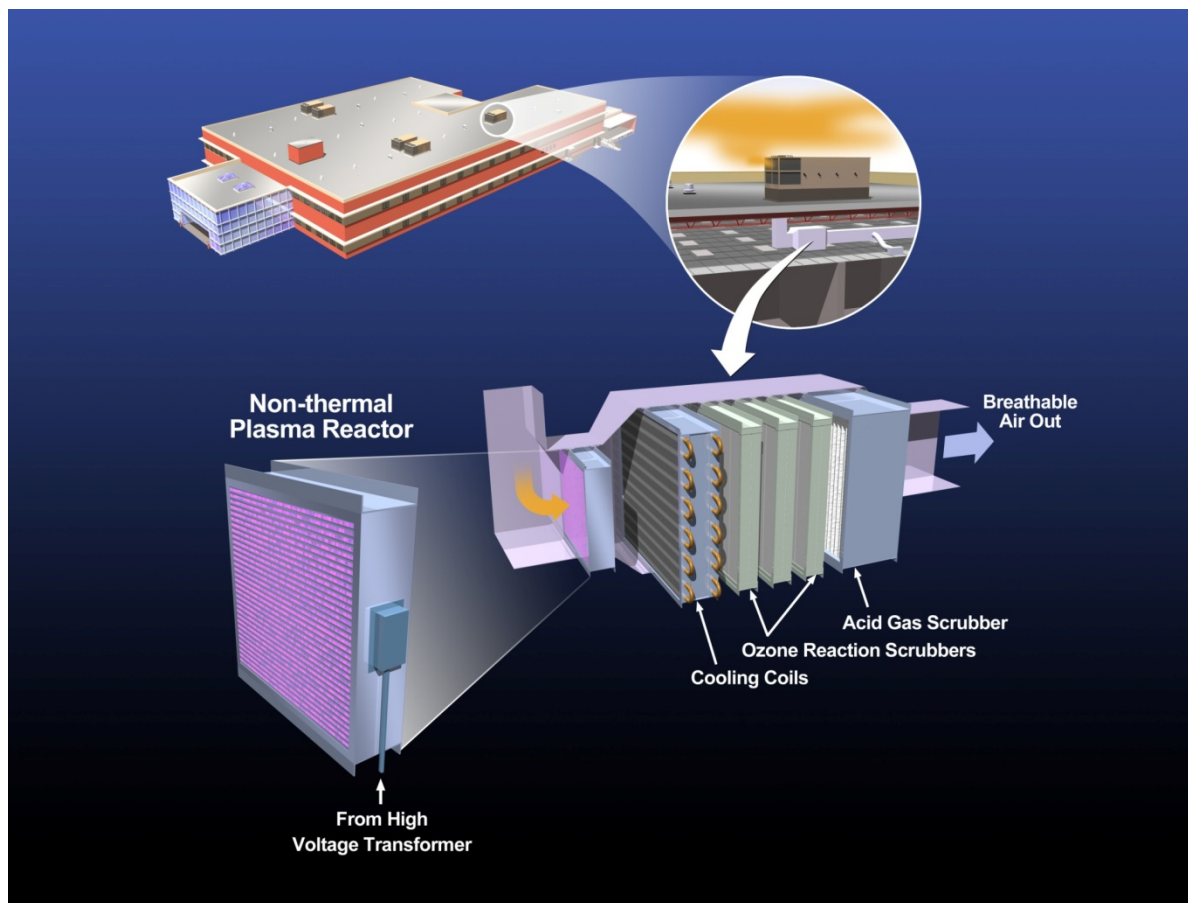
Figure 34. Hybrid-Plasma Reactor Filter Conceptual Installation in a Building Air Intake

The Hybrid-Plasma System is composed of three vapor control components: NTP reactor, O_3 reactor/filter and acid-gas filter. These are shown as modular components in Figure 34. In addition to the vapor control components the conceptual design includes heat exchanger cooling coils. The cooling coils are to remove heat input into the air from the NTP reactor. During an attack the NTP reactor will deliver 200 J/l of plasma power. This energy input will result in an increased temperature of the building air that must be removed. The cooling coils may be used or not during normal operation depending upon weather and "idle" power input to the NTP reactor.

Table 8 shows the performance thresholds for air purification units and the estimated specifications for a Hybrid Plasma Reactor/Filter.

Table 8. Hybrid Plasma Reactor/Filter Performance Specifications[1]

Attribute	Performance Threshold	Hybrid Plasma
Chemical Performance		
CH_3Br	55,000 mg-min/m^3	Conceptual design to 110,000 mg-min/m^3 (2 exposures)@ 2000 mg/m^3 conc.
Acid-gas (Cl_2)	100,000 mg-min/m^3	Conceptual design to 200,000 mg-min/m^3 (2 exposures)@ 2000 mg/m^3 conc.
Unit Weight	5 lbs/cfm	4.2 lbs/cfm [2]
		NTP reactor— 0.9 lbs/cfm

		Transformer—	1.1
		Pwr. Control—	TBD
		Ht. exch—	0.3
		O_3 reactor—	1.9
		Acid/gas—	<0.1
		Structure—	TBD
Unit Volume	0.3 ft^3/cfm	0.055 ft^3/cfm[3]	
		NTP reactor—	.007ft^3/cfm
		Transformer—	.01
		Pwr. Control—	TBD
		Ht. exch—	.006
		O_3 reactor—	.03
		Acid/gas—	<0.001
		Structure—	TBD
Unit Power	0.12 kW/cfm	Continuous Power—0.014kW/CFM	
		Peak Power—0.1 kW/CFM	
Consumables	5 yrs.	TBD	

[1]Performance specifications are estimates based upon laboratory studies scaled to 220CFM. Scaling is described in follow sub-sections

[2]Weight estimates are based upon the process functional elements (packing, electrodes, heat exchanger surfaces, and transformer). Weights of vessel shells, controls, and supporting structure have not been estimated.

[3] Volume estimates are based upon the active process volumes only. Equipment is expected to be close-packed as shown in Figure 33, but no open space has been estimated between elements. Volume of supporting structure is not included.

Table 9. Hybrid Plasma Reactor/Filter Conceptual Design Component Specifications

	NTP reactor:							Heat Ex.		O3 scrubber reactor			acid gas scrubber	
	power, J/L	destruction in NTP	Power for 220CFM		Reactor vol. ft3	dim.	~ wt. lbs	ft2	lbs.	packing wt. lbs.	bulk density lb/ft3	packing vol. ft3	Zr(OH)4 wt. lbs	Zr(OH)4 vol. ft3
Normal Operation	30		3.1	kW										
Attack Operation	200	95%	20.8	kW	1.5	1.9'x2'x6"	200	284	67	412	62	6.6	6.2	0.05

The 95% is considered conservative based upon NTP reactor test using a 7cc reactor of Ag-ZSM5+Ag at 200 J/L (see chart)
During this test 510 ppm was added for 28 min. Initially, 0 CH3Br came through the reactor until the last few min.
The overall destruction was 99%.

Assume Zr(OH)4 @ 50% availability of total alkalinity

Reactor volume is based upon 7 cc of catalyst treating 2SLM scaled up to 220 CFM
The reactor volume is then doubled to provide spare capacity for a second attack.

wt. does not include housing

Description of the design basis for each component is described below.

NTP Reactor:

The NTP reactor design is based upon a proportional scale-up of the lab-scale test using 7cc of Ag-ZSM5 packing which achieved a 99% destruction of CH_3Br with 200 J/l input power shown in Figure 5. The design basis is to provide protection for two sequential attacks where the unit could not be refurbished between. The NTP reactor will oxidize and remove accumulated organic material, but testing has shown that phosphorous, sulfur, and Br^- are not cleaned and poison the Ag catalyst. The reaction with CH_3Br actually consumes Ag in a stoichiometric reaction with Br. To compensate for loss of activity the amount of packing has been doubled in the conceptual design. A direct proportional scale-up required 0.75 ft^3 of packing in the NTP reactor. The conceptual design includes 1.5ft^3 of Ag-exchanged ZSM5 packing. For 220 CFM the NTP reactor would be approximately 2'x2'x4½" deep.

Humidity has a big impact on the formation of active species and their reactivity in a NTP. The majority of testing was conducted at 80% RH. Some testing was also conducted at 15% RH, which confirmed that performance was poorer at higher humidity (i.e. 80%RH). The design is based upon 80%RH performance, which is worst-case for the specified humidity range of operation.

NTP reactors can be made in two basic designs that can be scaled to large volume reactors, parallel-plate and tube array. Parallel plate designs are advantageous when high energy density is needed. Parallel plate designs can also be built with lower operating voltages by minimizing required discharge gaps. Parallel plate reactors are especially useful when used with an open gap. This project initially anticipated a parallel plate design because it could be more compact. More consideration was given to the tubular design when the lab testing indicated that better performance could be achieved by increasing the volume of the Ag-ZSM5 packing with the same power delivery.

Calculations of the reactor weight also supported a tubular array design. The parallel plate design includes a greater volume fraction of alumina dielectric barriers in the reactor and they are very dense. The parallel plate reactor is smaller, but heavier.
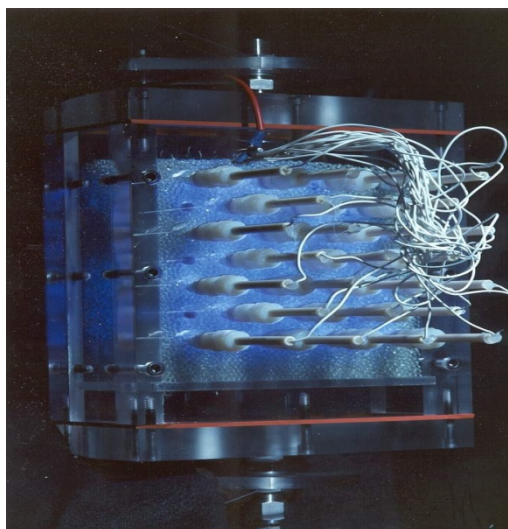

Figure 35. NTP reactor Scale-up approaches parallel plate (left) tube array (right)

O$_3$ Reactor/Filter:

The conceptual design of the O$_3$ reactor/filter is based upon a simplified kinetics model of CH$_3$Br destruction. The model was based upon kinetic equations for reactions that were consistent with the observed test results. The laboratory experiments showed that ozone did not react with CH$_3$Br in the gas phase; rather the reaction included some type of species on the surface. Additionally, O$_3$ and Ag were needed for the reaction with CH$_3$Br. The reaction didn't proceed unless either Mn or Fe was on the packing. Both of these are known to decompose O$_3$ to O$_2$ and a stabilized O• species, so the model assumed a surface O• was a reactant with adsorbed CH$_3$Br and Ag on the surface. The model further recognized that CH$_3$OH was the initial reaction product. Because CH$_3$OH continued to emerge in a long tail after the CH$_3$Br was stopped the initial CH$_3$OH was assumed to be formed on the surface. The final production of CO$_2$ was considered to come from oxidation of CH$_3$OH to CO$_2$. All of the reaction equations are shown in Table 10 below:

Table 10. Hybrid Plasma Reactor/filter model reactions

Rate coefficient	Reaction
k1:	CH3Br(g) + n → nCH3Br
k2:	nCH3Br → CH3Br (g)
k3:	CH3Br(g) + Ag → AgBr + nCH3OH
k4:	CH3Br(g) + AgO → AgBr + CO2
k5:	O3(g) + n → nO3
k6:	nO3 → O3 (g)
k7:	O3(g) + Mn → nO + O2(g)
k8:	O3(g) + Ag → AgO
k9:	O3(g) + nCH3OH → CO2(g) + n
k10:	nCH3OH → CH3OH (g)
k11:	nO + Ag → AgO
k12:	3nO + nCH3OH → CO2 + 2H2O + n

In Table 10 n represents a site on the packing material, nCH3Br represents adsorbed CH3Br.

The changes of each chemical over time were expressed as differential equations, which were then simplified as changes over small time (Eulerian method of numerical integration).

Gas phase components:

$$\frac{\partial CH3Br}{\partial t} = (\rho/\varphi) \times (-k1 \times CH3Br \times n + k2 \times nCH3Br - k3 \times CH3Br \times Ag - k4 \times CH3Br \times AgO)$$

$$\frac{\partial O3}{\partial t} = (\rho/\varphi) \times (-k5 \times O3 \times n + k6 \times nO3 - k7 \times O3 \times Mn - k8 \times O3 \times Ag - k9 \times O3 \times nCH3OH)$$

$$\frac{\partial CO2}{\partial t} = (\rho/\varphi) \times (k4 \times CH3Br \times AgO + k9 \times nCH3OH \times O_3 + k12 \times nO^3 \times nCH3OH)$$

$$\frac{\partial CH3OH}{\partial t} = (\rho/\varphi) \times (k10 \times nCH3OH)$$

Surface adsorbed components:

$$\frac{\partial nCH3Br}{\partial t} = k1 \times CH3Br \times n - k2 \times nCH3Br$$

$$\frac{\partial nO3}{\partial t} = k5 \times O3 \times n - k6 \times nO3$$

$$\frac{\partial nCH3OH}{\partial t} = k3 \times CH3Br \times Ag - k9 \times O3 \times nCH3OH - k12 \times nCH3OH \times nO^3$$

$$\frac{\partial nO}{\partial t} = k7 \times O3 \times Mn - k11 \times nO \times Ag - 3 \times k12 \times nO^3 \times nCH3OH$$

$$n = n^0 - nO3 - nCH3Br - nCH3OH - nO$$

Metals:

$$\frac{\partial AgO}{\partial t} = k8 \times O3 \times Ag + k11 \times nO \times Ag - k4 \times CH3Br \times AgO$$

$$\frac{\partial AgBr}{\partial t} = k3 \times CH3Br \times Ag + k4 \times CH3Br \times AgO$$

$$Ag = Ag^0 - AgO - AgBr$$

The initial step of the O_3 reactor modeling was to determine the adsorption kinetics and capacity (k1 and n, respectively) using adsorption data alone on the simple substrate with no reaction. Using the equation for the disappearance of CH_3Br from the gas phase k1 and n were determined by trial and error to provide a "visual best fit" to the adsorption curve determined for CH_3Br on ZSM5 as shown in Figure 36.
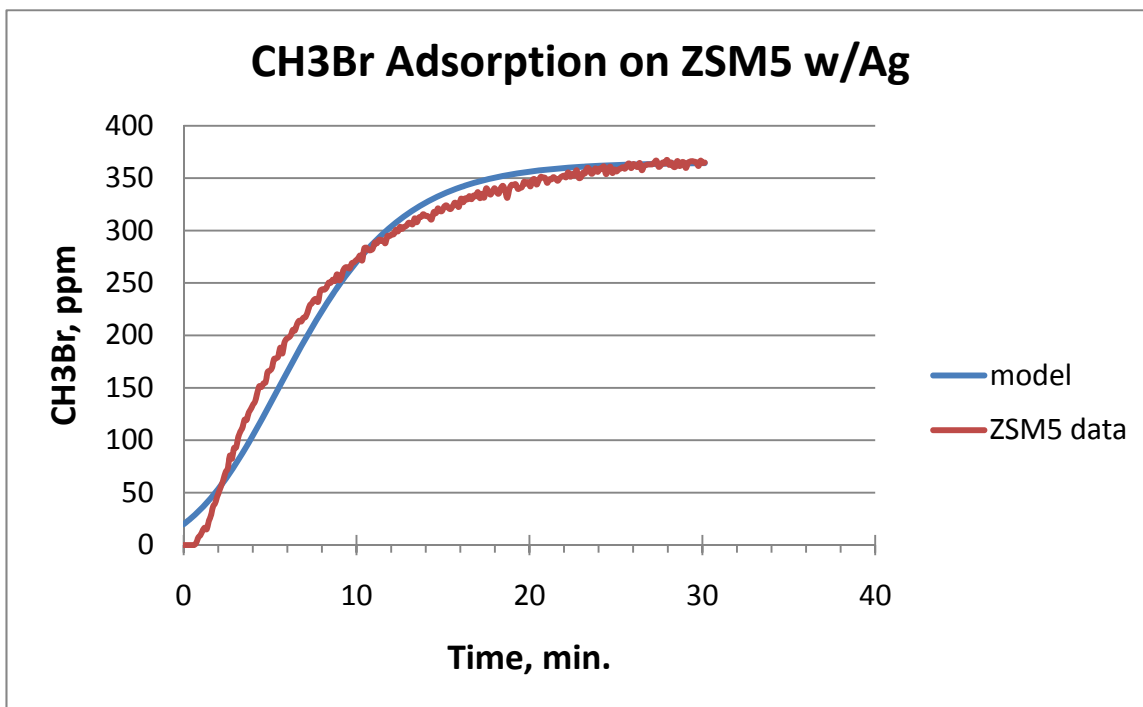
Figure 36. CH$_3$Br adsorption on ZSM5 with no reaction.

The best-fit was achieved with an adsorption rate constant of 1.70x10^4 L(gas)/mole-min and total packing capacity of 5.48x10^{-5} moles CH$_3$Br/g ZSM5 (i.e. 5mg CH3Br/g).

The intent was to determine additional kinetics coefficients to fit additional lab data of more complex mixture. For example, the next step was to determine O$_3$ adsorption, desorption, and decomposition kinetics by matching lab data for O$_3$ decomposition only. Then to determine CH$_3$Br reaction rate constants and Ag capacity coefficients by matching lab data for CH$_3$Br reaction. Finally, CH$_3$OH and CO$_2$ coefficients were to be established by matching analytical data for these components. The initial models were set up in Excel spreadsheets. However, as additional components were added the number of components to track increased. The spreadsheets became too large to be executed. The project scope (budget and time) wasn't sufficient to undertake converting the full reaction set to another more suitable calculating tool so the scope was reduced to simply match the disappearance of CH$_3$Br so that a suitable volume of O$_3$ reactor could be estimated to meet the required system performance capacity and maintain an acceptable outlet concentration of CH$_3$Br (1ppm). The results of that model are shown in Figure 37.

Figure 37. O₃ Reactor CT Test with simplified CH₃Br model.

Figure 37 shows the input to the O_3 reactor as increasing linearly after about 7 min. of complete CH_3Br destruction by the NTP. This input mimics the performance of an NTP 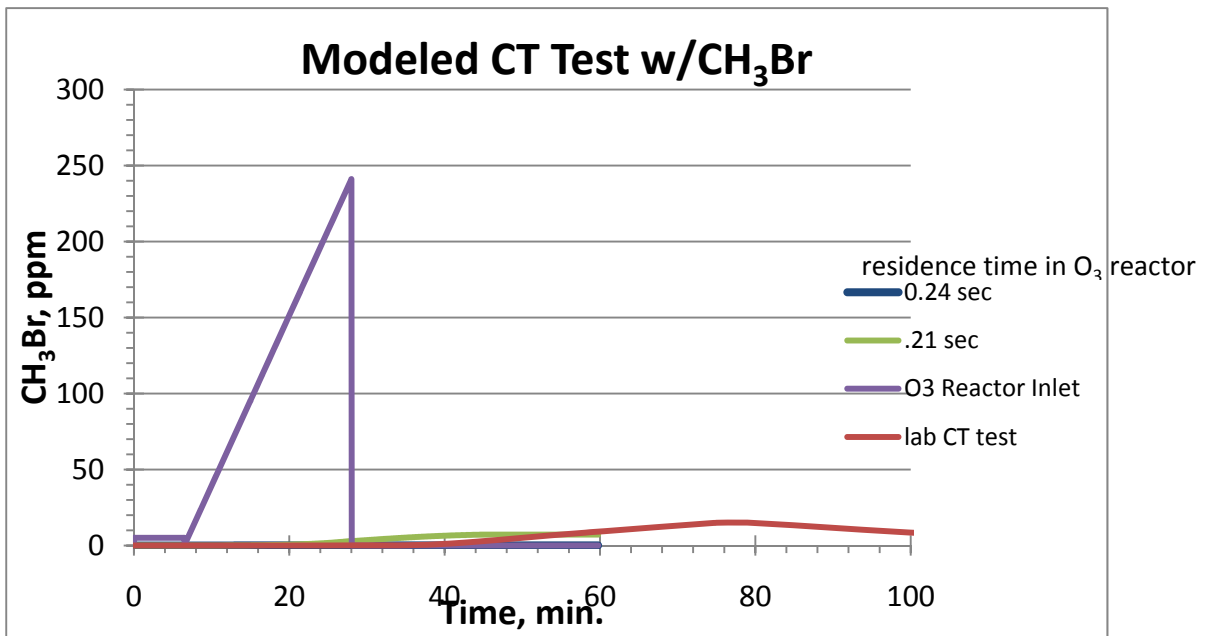reactor w/4cc of Ag-ZSM5 packing at 200 J/l. The model is pretty close but overestimates the performance of the O_3 reactor. Additional work needs to be done to improve the model and then apply similar modeling to the NTP reactor.

Acid Gas Scrubber:

Based on testing with CH_3Br or acrylonitrile an acid gas scrubber would not be needed. It was expected that the final fate of the Br would be as HBr, and acid gas which would need to be scrubbed. That is not what happened. The Br combined with Ag on the packing and formed immobile AgBr. The high power plasma was expected to also form NO_x, primarily as NO_2. Those emissions were also missing from the effluent of the O_3 reactor scrubber. Nitric acid, HNO_3, was also formed in the NTP reactor, but it wasn't in the emissions following the O_3 reactor.

The fate of acid gases in the O_3 reactor needs to be investigated further. Perhaps the ZSM5 packing has considerable capacity to react (absorb?) acid gases. Until acid specific studies are done it is assume that control of acid gas threats (e.g. Cl_2, HCl, HF, HNO_3, HCN, etc) will be controlled by an acid gas scrubber. For assessment purposes it was assumed that $Zr(OH)_4$ would be the primary control material in the acid gas scrubber. Fifty percent of the total hydroxide in the $Zr(OH)_4$ was assumed available for reaction and total mass of the $Zr(OH)_4$ was calculated to neutralize two sequential attacks of 100,000 mg-min/m³ of Cl_2. Chlorine gas was chosen as the design basis because Cl_2 has the highest specified capacity of all acid gases in the performance specifications of chemical vapor air purification technologies (ref. TTA#08-JECP-07-003 rv.6).

The hybrid plasma reactor filter includes an acid gas filter with 2.8 kg of $Zr(OH)_4$.

A more detailed design of an acid gas filter is proposed as part of preparation for agent/simulation tests to advance this technology to TRL level 5.

Finned heat exchanger:

During an attack the proposed operation is to turn on the NTP reactor at 200 J/l. For a 220 CFM air stream this would require ~21 kW. This power input to generate the nonthermal plasma will be thermalized and result in an adiabatic temperature rise of approximately 300F. This heat must be removed immediately. Air handling systems handle large heat transfers efficiently with finned heat exchanges. The conceptual design includes a 284 ft^2 finned heat exchanger flowing 20 gpm of cooling water @ 55F.

Based on discussion with Vimco Heating and Air Conditioning of Spokane, WA, a compact 8"x8"x8" finned heat exchanger provides 64ft^2 of heat transfer area and weighs ~15 lbs. Scaling proportionately, the 284ft^2 required for the hybrid plasma system would occupy 1.32 ft^3 and weigh 67 lbs.

5 Appendix A—Catalyst Synthesis Methods

All of the catalysts prepared for this program were prepared in either a granular or extrudate engineered form. ZSM-5, Silicalite, Na-Y-Zeolite, and Zeolite Beta were obtained in 12-30 mesh granular form (containing ~ 20wt% ZrO2 as a binder except for the Silicalite which used ~ 20wt% silica as the binder) from Dr. Joe Rossin of Guild Associates. Exxon/Mobil MCM-41 mesoporous silica was formed into 0.6mm diameter extrudates using either an alumina binder, or a silica binder.

The MCM-41 extrudate containing the alumina binder is designated as MC-1381 (avg. pore dia. ~ 30-34Å). The MCM-41 extrudate containing the silica binder is designated as MC-1382 (avg. pore dia. ~ 30-34Å). Perlkat 97-0 (a more macroporous silica : avg. pore dia. ~ 95Å) obtained from BASF was ground and sieved to a 12-30 mesh size fraction prior to use.

1st Generation MCM-41 Catalysts

These catalysts were prepared on the baseline MC-1381 extrudate material. Four catalysts were prepared on this material via impregnation of aqueous metal precursors solutions (Cu & Mn Acetates and Ag Nitrate). One catalyst was prepared with 5wt% of Mn, one with 5 wt% of Cu, one with 5 wt% of Ag, and one with ~2.5wt% each of Cu and Mn. Following the metal precursor addition, the catalysts are dried to remove water, then calcined to decompose the precursor materials to the oxides. The catalysts were tested in this form.

2nd Generation MCM-41 Catalysts (SAMMS Catalysts)

These catalysts were prepared on the MC-1382 extrudate material onto which a hydrophobic surface coating was attached. Catalytic metals were then added to the hydrophobic supports. The objective was to determine if the hydrophobic support surface would possess a greater affinity for capturing CH_3Br and degrading it when tested as an ozone catalyst, than do the more hydrophilic counterparts prepared above. The syntheses of these catalysts were somewhat complicated and time consuming, so only small quantities of each of 2 catalyst compositions (one containing Mn & the other containing Cu) were made for testing.

The first step in preparing these catalysts, involves refluxing the MC-1382 base material in a water-toluene mixture to hydrate the pore surfaces of the support. After this has been done, the hydrated support is treated with perfluorooctyltriethoxysilane, then filtered, washed with isopropyl alcohol to remove unreacted silane, then air-dried. After the now "Teflon-like" surface coated support has been prepared, the catalytic metals with similar hydrophobic ligands were prepared. The metal compounds that were prepared were $Cu(II)(perfluorobutyrate)_2$ and $Mn(II)(perfluorobutyrate)_2$. These compounds were prepared by refluxing the corresponding acetate salts with perfluorobutyric acid, taking up the reaction product in a solvent, then impregnating the hydrophobic supports with the perfluorobutyrate solutions.

The solvents are then removed by drying in a vacuum oven. The resulting $Mn-C_8F_{13}$ SAMMS and $Cu-C_8F_{13}$ SAMMS catalysts both contained ~ 1% of the catalytic metal by weight.

Two additional catalysts similar to the two described above were prepared by impregnation of the MC-1381 supports with $Ag(I)(perfluorobutyrate)$ and $Cu(II)(perfluorobutyrate)_2$ precursors respectively.

Catalysts Preparations on Silicalite

Silicalite has the same crystalline structure as ZSM-5 zeolites, except that it has higher silica to alumina ratios than do most ZSM-5 materials. As a consequence, Silicalite has very few cation exchange sites and is considerably more hydrophobic in nature. Therefore, catalytic metals that are to be placed inside of the Silicalite structure are unlikely to be atomically dispersed, as are metals that are attached to discrete cation exchange sites. Catalytic metals are more likely to form small multi-nuclear clusters. Catalytic metals were added to the Silicalite support via simple impregnation, but using an alcohol as a solvent instead of water. After impregnation of the catalyst metals, the solvent was removed by either drying with a heat gun or in a drying oven. After drying, the impregnated catalysts were calcined to decompose the precursor salts to oxide or elemental form. The catalysts were typically tested in this form.

Catalyst Preparations on ZSM-5

The granular ZSM-5 material were provided by Guild Associates in the Na form, and therefore needed to be exchanged in order to incorporate catalytic metals into the zeolitic structure. The initial batch of material had a silica to alumina ratio of ~ 35. A 2nd batch of material received later had a silica to alumina ratio of ~38. Therefore, the later batch of material had a slightly lower exchange capacity than the original material. Typically, cation exchanges were conducted using ~ a 10 times stoichiometric excess of the desired ion. The exchanges were typically carried out using an aqueous solution of the desired metal nitrate at ~60°C for 1-2 hours. Following the liquid phase cation exchange process, it is necessary to decant off the spent exchange solution, followed by a series of hot DI water washes to remove excess salt solutions. The washing is continued until the level of dissolved solids in the wash has been reduced to less than ~ 30ppm (~ 50 umhos). After exchange and washing, the catalyst is dried and then calcined to thermally decompose the nitrate portion of the precursor material. Some catalysts required that a second catalytic metal also be added to the already ion exchanged ZSM-5 catalysts. This was typically accomplished via impregnation with a solution of the desired salt. A second drying and calcination followed the addition of the second component.

Catalyst Preparations on Y Zeolites

The granular Y-zeolite material provided to us by Guild Associates also was provided in the Na form, and also needed to be exchanged to incorporate catalytic metals into exchange sites. The silica to alumina ratio of the Y-zeolite material supplied to us was reported to be ~ 5. As a consequence of the lower silica to alumina ratio the Y-zeolite material contains on the order 6-8 times as many cation exchange sites as does the above ZSM-5 materials. Similar ion exchange and washing procedures were used for the Y-zeolite material as were described above for the ZSM-5 catalysts.

Brief Description of Catalyst Preparations

1ˢᵗ and 2ⁿᵈ Round Catalyst Preparations

60433-1-1   "As received" Silicalite preparation obtained from Joe Rossin at Guild Associates. This material was 12-20 mesh granular preparation reportedly containing ~20 wt% of a silica-based binder.

60433-1-2   A sample of commercial Perlkat 97-0 silica (Spheres) was crushed an sieved to a 12-20 mesh size fraction. BET surface area is reported to be ~ 343m2/g with internal pore volume of ~ 0.81cc/g. Mean pore diameter is reported to ~95angstroms.

60433-1-3   This was a H-exchanged version of Joe Rossin's Na-ZSM-5 preparation. His Na-ZSM-5 preparation was a 12-20 mesh granular material containing ~ 20 wt% of a zirconia-based binder. The Na-ZSM-5 material contained in it had a SiO_2/Al_2O_3 ratio of ~ 35:1. The H-exchange was conducted using ~ 10 wt% Acetic Acid solution (~500g) , followed by D.I. water washing, drying, the calcination at 550C for 4 hours.

60433-5-1   ~ 1wt% Au on the above Silicalite material, prepared by impregnation of the support with an isopropanol solution of chloroauric acid, followed by drying, then rinsing with 29% aqueous ammonia solution to immobilize the gold and to rinse out chloride by-product. The catalyst was re-dried, then calcined at 400C for 2 hours. The finished catalyst was violet to purple in color indicative of colloidal size gold particles.

60433-8-1R   ~ 1wt% Pt on the above Silicalite material, prepared by impregnation of the support with an isopropanol solution of platinum nitrate, followed by drying, and reduction at 250C for 3 hours with hydrogen gas.

60433-11-1   ~ 0.5wt% Au + ~ 0.14% Mn on the above Silicalite material, prepared by impregnation of the support with an isopropanol solution of chloroauric acid and manganese nitrate, followed by drying, then rinsing with 29% aqueous ammonia solution to immobilize the manganese and gold and to rinse out chloride by-product. The catalyst was the re-dried, then calcined at 400C for 2 hours.   The finished catalyst was also a violet to purple color like the 60433-5-1 catalyst above.

60433-14-1R   ~ 3.00wt% Pt + ~ 2.86% Re on the Perlkat 97-0 silica material, prepared by impregnation of an aqueous solution of platinum nitrate and perrhenic acid, followed by drying, and reduction at 250C for 3 hours with hydrogen gas.

60433-18-1R   ~ 2.95wt% Re on the Perlkat 97-0 silica material, prepared by impregnation of an aqueous solution of perrhenic acid, followed by drying, and reduction at 250C for 3 hours with hydrogen gas.

60433-21-1   Ag-exchanged Na-ZSM-5 material was prepared by conducting 2- 60C hot exchanges on the base material using a total of ~ 10X stoichiometric excess of Ag (as AgNO3). Afterwards the Ag-exchanged ZSM-5 material was washed with D.I. water until the spent wash water conductivity measured < 50 micro mhos, then was dried, and calcined at 400C for 2 hours.

60433-25-1R   ~ 1.9wt% Mn + ~ 1.9wt% Pt on ZSM-5. Mn-exchanged Na-ZSM-5 material was prepared by conducting 2-60C hot exchanges on the base material using a total of ~ 10X stoichiometric excess of Mn (as Mn Nitrate). Afterwards, the Mn-exchanged ZSM-5 material was washed with D.I. water until the spent wash water conductivity measured < 50 micro mhos, then dried, and calcined at 400C for 2 hours. The amount of Mn added to the ZSM-5 was estimated to be ~ 1.9wt%. Next, approximately an equal wt. of Pt was added to the Mn-exchanged ZSM-5 material by impregnation with an isopropanol solution of platinum nitrate. The catalyst was subsequently dried and reduced at 250C for 3 hours with hydrogen gas.

60433-33-1   Mn-exchanged Na-ZSM-5 was prepared by conducting 2-60C hot exchanges on a large batch of the Na-ZSM-5 material. As done previously an ~ 10X stoichiometric excess of Mn (as Mn nitrate) was used during the exchange procedure. DI water washes were employed to remove excess material and by-product Na nitrate. Washing was terminated when the spent wash water conductivity measured < 50 micro mhos. The material was subsequently dried and

calcined at 400C for 2 hours. The Mn content of the finished 60433-33-1 material is estimated to be ~1.9wt% Mn, but no analyses were conducted on the material at this time. A portion of this material was submitted for testing and the remainder of this material became the precursor material used to make both the 60433-43-1 and 60433-46-1 catalyst materials described below.

60433-37-1   ~ 3.6wt%Mn + ~1.0wt% Ag was made on the Silicalite support via impregnation using an isopropanol solution of manganese nitrate and silver nitrate. The impregnated material was then dried, and calcined at 400C for 2 hours.

60433-40-1   Cu-exchanged ZSM-5 material was prepared by conducting 2-60C hot exchanges of the Na-ZSM-5 base material using ~ 10X stoichiometric excess of copper (II) nitrate solution. Following the exchange, D.I. water washes were performed as described above, followed by drying, and finally by calcination at 400C for 2 hours.

60433-43-1   A portion of the previously prepared Mn-exchanged ZSM-5 material (60433-33-1) was used as the precursor for this preparation. An additional ~ 1.8wt% of Mn was added via impregnation of the 60433-33-1 material using an aqueous Mn nitrate solution. The impregnated material was then dried and calcined at 400C for 2 hours.

60433-46-1   A portion of the previously prepared Mn-exchanged ZSM-5 material (60433-33-1) was used as the precursor for this preparation. An additional ~ 1.8wt% of Mn + ~ 3wt% Ag was added via impregnation of the 60433-33-1 material using an aqueous Mn nitrate and Ag nitrate solution. The impregnated material was then dried and calcined at 400C for 2 hours.

60433-49-1   An Fe-exchanged ZSM-5 material was prepared by conducting 2-60C hot exchanges of the Na-ZSM-5 base material using a ~10X stoichiometric excess of iron (III) nitrate solution. Following the exchange, D.I.water washes were performed as described above, followed by drying and calcination at 400C for 2 hours. After calcination, ~3wt% of Ag was added to the Fe-exchanged ZSM-5 by impregnation using an isopropanol solution of silver nitrate. The impregnated catalyst was the re-dried, the calcined at 400C for 2 hours.

60433-54-1   We wished to add ~ 3wt% of Ag to Joe Rossin's FeO(OH) preparation, but we were afraid that we wouldn't be able to add Ag nitrate solution to his material, then do a calcination at ~ 400C to decompose the nitrate. Joe verified our fears and suggested that we add the silver as an amine complex of silver carbonate or hydroxide. A freshly precipitated and washed silver hydroxide material was prepared, then dissolved in a 29% aqueous ammonia solution. The solution was then impregnated onto the "as received" FeO(OH) material. After impregnation, the catalyst was placed into a vacuum oven (set at 50C & under house vacuum) to dry over night. The "dried-only" catalyst was then submitted for testing.

1st generation MCM-41 catalysts

These catalysts will evaluate the impact of nanoporous architecture on Cu and Mn catalysts, which were used in the commercial catalyst demonstrated last year.

[1] bare MCM-41 extrudate (baseline)
[2] MCM-41 extrudate + Cu salt (acetate)
[3] MCM-41 extrudate + Mn salt (acetate)
[4] MCM-41 extrudate + Cu salt + Mn salt

These systems will allow us to see how much better the MCM-41 supported catalysts perform relative to the commercial CuO on MnO$_2$. Better capillary condensation for capturing the organics in the nanoporous structure, more surface area to disperse the catalyst for greater activity, etc.

We added the Ag salt into the matrix due to the interest in using Ag for this type of catalyst (especially for methyl bromide).

[5] MCM-41 extrudate + Ag salt (nitrate)

Support characteristics

MC-1381 Silica (ExxonMobil extrudate made from MCM-41 with an alumina binder)
0.6 mm diameter x 5-18 mm long
Surface Area to Mass Ratio = 747.9 m^2/g
Average Pore Diameter = ~30-34 Å
Pore Volume = 1.4015 cc/g

25 cc of MC-1381 is approximately 6.5 g
6.5 g x 1.4015 cc/g = 9.11 cc pore volume
5 wt% of 6.5 g = 0.325 g of catalyst metal

Mn catalyst on MC-1381
For Mn 0.325g = 5.92 mmole Mn
5.92 mmole of Mn(OAc)$_2$-4H$_2$O = 0.00592 mole x 245.09 g/mole = 1.45 g of Mn(OAc)$_2$-4H$_2$O

1.500g of Mn(OAc)$_2$-4H$_2$O was dissolved in 9 mL of DI water, and was manually mixed with 6.511 g of MC-1381. This material was then placed in vacuum oven at 100°C and ~25 in. Hg over the weekend to remove the solvent. Final product weighed 7.500g. Mass gain = 0.989 g; if the Mn were present as the anhydrous acetate (173.03 g/mole) then the predicted mass gain would be 1.024g, so it appears that the Mn is predominantly present as the anhydrous acetate, with a small amount of the oxide or silicate also present.

BET surface area analysis
Surface area = 563 m^2/g
Pore volume = 1.1 cc/g
Average pore diameter = 27Å

Cu catalyst on MC-1381
For Cu 0.325g = 5.12 mmole Cu
5.12 mmole of Cu(OAc)$_2$ = 0.00512 mole x 181.64 g/mole = 1.075 g of Cu(OAc)$_2$

1.084g anhydrous Cu(OAc)$_2$ was dissolved in 18.7 mL of DI water (it was not sufficiently soluble to dissolve in less than the total pore volume). This solution was added to 6.584 g of MC-1381 (which, as expected, did not soak all of the solution up). This sample was heated to 100°C in vacuum oven overnight (~25" Hg) to remove the solvent. Final product weighed 7.491g. Mass gain of 0.907g (again it appears that the Cu is present primarily as the anhydrous acetate, with a small amount of the oxide or silicate).

BET surface area analysis
Surface area = 594 m^2/g
Pore volume = 1.1 cc/g
Average pore diameter = 30Å

Mixed Cu/Mn catalyst on MCM-41
0.721g Mn(OAc)$_2$ (2.94 mmole) and 0.416g Cu(OAc)$_2$ (2.29 mmole) were dissolved in
10 mL DI water (originally aimed for 9 mL, but that didn't quite dissolve all of the Cu salt). This
solution was then combined with 6.492 g MC-1381, mixed thoroughly and placed in the oven
overnight at 80°C overnight (no vacuum was applied at there were other samples being treated at
the same time). The next morning the heat was turned up to 100°C and vacuum (~25" Hg)
applied for 6 hours in an effort to remove residual solvent. Final product weighed 8.389g (still
contains residual water).

BET surface area analysis
Surface area = 607 m^2/g
Pore volume = 0.66-0.81 cc/g (notably lower than the others, may have been some
hydrolysis/condensation going on leading to colloidal oxide formation?)
Average pore diameter = 28Å

Ag catalyst on MCM-41
For Ag 0.325g = 3.01 mmole Ag
For AgNO$_3$ MW = 169.88 g/mole, so 3.01 mmole is 0.512 g

Dissolved 0.517 g AgNO$_3$ in 9.0 mL DI water, and combined this solution with 6.525g MC-1381
and mixed the two components thoroughly. This mixture was then placed in
the vacuum oven overnight at 100°C and ~25 in. Hg. The final product weighed 6.953g. Mass
gain = 0.428g (suggesting that the Ag is present as a mixture of the nitrate and oxide/silicate)

BET surface area analysis
Surface area = 667 m^2/g
Pore volume = 1.2 cc/g
Average pore diameter = 30Å

Notes on second generation SAMMS catalysts

Silica characteristics
Both of these extrudates are made using Exxon/Mobil MCM-41 as the feedstock.

MC-1381 Silica (granulation = 0.6 mm diameter x 5-18 mm long)
Alumina binder
      Surface Area to Mass Ratio = 747.9 m^2/g
      Average Pore Diameter = ~30-34 Å
      Pore Volume = 1.4015 cc/g

MC-1382 Silica (granulation = 0.56 mm diameter x 2-10 mm long)
Silica binder (well-suited for silane chemistry)
      Surface Area to Mass Ratio = 665.3 m^2/g
      Average Pore Diameter = ~30-34 Å
Pore Volume = 1.392 cc/g

25 cc of MC-1381 is approximately 6.5 g
6.5 g x 1.4015 cc/g = 9.11 cc pore volume
5 wt% of 6.5 g = 0.325 g of catalyst metal

Perfluorobutyrate (pfb) complexes
The literature method (IC, 1982, 21, 2196-2202) calls for dissolving 1 g of the metal acetate salt in 30 mL of perfluorobutyric acid + 3 mL of perfluorobutyric anhydride and heat to reflux for 15 minutes under N_2. Distill the solvent off, wash with pentane and dry under vacuum.

$Rh_2(pfb)_4$ is soluble in CH_2Cl_2 and picks up water (and other bases) readily. Not soluble in CCl_4 or toluene.

$Mo_2(pfb)_4$ is soluble in toluene and decomposes slowly in air. Only slightly soluble in CH_2Cl_2.

Ag(pfb) was made from the oxide (in water!) (JACS, 1951, 73, 2461-2463)
Also in JACS 1953, 75, 4525-4528 – both Ag and Cu (made from Cu metal and air in the acid at reflux, reported to be slow).

Ag(pfb) is commercially available from Aldrich.

Cu(pfb)₂ catalyst
CuO 79.54 g/mole
Aiming for 0.325 g of Cu, or 5.11 mmole, or 0.407g CuO
Perfluorobutyric anhydride (410.06 g/mole, 1.665 g/mL) 5.11 mmole = 2.095g or 1.26 mL
Perfluorobutyric acid (214.04 g/mole; 1.645 g/mL), 5.11 mmole = 1.094g or 0.665 mL

0.433g of CuO were added to an oven-dried flask, and purged with N_2. Next 1.25 mL of perfluorobutyric anhydride and 1.35 mL perfluorobutyric acid were added and the mixture heated to reflux overnight. Perfluorobutyric acid was distilled off and the product dried under vacuum. $Cu(pfb)_2$ was dissolved up in a total of 10 mL of trifluoroethanol to form a deep turquoise blue solution. MC-1381 (6.595g) was added and the mixture shaken to disperse the solution, which was soaked up almost instantly. The MC-1381 was then dried in a vacuum oven overnight at ~100°C and 25" Hg. The product was blue-gray (not uniform, some dark powder) and the yield was 7.110g (mass gain 0.515g).

Metal content of this catalyst
pfb ligand = 213 g/mol, Cu = 63.5 g/mole, so $Cu(pfb)_2$ = 489.5 g/mole
So .515g/489.5 = 1.05 mmole
%Cu = 63.5/489.5 = 13% by weight
13% of .515 = 67 mg Cu
.067/7.11 = 0.94% Cu by weight.

BET data
741 m²/g
1.46 cc/g
Pore diameter 31Å

Ag pfb catalyst
For Ag 0.325g = 3.01 mmole Ag
MW = 320.9 g/mole, so 3.01 mmole is 0.966 g

Used 0.957 g Ag(pfb) (from Aldrich), dissolved in 8.0 mL diglyme (TFE and CH_2Cl_2 did not dissolve the Ag(pfb)), on 6.515 g MC-1381, then placed in a vacuum oven at 90°C and ~25 in. Hg overnight. Final product was charcoal gray, and weighed 7.778g.

Mass gain = 1.263g (more that the Ag(pfb) added, so it appears that there is still a small amount of residual solvent left in the product).

BET data
620 m^2/g
1.14 cc/g
Pore diameter 31Å

Perfluorooctyl SAMMS on MC-1382
1h,1h,2h,2h-perfluorootyltriethoxysilane (Aldrich)
510.36 g/mole
1.341 g/mL

For a coverage of 5 silanes/nm^2, then this suggests we need 2.15 x 10^{22} silane molecules, or 35.7 mmole. This would be 18.2 g or 13.6 mL for C_8F_{13} silane.

6.470 g of MC-1382 was placed in 125 mL of toluene, treated with 2.0 mL of water and heated to reflux (no stirring!) for 5 hours in order to hydrate the pore surfaces of the support. 13.6 mL of C_8F_{13} silane was added and the mixture maintained at reflux for an additional 4 hours. Product collected by filtration and washed copiously with IPA and air-dried overnight to give 8.886 g of snow-white extrudate. This corresponds to a 2.416 g mass increase.

"HOSi(O)-R" approximation
MW of "HOSi(O)-R" approximation = 409.1 g/mole
5.91 mmole of silane in product
3.56 x 10^{21} silane molecules
6.470g of MC-1382 = 4303 m^2 surface area
0.83 silanes/nm^2

Mn(pfb)$_2$ on C_8F_{13} SAMMS catalyst
1.460g of Mn(OAc)$_2$-4H$_2$O was placed in a N$_2$ purged round-bottomed flask and treated with 2.0 mL of perfluorobutyric acid. The pink salt did not dissolve and was "clumpy". The mixture was heated to reflux, and the salt dissolved quickly resulting in a clear homogeneous solution. Reflux was maintained for 20 minutes, then the mixture was cooled and 4.0 mL of glyme was added and then the C8F13 SAMMS were added and mixed thoroughly. Dried in the vacuum oven for 7 hours to give 9.734g of product (0.848g mass gain)

Metal content of this catalyst
pfb ligand = 213 g/mol, Mn = 54.9 g/mole, so Mn(pfb)$_2$ = 480.9 g/mole
So .848g/480.9 = 1.76 mmole
%Mn = 54.9/480.9 = 11.4% by weight
11.4% of 0.848 = 96.8 mg Mn
.0968/9.734 = 1.0% Mn by weight.

2nd Batch of C8F13 SAMMS

6.473g of MC-1382 was placed in 35 mL of glyme and treated with 2 mL of water and allowed to stand for 24 hours to hydrate the silica surfaces. Next it was treated with 2.6 mL of C_8F_{13} silane (6.83 mmole) and heated to reflux for 4 hours. The product was collected by vacuum filtration, washed copiously with IPA and air-dried to give 7.373g of snow white extrudate. This corresponds to a mass increase of 0.900g.

MW of "HOSi(O)-R" approximation = 409.1 g/mole
2.20 mmole of silane in product
1.32 x 10^{21} silane molecules
6.473g of MC-1382 = 4305 m^2 surface area
0.31 silanes/nm^2

Cu(pfb)$_2$ on C$_8$F$_{13}$ SAMMS catalyst
0.446g of CuO was placed in a N_2 purged round-bottomed flask and treated with 1.5 mL of perfluorobutyric acid and 1.5 mL of perfluorobutyric anhydride and heated to reflux overnight, resulting in a dark blue solution. The solvents were removed under vacuum and the produce taken up in 6.0 mL of trifluoroethanol (dark green solution), to which was added the C_8F_{13} SAMMS prepared above and mixed thoroughly. Dried in the vacuum oven overnight to give 7.168g of a blue-green product (the slight mass loss suggests that the original C_8F_{13} SAMMS still had some solvent in it, the blue-green color of the final product clearly indicated that it contained $Cu(pfb)_2$).

3rd Round Catalyst Preparations

60433-63-1   This catalyst was prepared using some of Joe Rossin's granular Silicalite preparation (batch # 5-14-10 ; 12x30 mesh). The nominal catalyst composition was ~1.8wt%Mn + ~3 wt% Ag on the Silicalite support. The catalyst was prepared in two separate steps by first impregnating the support material with a 2-propanol solution of manganese (II) nitrate, followed by oven drying @ 120 C, then calcination @ 400 C for 2 hours. Next, the catalyst was impregnated a 2nd time with a silver amine nitrate solution, followed by a 2nd oven drying, and a second calcination @ 475 C for 2 hours.

60433-67-1   This catalyst was prepared by conducting two 60 C ion-exchanges on some of the granular Na-ZSM-5 zeolite preparation (batch # 5-12-10 ; 12x30 mesh) using a 10X stoichiometric excess of Mn(II) nitrate in aqueous solution. Following the exchange, the Mn-ZSM-5 material was hot washed with D.I. water until the spent wash water contained < 30 ppm of dissolved solids, then was dried @120 C, then calcined @400 C for 2 hours. After calcining, the Mn-ZSM-5 material was impregnated with a silver amine nitrate solution, redried, then recalcined @475 C for 2 hours. The nominal catalyst composition for the completed catalyst was ~1.8wt%Mn(via exchange) + ~3wt.%Ag (via impregnation) on ZSM-5.

60433-69-1   This catalyst was prepared on some of the granular Silicalite material, mentioned above, by first impregnating it with an aqueous Fe(III) nitrate solution, then immersing the Fe(III) nitrate impregnated catalyst in 29% aqueous ammonia solution to convert the Fe to the hydroxide form. The $Fe(OH)_3$ –containing catalyst was then dried in a vacuum oven overnight under house vacuum @80 C. After drying, the catalyst was re-impregnated with a silver amine hydroxide solution and redried again under house vacuum @ 80C overnight. The nominal catalyst composition for the completed catalyst was ~ 1.8wt%Fe(as Fe hydroxide or oxyhydroxide) + ~

3wt%Ag on Silicalite. The catalyst was tested without prior calcination to preserve the state of the Fe and Ag species.

60433-73-1   This catalyst was prepared on some of the granular Na-ZSM-5 material, mentioned above, by conducting two 60 C ion-exchanges of the material using a 10X stoichiometric excess of Fe(III) nitrate in aqueous solution. Following the exchange, the Fe-ZSM-5 material was hot washed with D.I. water until the spent wash water contained < 30ppm of dissolved solids, then was dried @120 C, then calcined @ 400 C for 2 hours. The nominal catalyst composition for the completed catalyst was ~1.32wt%Fe (via exchange) on ZSM-5.

60433-75-1   This catalyst was prepared on some of the granular Na-Y zeolite material also obtained from Joe Rossin at Guild Associates (batch #6-5-10 ; 12x30 mesh ; SiO_2 to Al2O$_3$ ratio = 5). This catalyst was prepared by conducting two 60 C ion-exchanges of the material using a 10X stoichiometric excess of Fe(III) nitrate in aqueous solution. Following the exchange, the Fe-Y zeolite material was hot washed with D.I. water until the spent wash water contained < 30ppm of dissolved solids, then was dried @120 C, then calcined @ 400 C for 2 hours. After calcining, the catalyst was impregnated with an aqueous AgNO3 solution, re-dried, then recalcined @ 475 C for 2 hours. The nominal catalyst composition for the completed catalyst was ~6.12wt%Fe (via exchange) + ~6wt%Ag (via impregnation) on Y zeolite.

60433-78-1   This material was prepared by adding an additional 3wt% of Ag to the previously prepared 60433-49-1 catalyst (60433-49-1 composition was ~1.28wt%Fe via exchange + 3wt%Ag via impregnation on ZSM-5). The additional silver was added as a 2-propanol solution of silver nitrate, followed by drying, and then re-calcination @ 475 C for 2 hours. The nominal composition of the finished catalyst is ~1.24wt%Fe (via exchange) + 5.91wt%Ag (via impregnation) on ZSM-5.

60433-81-1   This catalyst was prepared by conducting two 60 C ion-exchanges on some of the granular Na-ZSM-5 zeolite preparation (batch # 5-12-10 ; 12x30 mesh) using a 10X stoichiometric excess of Mn(II) nitrate in aqueous solution. Following the exchange, the Mn-ZSM-5 material was hot washed with D.I. water until the spent wash water contained < 30 ppm of dissolved solids, then was dried @120 C, then calcined @400 C for 2 hours. After calcining, the Mn-ZSM-5 material was impregnated with a silver amine nitrate solution, redried, then recalcined @475 C for 2 hours. The nominal catalyst composition for the completed catalyst was ~1.81wt%Mn (via exchange) + ~6wt.%Ag (via impregnation) on ZSM-5.

60433-81-2   This catalyst was prepared by conducting two 60 C ion-exchanges on some of the granular Na-ZSM-5 zeolite preparation (batch # 5-12-10 ; 12x30 mesh) using a 10X stoichiometric excess of Mn(II) nitrate in aqueous solution. Following the exchange, the Mn-ZSM-5 material was hot washed with D.I. water until the spent wash water contained < 30 ppm of dissolved solids, then was dried @120 C, then calcined @400 C for 2 hours. After calcining, the Mn-ZSM-5 material was impregnated with a silver amine nitrate solution, redried, then recalcined @475 C for 2 hours. The nominal catalyst composition for the completed catalyst was ~1.70wt%Mn (via exchange) + ~12wt.%Ag (via impregnation) on ZSM-5.

60433-85-1   This catalyst was prepared using the granular Na-ZSM-5 material described above. This material was prepared by an alternative ion exchange method where $FeCl_2$ was used as the precursor material, and the exchange was conducted at room temperature in aqueous solution under nitrogen gas sparge. A 10X stoichiometric excess of the $FeCl_2$ reagent was used,

and only a single exchange conducted. Following the exchange, the material was hot washed with D.I. water until the spent wash water contained <30 ppm dissolved solids, then was dried @ 120C. The dried exchanged solids were the impregnated with a silver amine nitrate solution, redried, and calcined at 475 C for 2 hours. The nominal composition of the catalyst is~1.91wt%Fe (via exchange) + 3wt%Ag (via impregnation) on ZSM-5.

60433-88-1   This catalyst was prepared on some of the granular Na-Y zeolite material also obtained from Joe Rossin at Guild Associates (batch #6-5-10 ; 12x30 mesh ; SiO_2 to Al2O$_3$ ratio = 5). This catalyst was prepared by conducting two 60 C ion-exchanges of the material using a 10X stoichiometric excess of Mn(II) nitrate in aqueous solution. Following the exchange, the Mn-Y zeolite material was hot washed with D.I. water until the spent wash water contained < 30ppm of dissolved solids, then was dried @120 C. After drying, the catalyst was impregnated with an aqueous AgNO3 solution, re-dried, then calcined @ 475 C for 2 hours. The nominal catalyst composition for the completed catalyst was ~8.20wt%Mn (via exchange) + ~12wt%Ag (via impregnation)on Y zeolite.

60433-91-1   This material was prepared on the granular Silicalite material mentioned above. This catalyst was prepared by impregnating the support material with a 2-propanol solution of Mn(II) nitrate and silver nitrate, followed by drying @120 C, then calcination @ 475 C for 2 hours. The nominal composition of the completed catalyst is ~ 0.05wt%Mn + ~3wt%Ag (both by co-impregnation) on Silicalite.

Final Round Catalyst Preparations

60433-96-1   This catalyst was ~ 300cc batch size re-make of the 60433-81-2 catalyst described above. The nominal composition is ~1.70wt%Mn (via exchange) + ~12wt.%Ag (via impregnation) on ZSM-5.

60433-105-1   This catalyst was ~300cc batch size re-make of the 60433-78-1 catalyst, also described above. The nominal composition is ~1.24wt%Fe (via exchange) + 5.91wt%Ag (via impregnation) on ZSM-5.

60433-99-1   This catalyst was prepared by impregnating ~ 30cc of the Sasol 1mm diameter alumina beads with $NaMnO_4$ solution. The impregnated beads were dried @ 120 C, then given a short (60 minutes) calcination @ 500C, to thermally decompose the permanganate. After calcination, hot D.I. water washes were performed on the material (to remove soluble Na salts) until the spent wash water contained < 30 ppm of dissolved solids. The washed catalyst was dried @ 120 C for 2 hours, but was not further calcined in order to maintain the MnO_x in a more hydrated form prior to testing. The catalyst nominally contains ~ 10wt%Mn as either oxide(s) or hydrous oxide(s).

60433-109-1   This catalyst prep was essentially a repeat of the 60433-21-1 prep (Ag-Exch'd Na-ZSM-5), except that this catalyst was prepared on the later Na-ZSM-5 batch of material that was reported to have a silica to alumina ratio of ~ 38:1 instead of the ~35:1 ratio material that was used in the 60433-21-1 catalyst prep.

6 Appendix B—NTP Testing with Other Materials

6.1 *Glass Beads*

The figure below shows measurements with glass beads at two different relative humidities. In the first plot I show some time data in order to illustrate how quickly CH3Br attained steady state with a glass bead packing. In contrast to the ZSM5. However in agreement with the ZSM5 work, the main product is CO. It seems likely that the primary reaction releases CO, which dominates the final distribution in the case of glass beads simply because it escapes the plasma quickly.
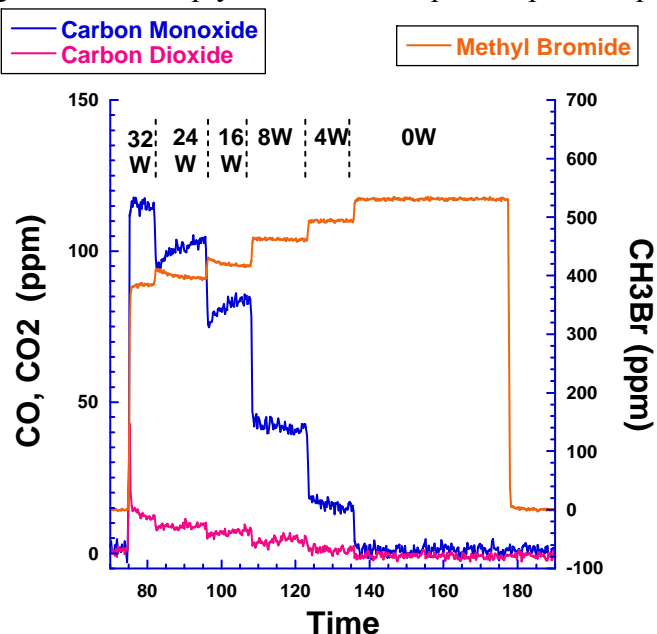
I did not find any indication of what happened to the Br in these experiments. I do believe if HBr made it to my FTIR I would have detected it, but that is as much as I can say.

Similar data was obtained at 80% RH and the two sets of data are plotted vs. plasma energy below. As you can see the data look exponential in power input but evidently there is a limit (~ 30% destruction) to the extent of reaction in either case. At lower relative humidity the energy efficiency is improved, but the net destruction is limited to the same value.

At 80% RH: β ~ 580 J/l
Minimum CH3Br ~ 370 ppm

At 15% RH: β ~ 410 J/l
Minimum CH3Br ~ 370 ppm
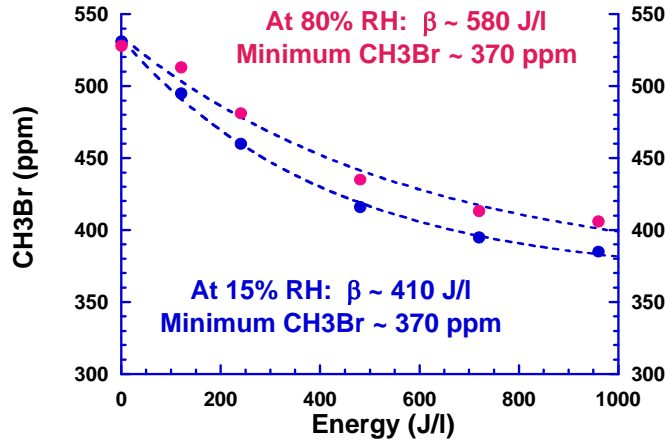
Glass beads obviously offer a minimal surface area and along with this are limited in their use in CH_3Br destruction. Another problem is that at such extremely high plasma powers the production of NOx (mainly NO2) is problematic.

6.2 *1% Pt on silicalite*

As can be seen in the following two slides, 1% Pt on silicalite is not useful for CH_3Br destruction. The only positive aspect is that most of what does get oxidized becomes CO_2 rather than CO. Unfortunately there is almost no adsorption and very little destruction. What's worse, this catalyst seemed to enhance HNO3 and NO2 formation in the plasma.

1%Pt/Silicatlite in Plasma

$y = 531 * e^{(-0.000555x)}$ $R^2 = 0.995$

β ~ 1800 J/l!

O3 (Pt/Sil)
CH3Br
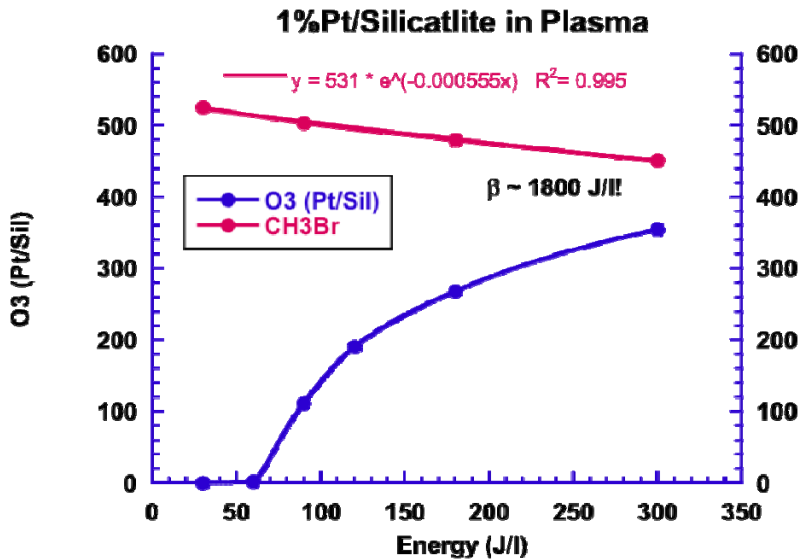
6.3 *Amorphous Manganese Oxide [AMO]*10% MnOx on Alumina (Sasol) beads

I ran one survey test 10% MnO_2 on Sasol beads in the plasma reactor. The idea is that since Mn is known to react catalytically with ozone, perhaps this reaction would lead to

oxidation of the CH$_3$Br also present in the reactor. I ran only one test of this material at very high power and at very low (15%) relative humidity.   Since I was using a large volume NTP reactor (24 cm^3) the GHSV was quite low, approximately 5000/Hr. This is probably unrealistically low, but the results were nevertheless promising. The plots below show the overall results for an extremely long exposure to 540 ppm of CH3Br. The first exposure was for 72 minutes and the latter one for approximately 200 minutes. The large volume plasma reactor did not operate well with this packing material, which could be due to unknown properties of the catalyst itself. I did not explore this issue further, but it would be worth another look in the future.

It should be noted that a large amount of CO$_2$ was formed, with only minimal CO. Furthermore the overall carbon balance is excellent, evidently improving with time as the catalyst efficiency dropped. We have no indication of where the Br atom goes, but a good guess would be that it stays behind, eventually removing active sites.

The first 77-minute exposure produced a destruction of 82%--which is quite good.   A calculation at 28 minutes for comparison to AgZSM5 yields an estimated 92% destruction of CH3Br.   Evidently the catalyst is immediately compromised by the
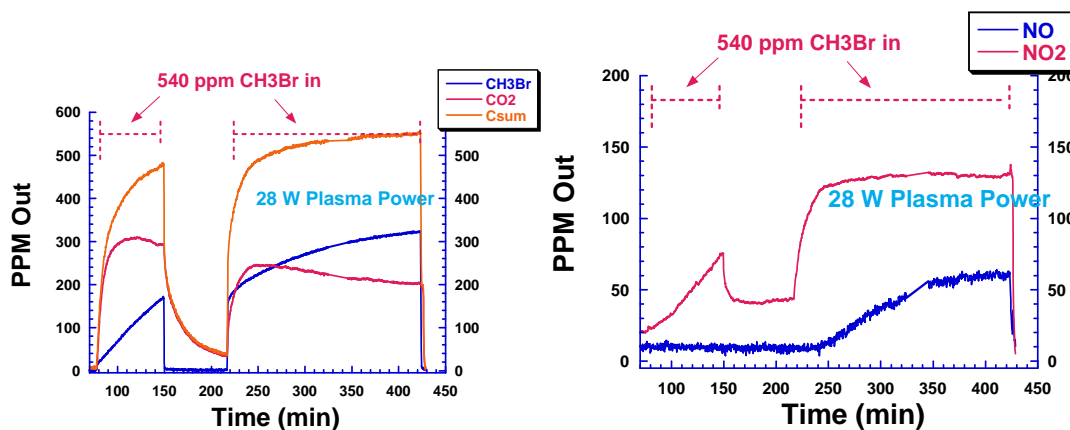

reaction and loses efficiency. We conclude that this material is acting as a reactant rather than a catalyst in these circumstances. Finally as the plot on the right shows, unless the power requirements were to come down dramatically the production of NOx is too high with this material.

6.4 *10% Pr doped-CeOx on alumina beads*

The final NTP packing we considered was a Pr-doped CeOx catalyst that was designed originally as a low temperature CO oxidation catalyst. The thought was that perhaps it could operate as a low temperature CH$_3$Br catalyst as well. This material was reasonably effective at CH$_3$Br destruction, but required fairly high power and had the somewhat unusual property that the efficiency initially improved with time when the plasma power was turned on. We attributed this to the gradual equilibration of the catalyst temperature over time. Evidently the effectiveness improves with temperature, even inside a non-

thermal plasma environment. We confirmed this hypothesis by insulating the NTP reactor and observing a noticeable improvement in the CH₃Br destruction. In fact with an insulated reactor we actually reached essentially 100% destruction, albeit at very high power inputs. It would have been an interesting test to see if this material is useful as a low temperature thermal catalyst but we did not explore this possibility.

This observation as well as the reasonably level steady state CH_3Br concentrations suggests that the reaction is catalytic in nature. In support of this we did find a very small band in the FTIR that was eventually identified as $BrNO_2$. This was a very small band, but it does prove that at least some of the Br escapes the plasma. Furthermore the carbon balance was pretty good overall, with CO_2 always the majority oxidation product for carbon. The next slides illustrate these points.
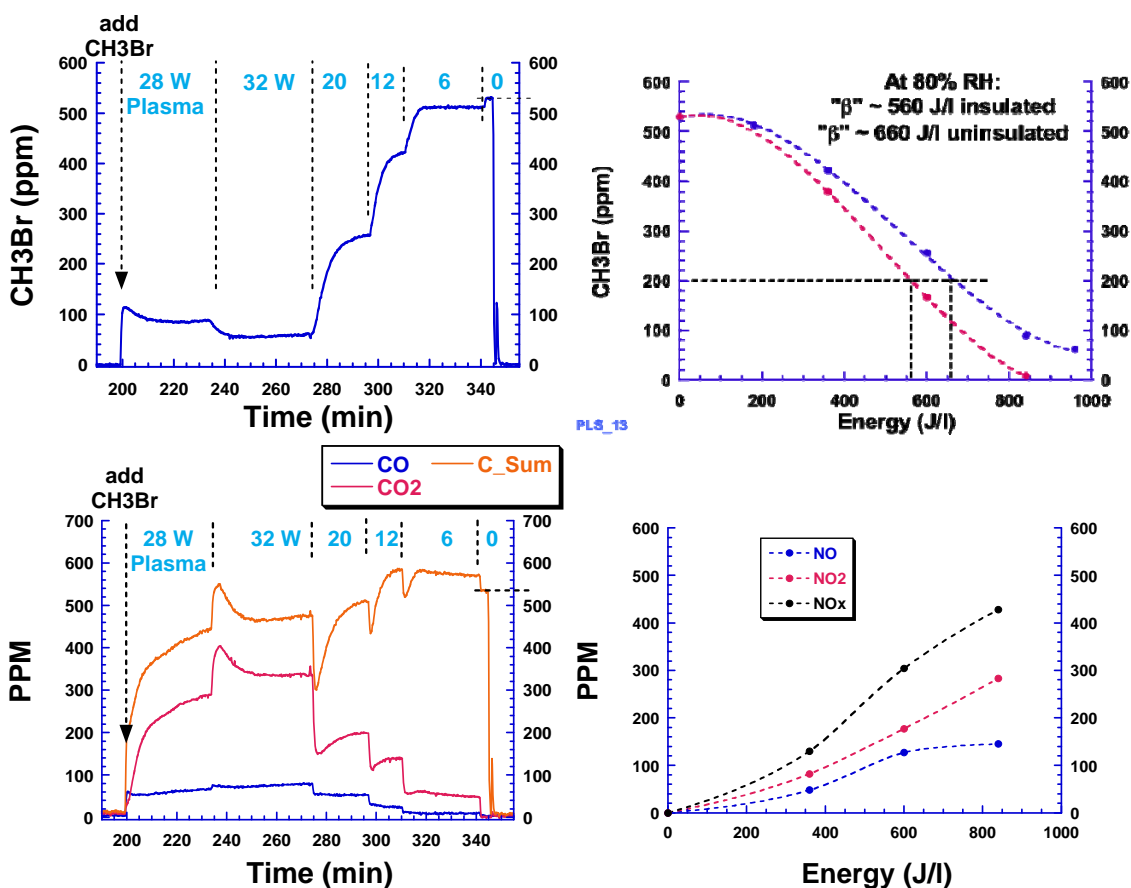
We show below one final test with the Pr-CeO2 catalyst beads. We ran one steady-state measurement of destruction at approximately 2500 ppm just to see what would happen in such a case. We presume at this point that ozone becomes the limiting reagent. The first plot shows the time behavior and the second compares the result to a 540 ppm test on a relative efficiency scale.
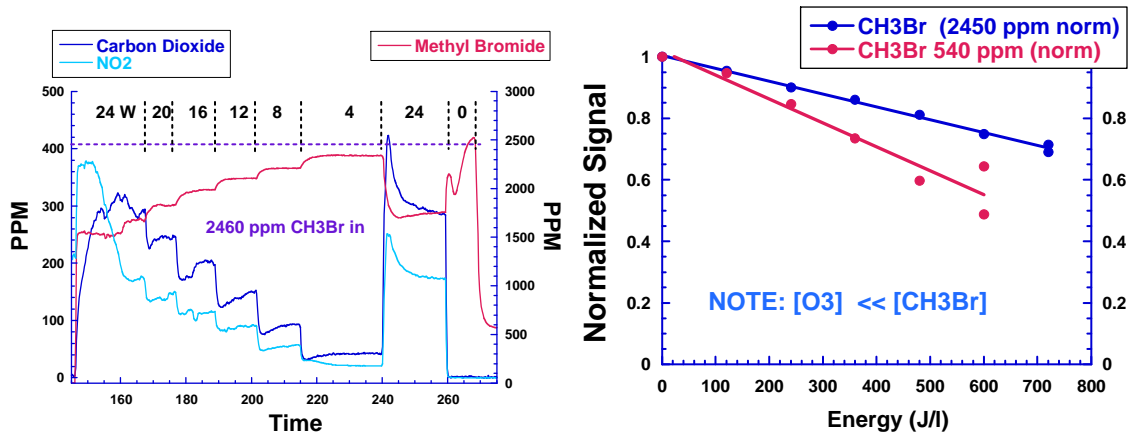
Even at extremely high concentrations the CH_3Br output looks quite level at steady-state. This supports the idea that this material is not being poisoned, but is in all likelihood the only material that actually catalytically destroys CH_3Br.

Unfortunately the conditions required to destroy significant quantities of CH3Br lead to quite high levels of NOx formation. Unless this issue can be addressed the usefulness of this catalyst in the context of breathable air production is minimal. It would be very interesting to test this material as a low temperature oxidation catalyst.

7 Appendix C—Reactor Packing Characterization

Scanning electron and optical microscopy on ZSM5 particles

7.1 Methods

Five different specimens were examined:
1) Ag-ZSM5 + CH_3Br
2) Mn-Ag-ZSM5 + CH_3Br
3) Mn-Ag-ZSM5 + CH_3Br (**black particles**)
4) Unreacted Mn-Ag-ZSM5 + CH_3Br
5) Unreacted Ag-ZSM5

Optical microscopy (OM), scanning electron microscopy (SEM), energy dispersive spectroscopy (EDS), and x-ray diffraction (XRD) were used to characterize the specimens.

- OM Methods
  - Leitz Orthoplan and Olympus SZH10 microscopes were used for these observations.
  - Random particles were selected from each batch and adhered to separate aluminum SEM stubs with carbon tape
  - Some particles were cross-sectioned using a razor blade and the cut surface mounted upwards for observations
- SEM-EDS Methods
  - A JEOL 5900 SEM, an EDAX silicon drifted array energy dispersive spectrometer, a Robinson backscatter detector, and 4 pi software were used for these observations.
  - OM specimen mounts (see above) were coated with Pd following OM observations for analysis in the SEM.
  - Samples were analyzed with both a backscatter electron (BSE) and secondary electron (SEI) detector. The BSE provides elemental contrast where brighter regions are displayed with higher average atomic number and the SEI provides better surface contour information.
  - The SEM was also used to gather size statistics for the various metal deposits throughout the specimen.
- XRD Methods
  - A Bruker D8 Advance and a Lynxeye 1-D linear array detector were used to collect these measurements.
  - Small samples of specimens #1, #2, and #4 and ground them to a powder in an agate mortar/pestle and diffraction patterns analyzed.

7.2 Results
7.2.1 Particle size analysis

The optical mounts were used in the SEM to locate and measure the various metal deposits found on the surfaces and on the cross-sectioned views of the various samples. The individual silver particles ranged observed on the different specimens varied from ~1.3–29 μm and sizes were consistent across the specimens. However, it appeared that the Ag-ZSM5 particles analyzed might have had more of these silver "pools" than the other specimens. In some cases, agglomerates of smaller silver particles were observed (see Figure 39). Finding the particles on Specimen #1 proved much easier than the other specimens.

7.2.2 Specimen #1, Ag-ZSM5 particles reacted with CH₃Br

These particles appeared very similar in appearance, all a very similar shade of white. We observed metallic deposits on the inside of some of the cross-sections (red circular region in Figure 38). One of the bright deposits on #1-B (yellow box) was analyzed with EDS and it was composed mostly of silver, a high degree of oxygen, and some bromine.
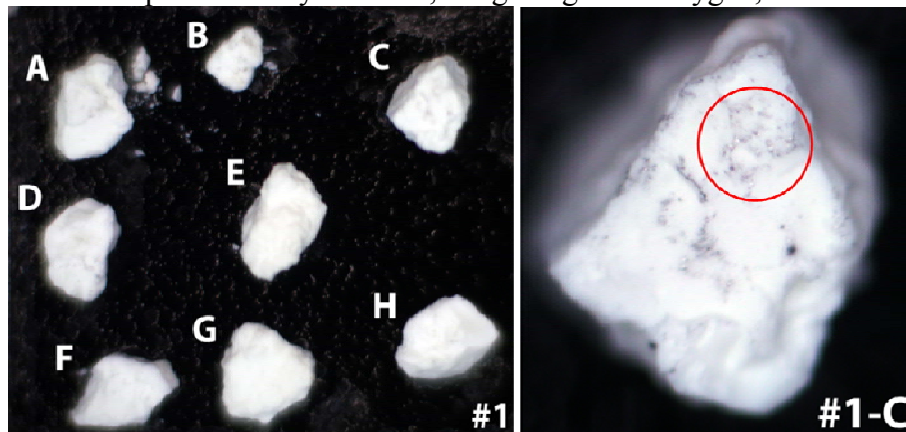

Figure 38. OM of Ag-ZSM5 particles reacted with CH₃Br. Some of these were cross-sectioned prior to analysis. The red circle denotes a region of metallic deposits. Field of view width in the left micrograph is ~7 mm.
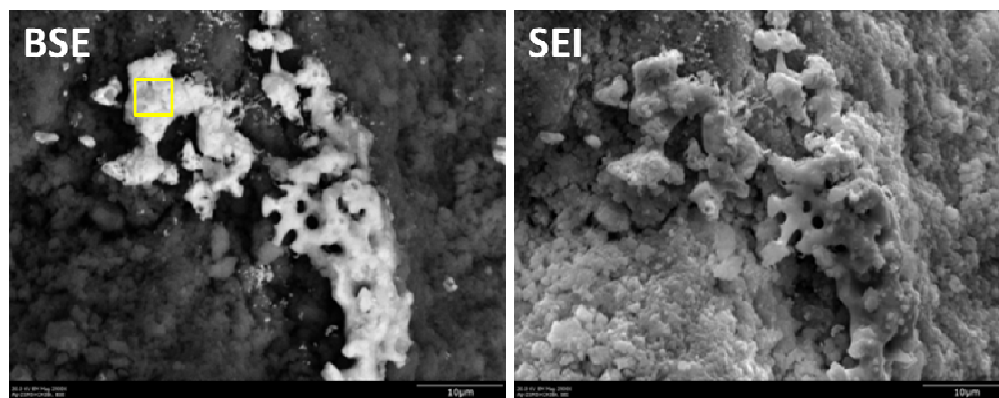
Figure 39. SEM micrographs collected with both BSE and SEI detectors. EDS region is defined by yellow box.

Table 1. EDS data from region in Figure 39.

Element	Weight %	Atomic %
C	1.28	6.65
O	6.55	25.47
Si	7.80	17.28
Fe	1.04	1.16
Br	5.22	4.06
Zr	3.13	2.13
Pd	1.12	0.66
Ag	73.85	42.58

7.2.3 Specimen #2, Ag/Mn-ZSM5 particles reacted with CH₃Br

These particles appeared very different in appearance, some white and some very dark (#2-G in Figure 40. Metallic deposits were observed on some of these particles on cross-sectioned surfaces (#2B, Figure 41). Also, red deposits were observed on some of the

particles (#2-H, Figure 41). Color gradients were observed along the perimeter of select particles (#2D and #2E, Figure 41) though this compositional gradient could not be verified with SEM/EDS (blue box on #2E, Figure 41).
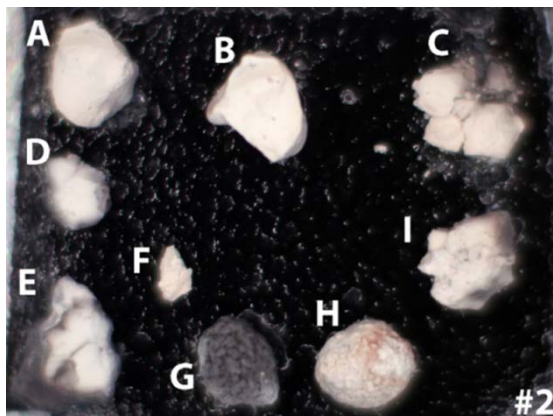
Figure 40. OM of various Ag/Mn-ZSM5 particles reacted with CH$_3$Br. Field of view width is ~7 mm.
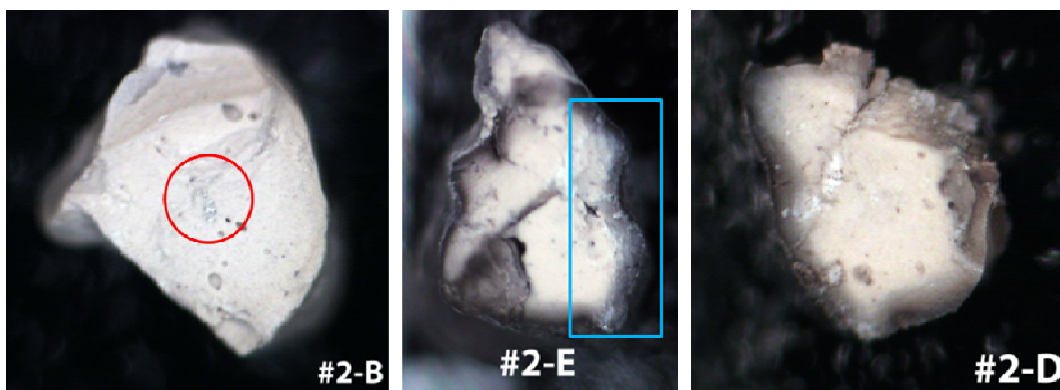
Figure 41. Higher magnification OM observations from Figure 40.
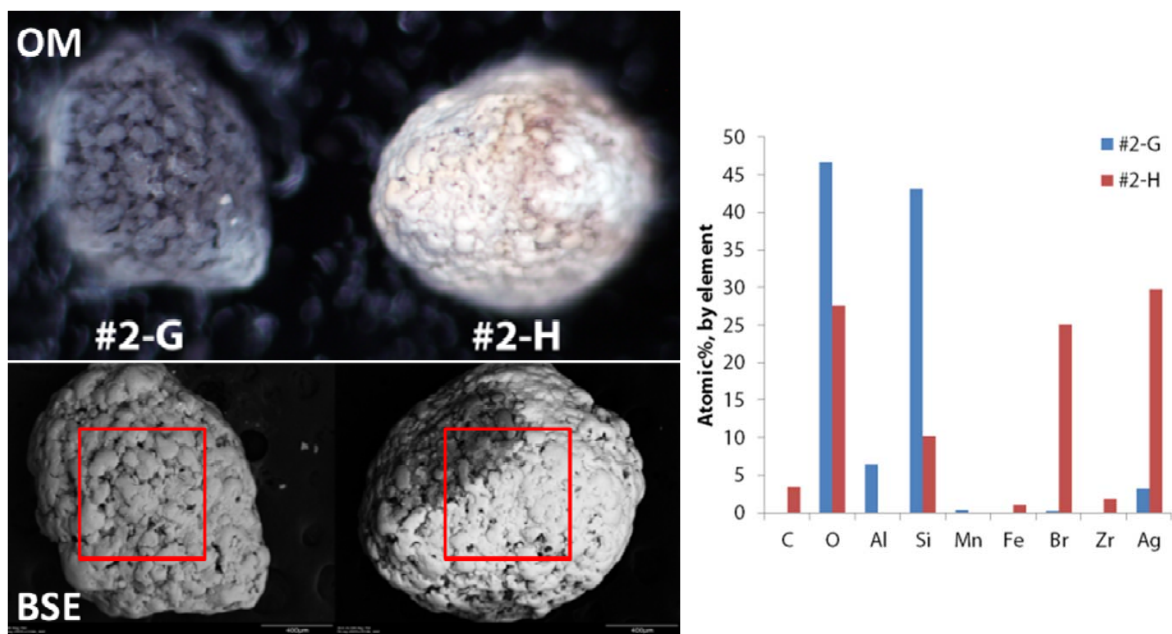
Figure 42. OM and BSE SEM on particles #2-G and #2-H (left). EDS was performed in the regions called out by the red boxes for each sample (right).

Figure 43. BSE SEM on particles #2-I.

Table 2. EDS data from region in Figure 43.

Element	Weight %	Atomic %
C	0.59	2.35
O	18.10	53.79
Si	3.54	5.99
Fe	0.66	0.56
Br	20.00	11.90
Zr	2.71	1.41
Pd	1.83	0.82
Ag	52.57	23.18

SEM dot mapping was performed on Specimen #2-B and #2-E in order to determine if the high concentration regions of Br overlapped with the high concentration regions of

Ag (see Figure 45 and Figure 46). The dot mapping technique revealed that this was, in fact, the case.
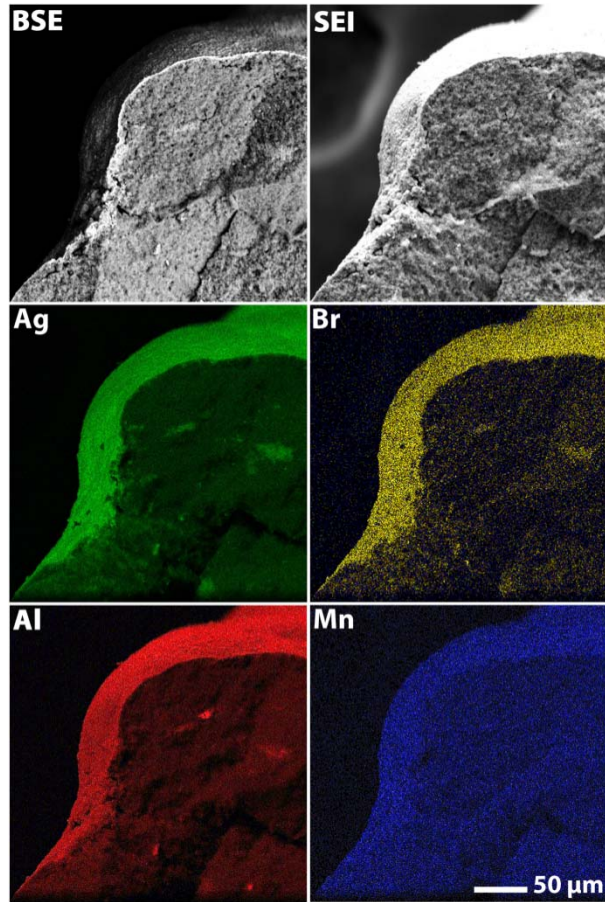
Figure 44. SEM dot map on Specimen #2-B.
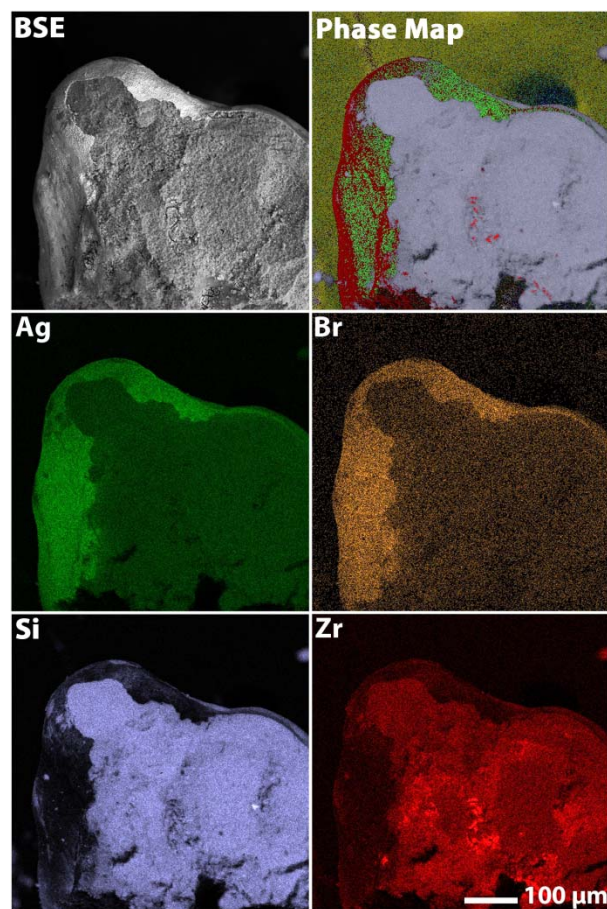
Figure 45. SEM dot map on Specimen #2-E.

7.2.4 Specimen #3, Ag/Mn-ZSM5 particles reacted with CH₃Br (dark particles only)

These specimens are the black particles from specimen #2. Two samples were mounted as-received (A & B) and two were cross-sectioned (C & D) – see Figure 46. The primary difference between the particles was the internal color: some were dark and some were light in color. A color gradients was observed along the perimeter of #3-D (as seen with Specimen #2) but not with #3-C. The red region observed in #3-B (see Figure 47) was analyzed with SEM-EDS.
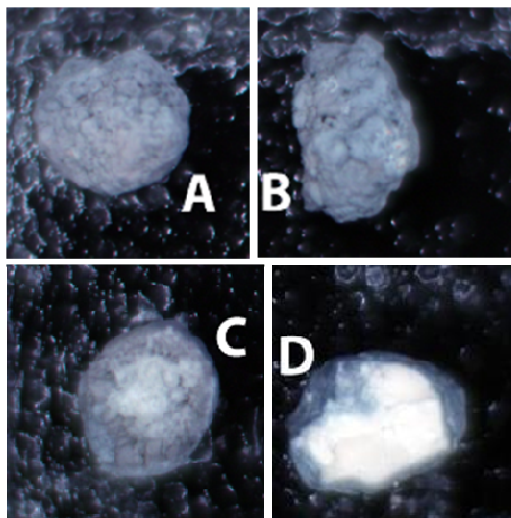
Figure 46. Optical micrographs of Specimen #3. Particles C & D were cross-sectioned (with cut surface up) and A & B were mounted as-received.
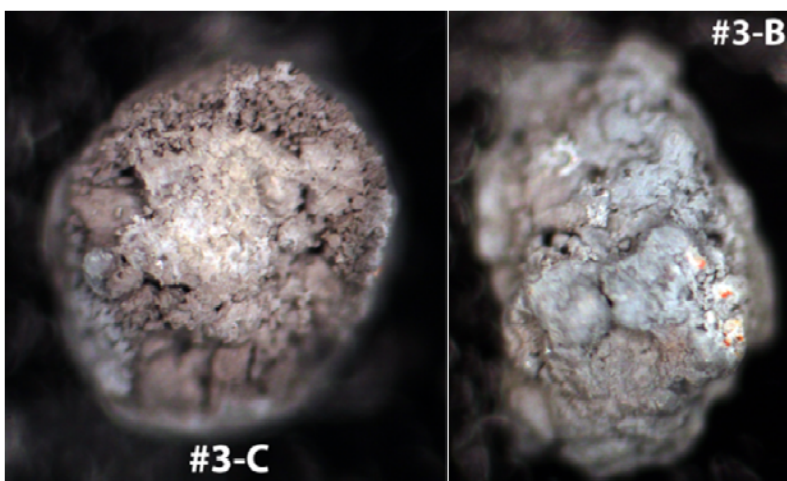
Figure 47. Higher magnification optical micrographs of #3-C and #3-B.

Specimen #3-A was analyzed by SEM/EDS for a bulk compositional measurement – see Figure 48.
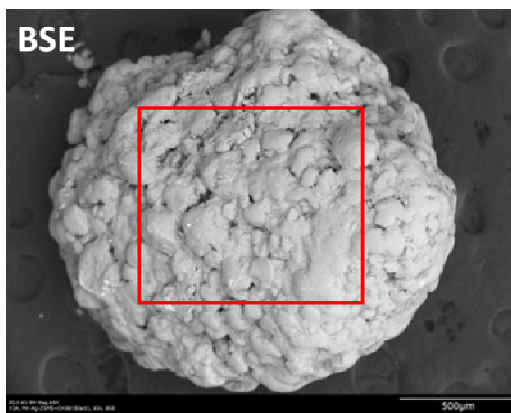
Figure 48. SEM micrograph on Specimen #3-A. EDS was performed on the red, boxed region.

Table 3. EDS results for region defined in Figure 48.

Element	Weight %	Atomic %
C	0.69	1.40
O	38.49	58.78
Si	39.54	34.40
Mn	0.63	0.28
Fe	0.53	0.23
Zr	8.51	2.28
Ag	11.61	2.63

The red regions found in #3-B (Figure 47) were analyzed using OM as well as SEM/EDS (Figure 49). The region bound by the red box was analyzed by EDS and was found to be composed of Ce, Ag, and Zr (Si-O signature is due to zeolite background).
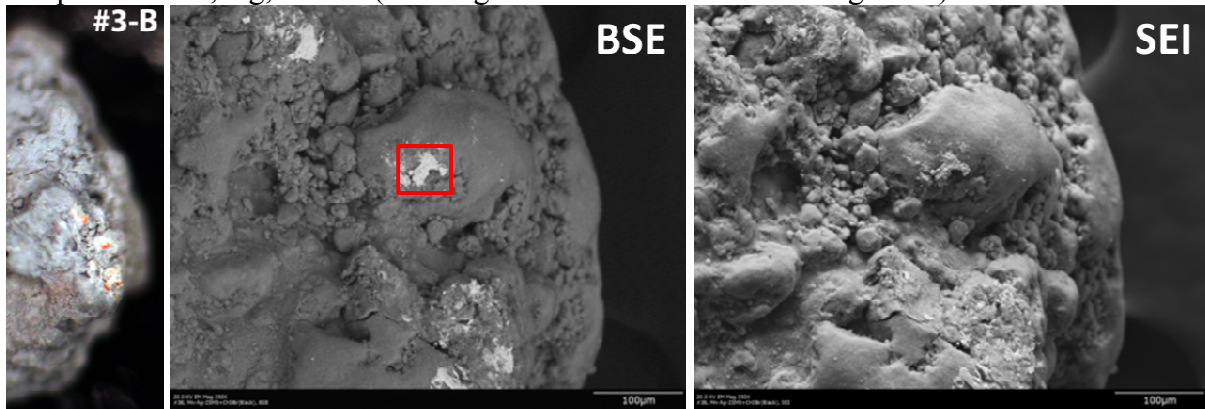
Figure 49. OM (far left), SEM-BSE, and SEM-SEI micrographs of Specimen #3-B. The region bound by the red box in the middle micrograph was analyzed by EDS and the results are presented in Table 4.

Table 4. EDS results from red, boxed region in Figure 49.

Element	Weight %	Atomic %
C	1.01	2.75
O	23.03	47.26
Si	32.27	37.73
Mn	0.92	0.55
Fe	0.42	0.25
Br	0.52	0.21
Zr	7.17	2.58
Ag	7.75	2.36
Ce	26.90	6.30

Specimen #3-D (see Figure 50) was analyzed using SEM-EDS for a compositional gradient using a high resolution dot map from the perimeter to the bulk of the particle though no variation was detected.
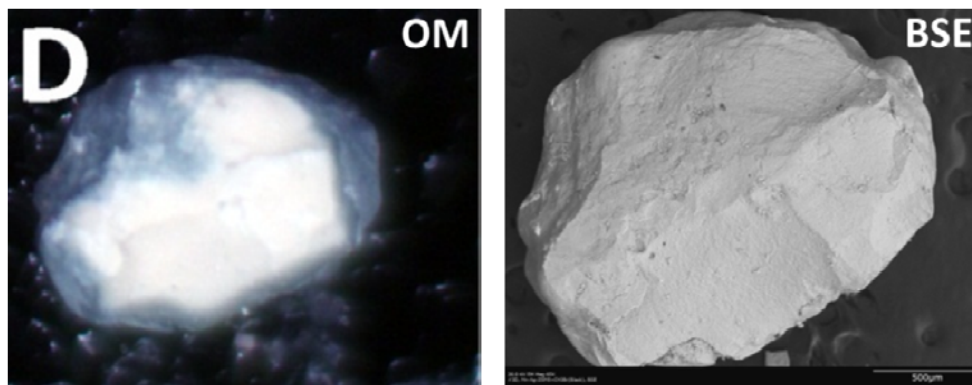
Figure 50. Optical (left) and SEM (right) micrographs of Specimen #3-D.

7.2.5 Specimen #4, Ag/Mn-ZSM5 unreacted particles

Separate particles from this batch appeared very differently (see Figure 51) from dark maroon (#4-E), light blue (#4-D), to yellow (#4-J). The surface morphology was highly variable as well from smooth (#4-D) to rough (#4-B). As with the reacted Ag/Mn-ZSM5 particles (Specimens #2 and #3, described previously), some particles showed a perimeter color gradient when cross-sectioned (#4-L and #4-M). See Figure 52 for more detail on #4-C and #4-M.
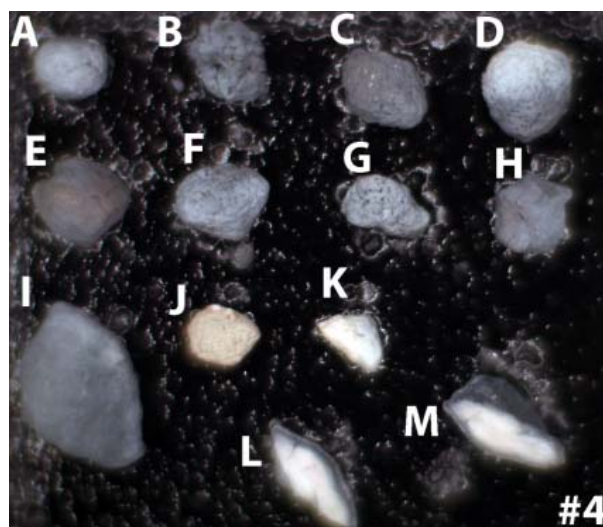
Figure 51. OM of 13 different particles from this batch. Particles #4-L & #4-M were cross-sectioned with the sectioned side mounted upwards and the rest were not cross-sectioned.
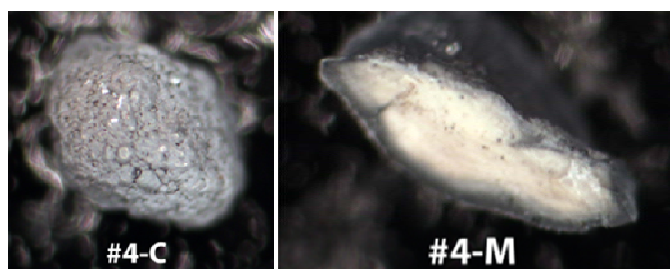
Figure 52. Higher magnification #4-C and #4-M as captured using OM.
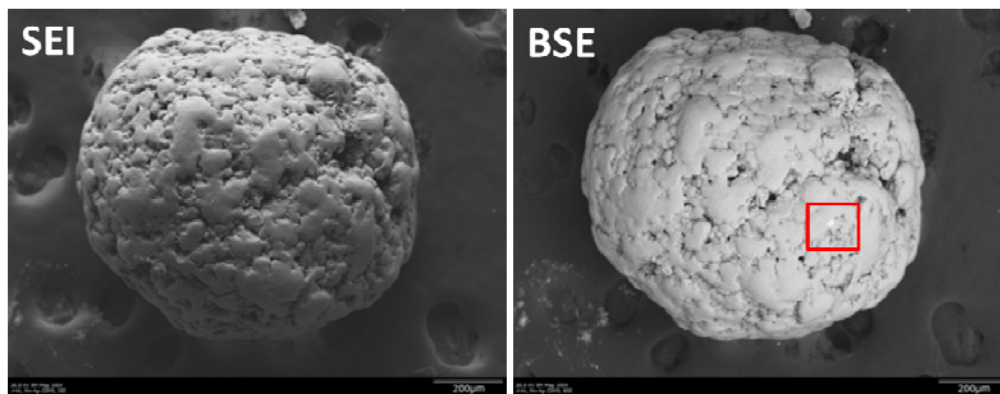
Figure 53. SEM captured on Specimen #4-A using both SEI and BSE detectors. EDS was performed on the red, boxed region and the data is presented in Table 5.

Table 5. EDS results from region defined in Figure 53.

Element	Weight %	Atomic %
C	1.87	7.27
O	10.72	31.25
Si	22.53	37.42
Mn	1.12	0.95
Br	1.05	0.61
Zr	4.32	2.21
Ag	8.58	3.71
Ce	49.81	16.59

7.2.6 Specimen #5, Ag-ZSM5 unreacted particles

The unreacted Ag-ZSM5 particles (Specimen #5) appeared very similar to those reacted with CH_3Br (Specimen #1). Most of the particles observed had regions with metallic deposits. SEM-EDS was performed on several different particles. The particles consisted of varying amounts of Fe, Ag, and they were found to contain large amounts of Fe, Cr, and Ag. Also, inter- and intra-particle Zr variations were observed throughout. Detailed EDS on the various particles analyzed is presented in 7.4 Supplemental Analyses on Specimen #5 (unreacted Ag-ZSM5) *EDS results*.
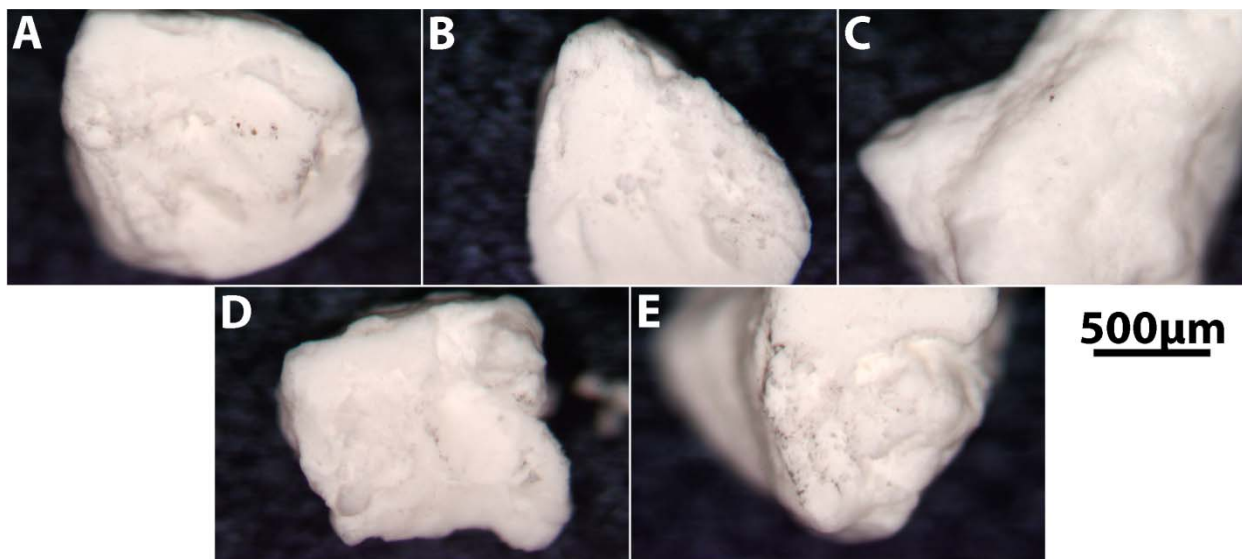
Figure 54. Optical micrographs of Specimen #5, unreacted Ag-ZSM5. Micrographs A, B, D, & E are cross-sections and C was mounted as-received. The scale-bar presented is valid for all micrographs.

7.3 XRD Results

All phases fit zeolite structure using Pawley refinement (Figure 55). A very small quantity of orthorhombic rare-earth manganate ($ErMn_2O_5$) was observed in the noise (near detection limits). Unit cell for #1 was largest and is most likely due to the large Ag ion. For Specimen #2, red/pink-colored particles were separated out from the rest, ground to a powder, mixed with ethanol and placed onto a zero-background silicon holder using a dropper. AgBr and Ag_2BrNO_3 phases were observed with this specimen (see Figure 56).
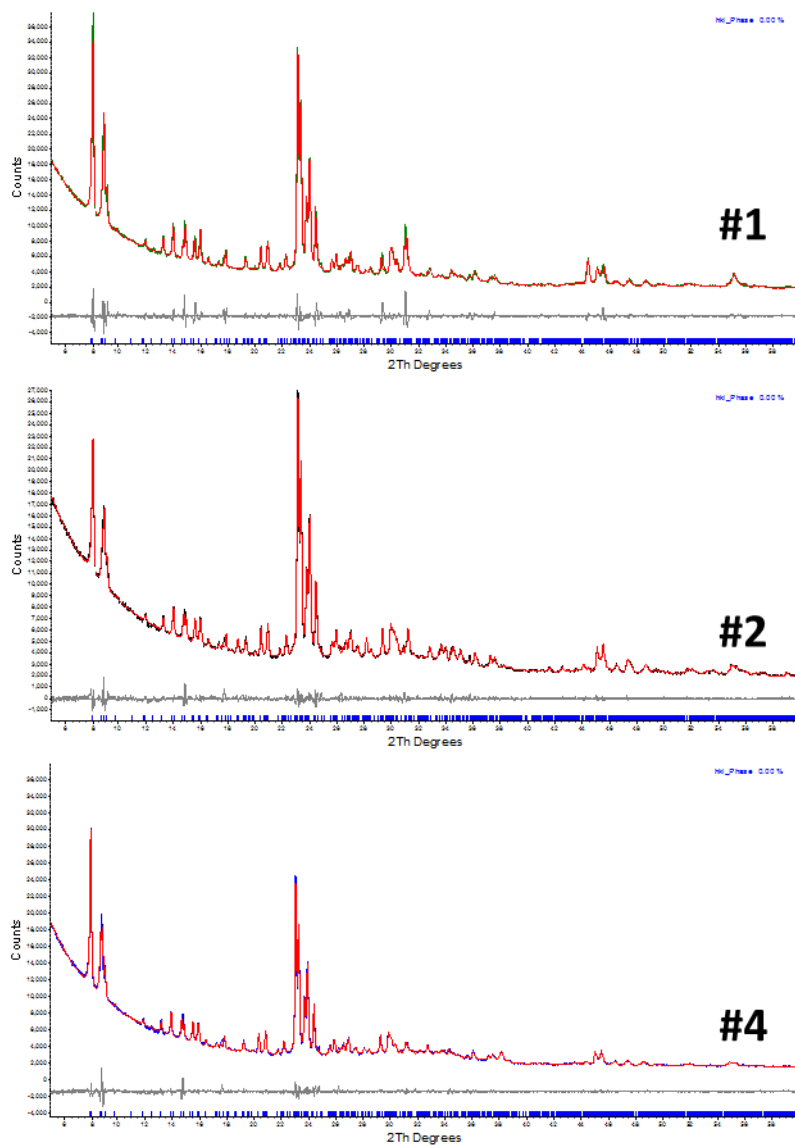
Figure 55. Pawley refinement for Specimens #1, #2, and #4 – see Table 6 for cell refinement parameters.

Table 6. Cell refinement parameters from Figure 55 data.

ID	SG	a (Å)	b (Å)	c (Å)	α(°)	β(°)	γ(°)
#1	Pnma	20.346	20.007	13.417	90.000	90.000	90.000
#2	Pnma	20.240	19.930	13.409	90.000	90.000	90.000
#4	Pnma	20.265	19.963	13.430	90.000	90.000	90.000
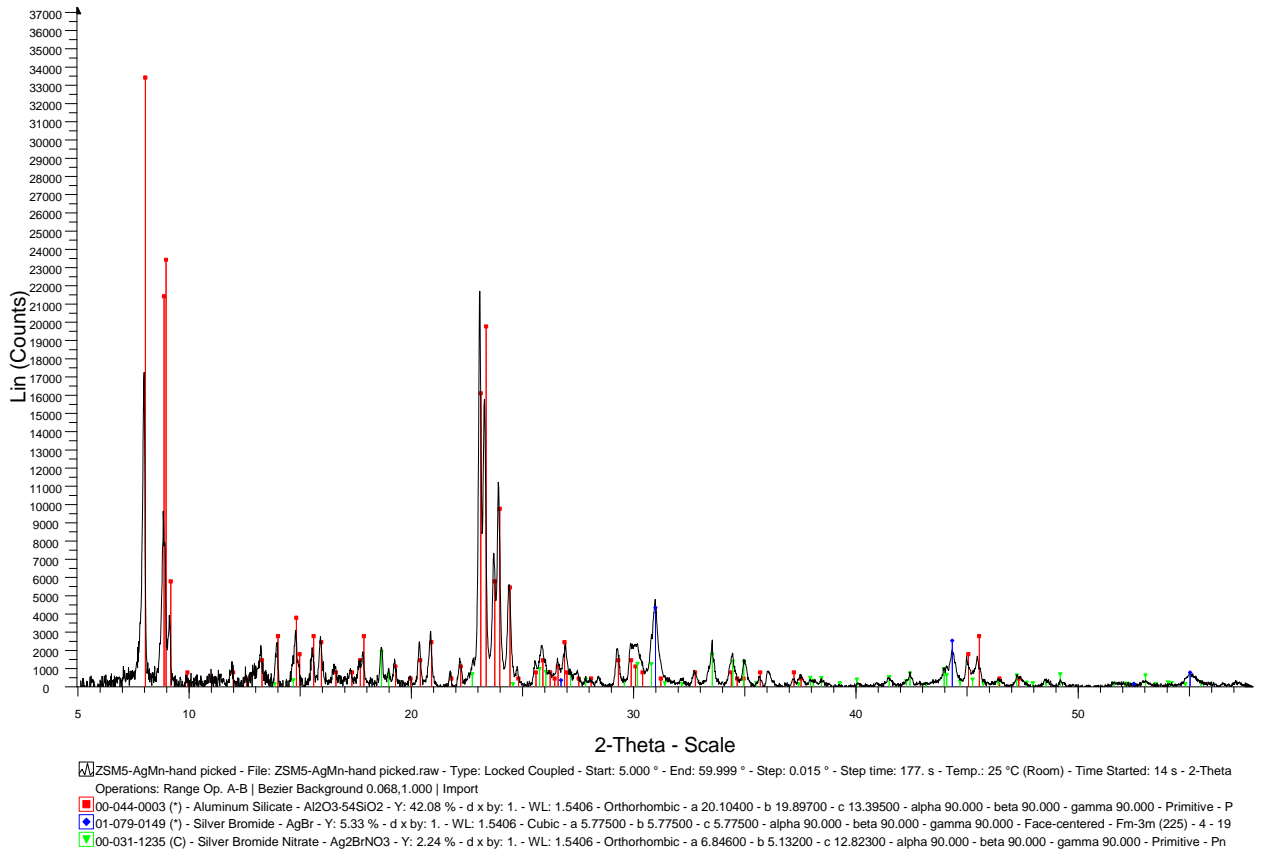
Figure 56. Phase identification for hand-picked red/pink-colored particles in Specimen #2.

7.4 Supplemental Analyses on Specimen #5 (unreacted Ag-ZSM5)
EDS results

Quantitative Results for Probe 1
Analysis: Bulk   Method: Standardless
Acquired 06-Jan-2011, 20.0 KeV @10 eV/channel

Element	Weight %	Std. Dev.	Atomic %
O	25.80	0.98	43.28
Al	6.77	1.02	6.74
Si	46.40	1.00	44.34
Fe	0.33	0.12	0.16
Cu	0.15	0.06	0.06
Zr	6.85	1.03	2.02
Pd	1.01	0.34	0.25
Ag	12.69	0.65	3.16
Total	100.00		

Quantitative Results for Probe 2
Analysis: Bulk   Method: Standardless
Acquired 06-Jan-2011, 20.0 KeV @10 eV/channel

Element	Weight %	Std. Dev.	Atomic %
O	28.03	1.00	45.10
Al	7.55	0.96	7.20
Si	46.98	1.01	43.06
Fe	0.25	0.09	0.11
Cu	0.03	0.01	0.01
Zr	9.60	0.64	2.71
Pd	0.64	0.22	0.16
Ag	6.93	1.02	1.65
Total	100.00		

Realtime: 58.3
Livetime: 20.0
Probe 3

56464
42348
28232
14116

Counts

X-Ray Energy (KeV)

O
Ag
Fe
Al
Zr
Zr
Cl
Cl
Pd
Ag
Pd
Ag
Pd
Ag
Si
Ag
Pd
Fe
Fe

Quantitative Results for Probe 3
Analysis: Bulk   Method: Standardless
Acquired 06-Jan-2011, 20.0 KeV @10 eV/channel

Element	Weight %	Std. Dev.	Atomic %
O	24.12	0.96	40.88
Al	6.38	1.04	6.41
Si	48.10	1.03	46.43
Cl	1.06	0.35	0.81
Fe	0.22	0.08	0.11
Zr	6.44	1.05	1.91
Pd	0.73	0.25	0.19
Ag	12.95	0.66	3.25
Total	100.00		

Realtime: 56.3
Livetime: 20.0
Probe 4

63788
47841
31894
15947

Counts

X-Ray Energy (KeV)

O
Ag
Fe
Al
Zr
Zr
Cl
Cl
Pd
Ag
Pd
Ag
Pd
Ag
Si
Fe
Fe
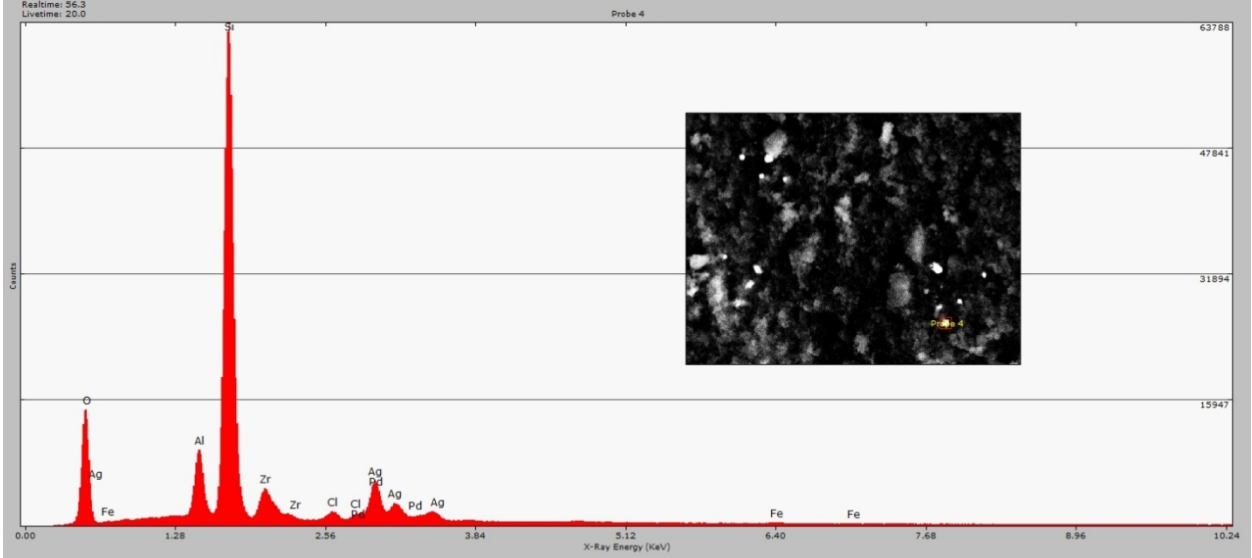
Quantitative Results for Probe 4
Analysis: Bulk   Method: Standardless
Acquired 06-Jan-2011, 20.0 KeV @10 eV/channel

Element	Weight %	Std. Dev.	Atomic %
O	30.52	1.00	47.49
Al	6.67	1.03	6.16
Si	47.61	1.02	42.20
Cl	0.66	0.23	0.47
Fe	0.24	0.09	0.11
Zr	6.74	1.03	1.84
Pd	0.64	0.22	0.15
Ag	6.93	1.02	1.60
Total	100.00		

Quantitative Results for Probe 5
Analysis: Bulk   Method: Standardless
Acquired 06-Jan-2011, 20.0 KeV @10 eV/channel

Element	Weight %	Std. Dev.	Atomic %
O	31.16	1.01	47.42
Al	6.87	1.02	6.20
Si	50.01	1.07	43.35
Cl	0.00	0.00	0.00
Fe	0.12	0.05	0.05
Zr	7.16	1.01	1.91
Pd	0.83	0.28	0.19
Ag	3.86	0.93	0.87
Total	100.00		

Quantitative Results for Probe 1
Analysis: Bulk   Method: Standardless
Acquired 06-Jan-2011, 20.0 KeV @10 eV/channel

Element	Weight %	Std. Dev.	Atomic %
O	4.73	1.01	13.07
Al	6.85	1.02	11.23
Si	12.33	0.62	19.44
Cr	9.55	0.64	8.13
Fe	56.33	1.23	44.65
Cu	0.64	0.23	0.45
Zr	1.72	0.53	0.83
Pd	1.13	0.37	0.47
Ag	0.52	0.18	0.21
Ta	6.22	1.05	1.52
Total	100.00		

Realtime: 46.3
Livetime: 30.0
Probe 2

Quantitative Results for Probe 2
Analysis: Bulk   Method: Standardless
Acquired 06-Jan-2011, 20.0 KeV @10 eV/channel

Element	Weight %	Std. Dev.	Atomic %
C	2.60	0.75	9.53
O	1.65	0.51	4.53
Al	6.90	1.03	11.24
Si	6.48	1.05	10.13
Cr	7.68	0.96	6.49
Fe	72.52	1.62	57.04
Cu	0.43	0.16	0.30
Zr	0.46	0.17	0.22
Pd	0.59	0.21	0.24
Ag	0.67	0.24	0.27
Total	100.00		

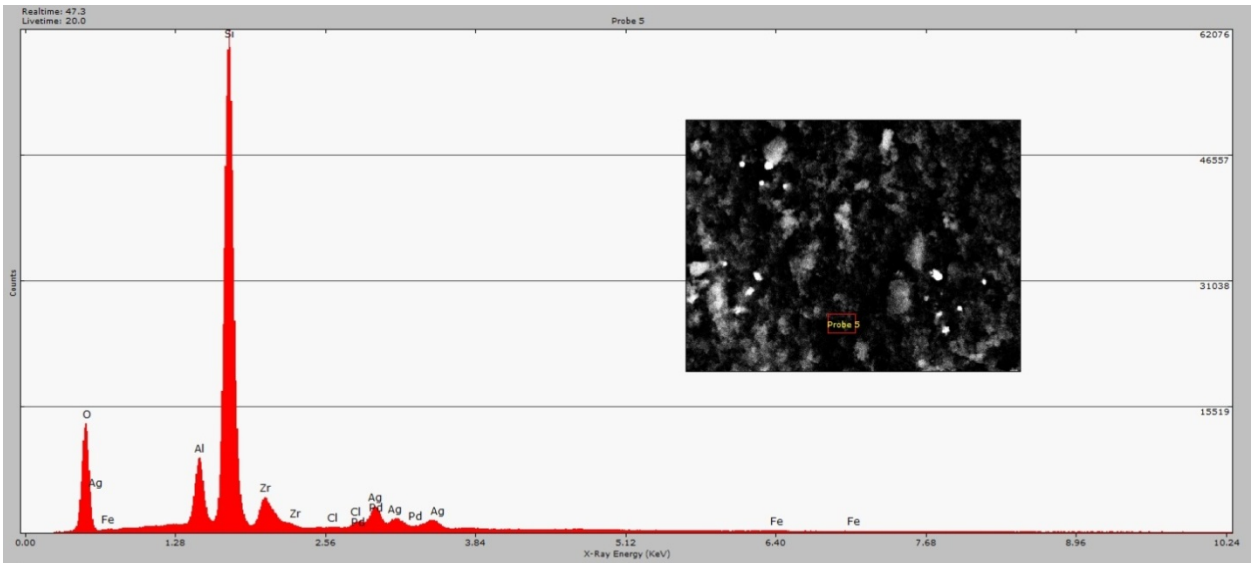Realtime: 28.2
Livetime: 20.0
Probe 1

Quantitative Results for Probe 1
Analysis: Bulk   Method: Standardless
Acquired 06-Jan-2011, 20.0 KeV @10 eV/channel

Element	Weight %	Std. Dev.	Atomic %
O	22.67	1.02	42.91
Al	6.43	1.07	7.22
Si	37.06	0.98	39.96
Cl	0.00	0.00	0.00
Fe	0.58	0.22	0.31
Zr	4.92	1.06	1.63
Pd	1.08	0.37	0.31
Ag	27.26	1.04	7.65
Total	100.00		

Realtime: 47.7
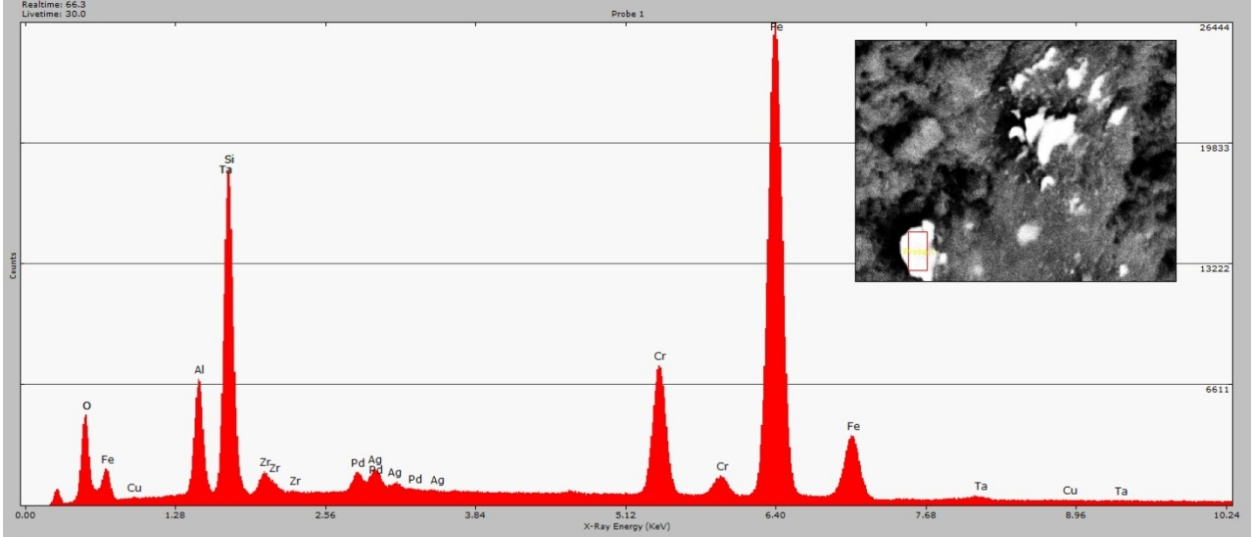Livetime: 13.3
Probe 1

Quantitative Results for Probe 1
Analysis: Bulk   Method: Standardless
Acquired 06-Jan-2011, 20.0 KeV @10 eV/channel

Element	Weight %	Std. Dev.	Atomic %
O	17.92	0.86	34.78
Al	6.67	1.04	7.68
Si	41.55	0.92	45.94
Cl	2.28	0.67	2.00
Fe	0.70	0.25	0.39
Zr	6.00	1.07	2.04
Pd	1.52	0.49	0.44
Ag	23.36	0.94	6.72
Total	100.00		

Realtime: 40.8
Livetime: 30.0
Probe 1

Quantitative Results for Probe 1
Analysis: Bulk   Method: Standardless
Acquired 06-Jan-2011, 20.0 KeV @10 eV/channel

Element	Weight %	Std. Dev.	Atomic %
O	14.41	0.79	29.87
F	1.93	0.62	3.38
Al	5.29	1.07	6.50
Si	26.29	1.00	31.05
Cr	5.55	1.08	3.54
Fe	38.94	1.02	23.13
Zr	4.35	1.01	1.58
Pd	1.37	0.45	0.43
Ag	1.32	0.44	0.41
In	0.01	0.01	0.00
Pm	0.54	0.21	0.12
Total	100.00		